Molecular Modeling of MOF Membranes and Polymer/MOF Mixed Matrix Membranes for Gas Separations

by

İlknur Eruçar

A Thesis Submitted to the
Graduate School of Engineering
in Partial Fulfillment of the Requirements for
the Degree of

Master of Science
in
Computational Sciences & Engineering

Koç University

July 2012

Koç University

Graduate School of Sciences and Engineering

This is to certify that I have examined this copy of a master's thesis by

İlknur Eruçar

and have found that it is complete and satisfactory in all respects,
and that any and all revisions required by the final
examining committee have been made.

Committee Members:

_____

Seda Keskin Avcı, Ph.D. (Advisor)

_____

Can Erkey, Ph.D.

_____

Özlem Keskin Özkaya, Ph.D.

Date: _____

ABSTRACT

Polymer membranes have been commonly used for gas separation applications due to their ease of fabrication and low cost. However, polymer membranes have a trade-off between gas selectivity and permeability. For the past two decades, there has been a growing interest in developing mixed matrix membranes (MMMs) by combining non-polymeric materials with the polymers to overcome this permeability/selectivity trade-off. Metal organic frameworks (MOFs) which are a new class of nanoporous materials present greater promise for being used as non-polymeric materials to fabricate MMMs due to their unique properties such as well-defined pores and large surface areas. Recently, combining MOFs with the polymers, MOF-based MMMs have been synthesized, and the high gas separation performance of MMMs has been reported. However, choosing the appropriate MOFs as filler particles in MMM applications is very difficult due to the very large number of existing MOF materials. Therefore, theoretical models play a critical role in predicting polymer/MOF combinations prior to experimental efforts. In this thesis, the methodologies for selecting MOFs as filler particles in polymers was examined using atomistic and continuum modeling. The validity of several theoretical permeation models was tested by comparing the predictions of these models with the available experimental data for CO_2/CH_4 and H_2/CH_4 separations. Combining detailed atomistic simulations with the theoretical permeation models, the performances of new-MOF based MMMs were estimated. The results found in this thesis demonstrated that selecting the appropriate MOF/polymer combinations can result in membranes with high CO_2 and H_2 selectivities and permeabilities relative to those of pure polymer membranes. The methodologies that were described in this thesis for screening MOFs in an efficient and easy way will provide conceptual hints for the assessment of the best MOF/polymer pairs to obtain high performance MMMs for CO_2/CH_4 and H_2/CH_4 separations.

ÖZET

Polimer membranlar, kolay üretimleri ve düşük maliyetleri sebebiyle gaz karışımlarını ayırma işlemlerinde yaygın olarak kullanılmaktadır. Fakat polimer membranlarda gaz seçiciliği ve geçirgenliği arasında ters bir ilişki bulunmaktadır. Son yirmi yıldır, seçicilik/geçirgenlik ters ilişkisini aşabilmek için polimer olmayan malzemeler ile polimerler kullanarak hibrit membran geliştirmeye yönelik artan bir ilgi vardır. Nanogözenekli malzemelerin yeni bir sınıfı olan metal-organik yapılı sistemler (MOF), geniş yüzey alanları ve karakteristik gözenekleri nedeniyle hibrit membran üretiminde polimer olmayan malzemeler olarak kullanıldıklarında ümit vermektedirler. Son yıllarda, MOF ile polimerleri birleştirerek hibrit membranlar sentezlenmiştir ve yüksek gaz ayırma performanslı hibrit membranlar elde edilmiştir. Fakat çok sayıda MOF'un bulunması sebebiyle, uygun olan MOF'u dolgu malzemesi olarak hibrit membran uygulamalarında seçmek oldukça zordur. Bu nedenle, teorik modeller uygun polimer/MOF kombinasyonunu deneysel çalışmalardan önce tahmin etmede önemli bir rol oynamaktadır. Bu tezde, polimerlerde dolgu malzemesi olarak kullanılan MOFları seçmek için hesaplamalı yöntemler kullanılmıştır. Teorik geçirgenlik modellerinin geçerliliği, CO_2/CH_4 ve H_2/CH_4 ayırımı için, modellerden elde edilen sonuçlar ile deneysel ölçümlerin karşılaştırılmasıyla test edilmiştir. Atomik simülasyon tekniklerini ve teorik geçirgenlik modellerini birleştirerek yeni MOF dolgulu hibrit membranların performansları hesaplanmıştır. Bu tezde elde edilen sonuçlar uygun MOF/polimer kombinasyonunun seçilmesiyle oluşturulan hibrit membranların CO_2 ve H_2 seçicilik ve geçirgenliğinin, saf polimer membranlara kıyasla önemli ölçüde arttığını kanıtlamıştır. Bu tezde MOFları hızlı ve etkili bir şekilde taramak için tanımlanan metotlar, CO_2/CH_4 ve H_2/CH_4 ayırımı için yüksek performanslı hibrit membran üretmede kullanılacak en iyi MOF/polimer çiftini bulmada kavramsal ipuçları sağlayacaktır.

ACKNOWLEDGEMENTS

Two years ago, I remember meeting my advisor, Asst. Prof. Dr. Seda Keskin. Her sincere attitudes, invaluable comments and her desire to research impressed me deeply. While I was leaving her office, I have already made my decision to study with her at Koç University. Now, I remember that day which was the beginning of my research career…

Asst. Prof. Dr. Seda Keskin, my exceptional advisor has been always my inspiration. Without her constant support and guidance, I have never finished my dissertation. I would like to express my sincere appreciation to my advisor for her motivation, constructive comments and her limitless patience. She was always helpful and she has always had time to answer all my questions. Throughout my master program, she has always encouraged me to reach my goals. My gratitude that I have for her is beyond words. Thank you my dear advisor for always believing in me…

My special appreciation goes to Prof. Dr. Özlem Keskin and Prof. Dr. Can Erkey for being my dissertation committee members. I would like to thank them for their time and insightful comments and suggestions.

I am grateful to my officemate, Erhan Atci. Sharing an office together for two years, we have learnt a lot from each other. I thank him for having so much patience with me these two years. Special thanks go to our group members Gamze Yılmaz and Yeliz Gürdal for their friendship and willingness to help me.

I owe special thanks to my dear friend Buse Aras for her great friendship. Throughout my master program, I have met many great people. My deepest gratitude goes to my dear homemates Zeynep Göksel Özsarp, Müge Bulu and İdil Arşık. My sincere thanks go to Zuhal Taşdemir for her close friendship. I also thank Hasan Şıldır, Deniz Çizmeci, Derya Aydın, Mehmet Tardu, Caner Nazlı, İbrahim Hocaoğlu, Ayşenur Kibar and Zehra Önen for their good friendship.

I am grateful to my dear parents, brother and my dear aunt Selma-Necmi-İlker Eruçar, Esma Biçer for their endless and unconditional support. Finally, I am deeply indebted my fiancé, Sinan Fındıkçı for his love, understanding and patience. He has always encouraged me to reach my goals and I am very lucky to have such a great family.

İLKNUR ERUÇAR

08.07.2012

TABLE OF CONTENTS

LIST OF TABLES

LIST OF FIGURES

NOMENCLATURE

c	adsorbate concentration
D_t	transport diffusivity
D_o	corrected diffusivity
f	bulk phase fugacity
J	steady state flux
L	membrane thickness
MMM	mixed matrix membrane
MOF	metal organic framework
P	gas permeability in a MOF/polymer membrane
P_d	gas permeability of dispersed phase
P_I	gas permeability of the rigidified interphase layer
P_m	gas permeability of continuous phase
P_r	relative gas permeability
S	selectivity

Greek letters

∇c	concentration gradient of the adsorbed species
Δp	pressure drop
$*\beta$	matrix rigidification factor
λ_{dm}	permeability ratio of P_d/P_m
λ_{Im}	permeability ratio of P_I/P_m
λ_{dI}	permeability ratio of P_d/P_I
ϕ	volume fraction of filler particles
ϕ_m	maximum packing volume fraction of filler particles

δ	ratio of outer radius of interfacial shell to core radius
φ	a parameter described for volume fraction of filler particles
β	a parameter for ratio of the interphase permeability to the polymer permeability
γ	a parameter described for ratio of the interphase thickness to the particle radius

Chapter 1

INTRODUCTION

Membrane-based gas separation processes have played an increasingly important role in industrial applications since 1980 when the first commercial polymer membranes were used[1]. The advantages of membranes such as low energy use and low capital investments make them promising candidates for gas separation applications. Membrane-based processes do not require phase change and there are no moving parts in membranes compared to conventional separation units such as distillation and crystallization[2]. Membranes are thin barriers that separate gas components from their mixtures based on the differential permeation of the components. Membrane-based gas separation applications include hydrogen separation, oxygen and nitrogen enrichment, natural gas purification (carbon dioxide/methane separation) and dehydration of air[3].

Permeability and selectivity are the two key parameters to assess the separation performance of a membrane. Permeability reflects the transport rates of the components (permeates) through a membrane and selectivity is the ratio of the permeability of the more permeable component to that of the less permeable one. For an efficient gas separation system, both high selectivity and high permeability are desired. High selectivity is needed to obtain components with high purity and high permeability will reduce the capital cost of the system due to the decrease in the membrane surface area[4].

Membranes can be classified into two main classes: porous and non-porous[4]. Porous membranes are rigid and have highly voided structures with inter-connected pores, and separation in these membranes depends on the molecular size of gases. Porous membranes

provide high permeability but low selectivity and only molecules that have different pore sizes can be separated effectively. Pore sizes can be classified into three groups: macropores (above 50 nm), mesopores (between 50 nm and 2 nm) and micropores (below 2 nm). Porous membranes separate gases based on various mechanisms such as Knudsen diffusion, convective flow and molecular sieving (surface diffusion). Knudsen diffusion and convective flow are based on the ratio of the pore radius of the membrane to the mean free path of the gas molecules[5]. The mean free path is the average distance traversed by a moving molecule between collisions. If this ratio is higher than 1, convective flow occurs. In Knudsen diffusion, this ratio is much less than 1. Thus, gas molecules collide with the wall and molecule-wall collisions are more dominant compared to the collisions between gas molecules[6]. Knudsen separation occurs in porous membranes having pore sizes below 50 nm and the selectivity achieved by both Knudsen and convective flow mechanisms is low compared to molecular sieve mechanism. Molecular sieve occurs when the membranes have pore diameters between those of the gas molecules. Zeolites are known as inorganic porous membranes and their gas transport mechanism is governed by the molecular sieve mechanism.

Non-porous (dense) membranes are polymer membranes which have the ability to control the permeation of different species by solution-diffusion mechanism. In the solution-diffusion mechanism, gas molecules diffuse through membrane due to the concentration gradient. Herein, permeability is related to both solubility and diffusivity. Polymer membranes are widely used for current gas separation processes due to the easy fabrication and low cost[5]. However, there is a trade-off between permeability and selectivity for polymer membranes. Robeson[7] showed that there is an upper bound for the log-log plot of selectivity versus permeability. The theory behind the upper bound can be explained by either transition state theory or free volume models[8].

Transition state theory explains activation energy for diffusion and the molecular size of the particle. Meares[9] explained the transition state theory presenting the relation between activation energy of diffusion and cross-sectional area of the gas molecules. In this theory, diffusion coefficients are correlated with the penetrants diameters. Diffusion coefficients indicate gas molecules mobility in the polymer matrix. Robeson[10] and Freeman[11] showed an empirical correlation between the kinetic diameters of the penetrants molecules and the slope of the upper bound. Thus, diffusion process has much more influence on the upper bound selectivity than the solubility process. As the size of gas molecule decreases, diffusion coefficient increases.

From the free volume viewpoint[12], diffusion coefficient rises with the increase in the fractional free volume. Hence, permeability of the penetrants increases. However, diffusion selectivity decreases with the increase in the free volume. Thus, selectivity of the overall system decreases despite the improvement in permeability. Rubbery polymers have flexible molecular chain mobility and this chain mobility causes weak size sieving ability. On the other hand, glassy polymers have restricted chain motion which provides free volume for the diffusion of small molecules, but big molecules cannot diffuse through these small chains. Therefore, rigid-glassy polymers have stronger size-sieving ability proving the upper bound relation[11].

Actually, these two approaches are related to each other since activation energies of diffusion and permeation are based on both transition state and free volume models. For example, polymers that have large free volume show low activation energies for diffusion.

In order to overcome selectivity/permeability trade-off of polymer membranes, inorganic porous membranes especially zeolite membranes have been considered for gas separation applications[13]. They have the advantage of being more chemically stable than polymer membranes. However, brittleness problem and high capital cost make zeolites less promising for large scale industrial applications. An alternative approach is to combine

advantages of both inorganic and polymer membranes to make mixed matrix membranes (MMM)[14]. Mixed matrix membranes (MMM) are consisted of inorganic fillers (dispersed phase) that are embedded into a continuous phase including a polymer matrix. Non-porous silica particles[15], carbon molecular sieves[16], fullerenes[17], zeolites[18], and carbon nano-tubes[19] have been used as filler particles in polymers to make MMMs. Recently, metal-organic frameworks (MOF) have been recognized as a new member of nanoporous materials. MOFs are crystalline materials consist of metal complexes with organic linkers, and they have well-defined pores and large surface areas (>3000m^2/g)[20]. MOFs have attracted attention especially for their exceptional potential in gas storage and gas separation applications due to their unique properties in terms of low density, high porosity and high surface areas[21]. MOFs have been also used as membranes, catalysis, and biomedical imaging devices[22]. Various types of MOFs can be synthesized by altering the combination of different organic linkers and metal-ions[23]. This tailorability makes MOFs promising candidates for separation applications compared to zeolites and other inorganic fillers and thousands of MOFs have been synthesized to date[24-26].

Incorporation of MOFs within the polymers to obtain high performance MMMs has started recently and the preliminary results revealed that MOF-based MMMs show better performance than pure polymers. The selection of appropriate MOF/polymer pairs is very important for experimental efforts to heighten the performance of MMMs. However, choosing the appropriate MOF as filler particles in MMM is challenging due to the high number of existing MOF materials. Therefore, theoretical models play a critical role in predicting the best performing polymer/MOF combinations prior to experimental efforts.

In this study, the challenge of selecting MOFs as filler particles in high-performance MMMs was examined using atomically detailed simulations and continuum modeling. Theoretical predictions were compared with the available experimental data. After validation of theoretical models, the performance of new MOF-based membranes

composed of different MOFs and different polymers was predicted for the separation of CO_2/CH_4 and H_2/CH_4 gas mixtures. The results obtained in this thesis show that selecting the proper MOF as filler particles in polymers can significantly enhance the performance of membranes by increasing both selectivity and permeability relative to pure polymer membranes.

Chapter 2 reviews the background of mixed matrix membranes and chapter 3 presents the computational methodology that was used in this thesis to predict gas separation performance of MOF-based MMMs. In chapter 4, the predictions of the theoretical permeation models were compared with the results that were obtained from experimental measurements. Chapter 5 demonstrates theoretical predictions for new MOF-based MMMs for CO_2/CH_4 and H_2/CH_4 separations, and the methodologies for selecting appropriate MOF/polymer pairs were presented. Finally, Chapter 6 concludes the results obtained in this thesis.

Chapter 2

LITERATURE REVIEW

This chapter reviews the background of mixed matrix membranes, their opportunities and challenges for gas separations.

2.1 Mixed Matrix Membranes (MMM)

MMMs offer the high selectivity of inorganic membranes and high permeability of polymer membranes. MMMs provide higher selectivity, permeability or both compared to pure polymer-based membranes. In addition, brittleness problem in the inorganic membranes can be tackled by using flexible polymers.

Fabrication of MMMs can be a difficult process if there is a poor contact and poor distribution of the inorganic fillers (dispersed phase) in the polymer phase. In addition, selecting the polymer and filler types, and controlling the particle size distribution and loading in polymers are challenging[27]. The weak contact between polymer and fillers contributes “sieve-in a cage” morphology[28] where an interfacial layer occurs. To maintain membrane separation performance and eliminate the poor contact between inorganic fillers and the polymer phase, manufacturing process requires additional steps such as using a plasticizer or silane coupling agents and melt processing.

MMMs are generally manufactured by the following steps: preparing a polymer and dispersed phase solutions, mixing these solutions. To prevent the formation of interfacial layer, silane coupling agents can be attached in the former step where filler solution is

prepared by using ultrasonic horn on a roll mill. The solution containing polymer and desired fillers is sealed with a septum and an inert purge flow is applied to the solution. The solution is heated until all the solvent is evaporated and dry polymer-filler mass is left in a flask. After cooling, the solvent that is used for film formation such as tetrahydrofuran is added into the flask and stirred. The prepared polymer-filler mass dissolves into this solvent and the films are casted on a glass surface at approximately 180°C-200°C in a vacuum oven with an inert purge. Each film is then annealed under vacuum and finally samples are cooled[29].

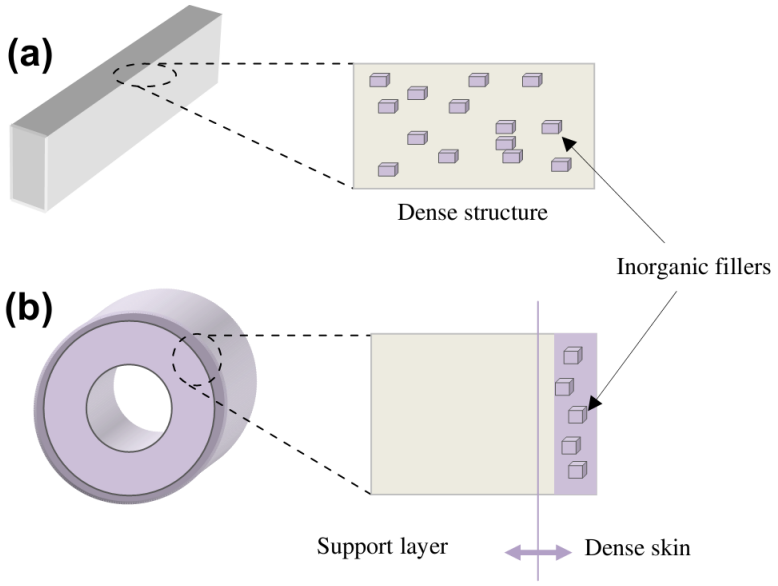

Figure 2.1: Mixed Matrix Membrane Configurations: (a) symmetric flat dense, (b) asymmetric hollow fiber [4]

Inorganic fillers are embedded into a polymer matrix forming either symmetric flat dense or asymmetric hollow fiber structures as it can be seen in Figure 2.1[4]. Negligible resistance for gas flow is provided by using a porous ceramic support where solution deposition occurs to obtain flat MMMs[3]. Hollow fiber MMMs are made by spinning method[30]. For industrial applications, hollow fiber membranes are preferred compared to flat dense MMMs due to their large gas transfer area per unit volume.

2.1.1 Zeolite-based Mixed Matrix Membranes

Zeolites have been comprehensively studied in MMM preparation due to their strong size-sieving ability. The first MMM for gas separation application was reported in 1970s by Paul and Kemp[31]. They investigated diffusion time lag for CO_2 and CH_4 molecules and implemented highly adsorptive molecular sieve 5A zeolite into polydimethyl siloxane (PDMS).Their experimental study revealed that diffusion time lag increased with the addition of zeolite particles into rubbery polymer due to the adsorption of gas molecules into zeolite.

Kulprathipanja et.al[32] in 1988 presented the first MMM that has high O_2/N_2 separation performance by incorporating silicalite (a particular zeolite) into polymer cellulose acetate (CA). The selectivity of O_2 was increased from 3.0 to 4.3 with the addition of silicalite particles into CA[32]. In another study, Mahajan and Koros[33] investigated zeolite 4A as inorganic fillers and they reported that zeolite 4A is more effective for O_2/N_2 separation compared to other zeolites since its pore size is 3.8 Å between the pore sizes of O_2 (3.75 Å) and N_2 (4.07 Å). They highlighted that addition of zeolite 4A into Matrimid polyimide enhances the performance of MMM for O_2/N_2 separation. (Figure 2.2) The MMM performance of SAPO-34 (silicoalumino-phosphate molecular sieve) for CO_2/N_2, H_2/CO_2 and CO_2/CH_4 separation has been investigated in

several studies and selectivity enhancements have been observed compared to pure Matrimid[34-35].

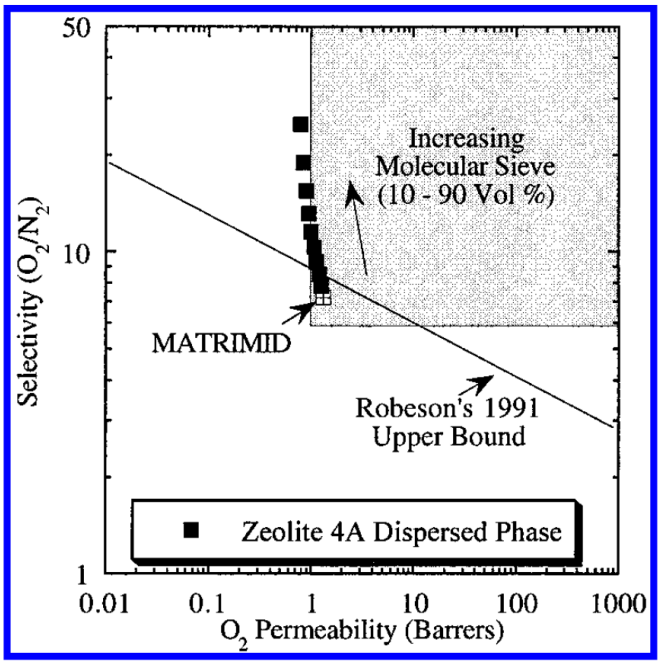

Figure 2.2: Performance of zeolite 4A- PI MMM for O_2/N_2 separation [33]

The main challenge in making zeolite-based MMMs is the poor contact between hydrophilic surfaces of zeolites and hydrophobic surfaces of polymers[36]. This poor contact causes "sieve-in-a-cage" morphology that affects the penetration of the gas molecules and decreases selectivity. In order to eliminate this void formation, coupling agents such as γ-aminopropyl-triethoxy silane,N-β-(amino-ethyl)-γ-aminopropyltrimethoxy silane, γ-glycidyloxy-pro-pyltrimethoxy silane and γ-aminopropyl-dimethylethoxy silane have been used to improve the adhesion at the interface[37]. Khan and co-workers[38] used amino-propyltrimethoxysilane as coupling agent to obtain good contact between

polysulfone (PSf) and zeolite 3A particles as can be seen in Figure 2.3. Gas selectivity for H_2/CO_2 mixture was increased from 1.53 (pure poly-sulfone) to 3.57 when the zeolite loading is 40%.

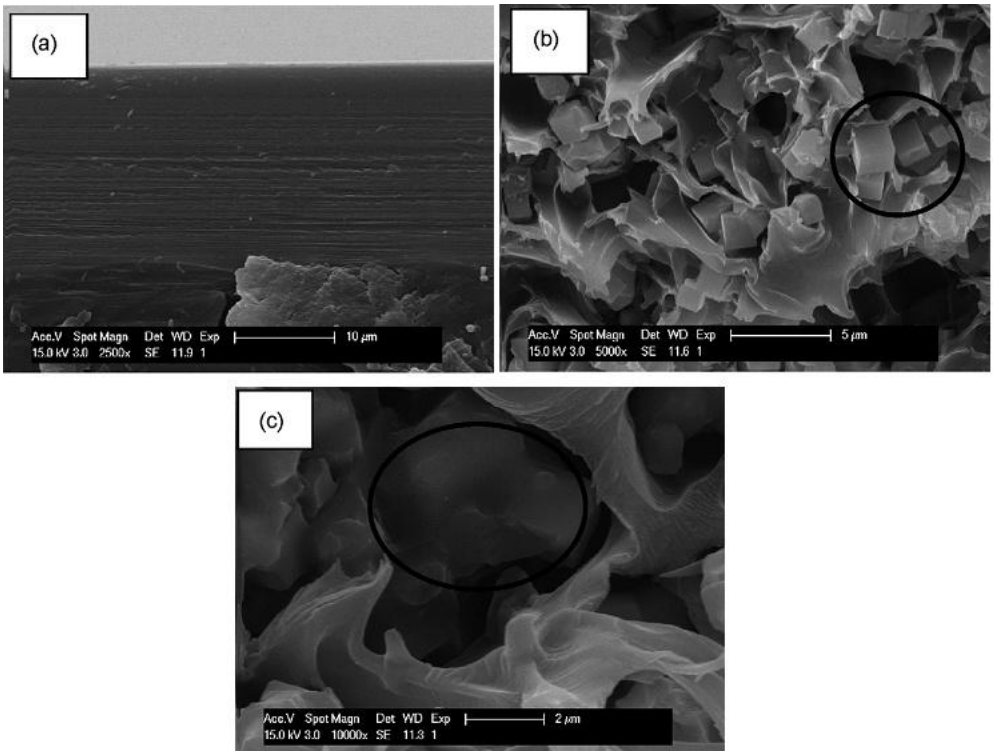

Figure 2.3: (a) pure PSf, (b) PSf-zeolite3A MMM, (c) PSf-coupling agent-zeolite 3A MMM [38]

One critical issue for zeolite-based MMM is the inconvenience for large scale industrial implementation due to limited chemical tailorability of zeolites[14]. Therefore, alternative fillers have been investigated to overcome these challenges.

2.1.2 Metal-Organic Framework-based Mixed Matrix Membranes

Recently, as an alternative to zeolites, metal-organic frameworks (MOFs) have attracted great attention for gas separation applications due to their excellent properties, such as large surface area and their well-defined pores. Their pore sizes can be adjustable and this makes them promising candidates compared to zeolites. In addition, synthesis of MOF-based MMM does not need high temperature and pressure conditions. Thus, fabrication of MOF-based MMMs requires less energy than zeolite-based MMMs. Moreover, structure directing agents are not required since calcination step is not required for MOF-based MMMs compared to zeolite-based MMMs[14]. During synthesis of zeolite-based MMMs, structure directing agents are used as templates for the formation of zeolite crystal structure. To separate this template from the zeolite membrane, calcinations step is applied. Thus, an open pore structure is obtained. Removing the template from the structure may cause micro-crack formation due to the thermal stress in the calcinations step. In addition, the lattice parameters of zeolites can change. Hence, MOF-based MMMs offer less expensive and energy intensive synthesis conditions compared to zeolite-based MMMs[39].

The history of metal-organic frameworks (MOFs) dates back to 1965 when Tomic[40] prepared a polymer solution composed of 3 ligands and selected metal-ions such as Zn, Ni, Al and Fe^{+3}. Today, the group of Yaghi[41] has synthesized numerous types of MOFs. MOFs are robust materials and they composed of metal ligand complexes that are connected with organic linkers. Coordination bonding occurs between the metal and organic linker in the MOF structure. This bond is kinetically weaker than covalent or covalent/ionic bonding[14].

Numerous types of MOFs can be fabricated by using different types of metal-ions and organic linkers. Thus, pore sizes of MOFs can be adjustable. Figure 2.4 demonstrates different type of IRMOFs that were synthesized by Yaghi and co-workers[41]. This figure

presents the tailorability of MOFs. IRMOFs have the same framework topology (octahedral Zn-O-C clusters that exhibits a cubic structure). Their pore sizes are arranged to be between 3.8 and 28.8 Å by using different organic linkers. Eddaoudi[42] and co-workers showed that changing linker type yields IRMOFs that have different free volume, crystal density and pore volume. Figure 2.5 shows the widely studied MOFs, MOF-5 and HKUST-1 in the literature. MOF-5 is also known as IRMOF-1 and it is constructed from octahedral Zn-O-C clusters that give three-dimensional cubic geometry.

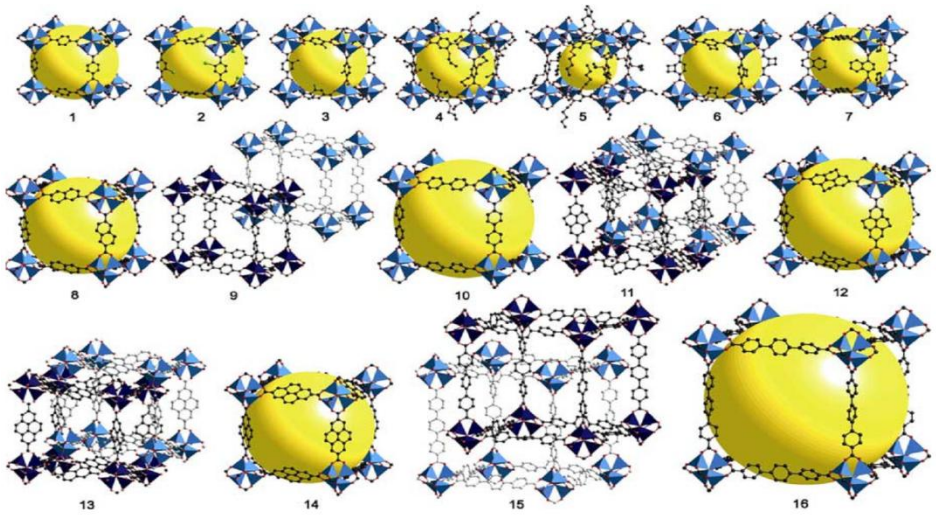

Figure 2.4: Series of isoreticular metal–organic frameworks (IRMOFs) [41]

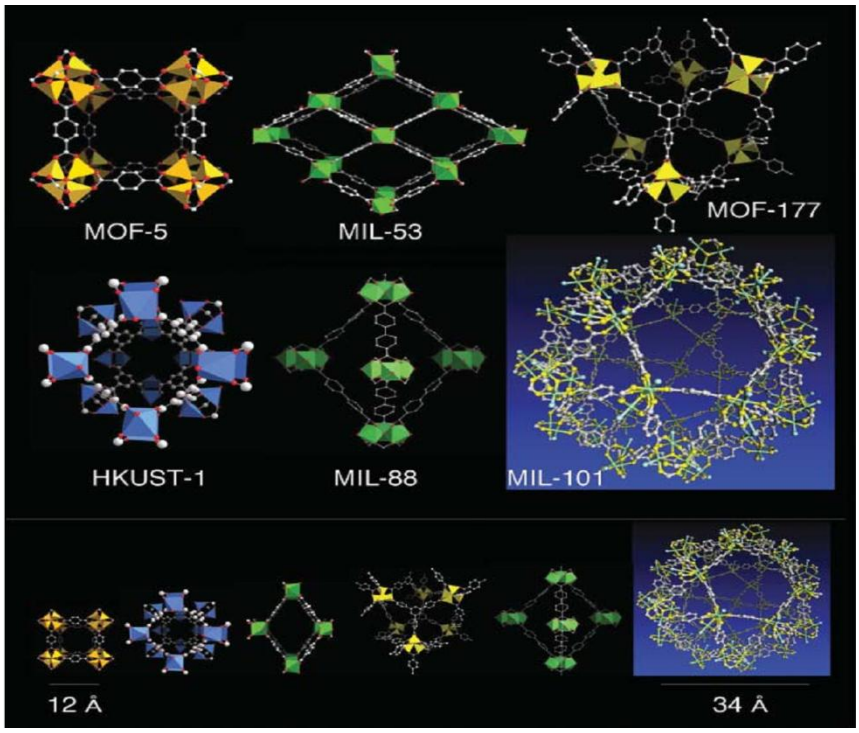

Figure 2.5: The widely studied MOFs and their cages and pore sizes [43]

HKUST-1 is also known as CuBTC which is constructed from Cu and benzene-1,3,5-tricarboxylate. Its structure is also cubic and it has main channels of a square cross-section of ca. 9 Å diameter and tetrahedral side pockets of ca. 5 Å, that are connected to the main channels by triangular windows of ca. 3.5 Å diameter[43].

Preparation of MOF-based MMMs in a lab-scale production consists of the following steps: dispersion of the MOF fillers in the solvent in an ultrasonic bath, addition of polymer by mixing a homogeneous solution and casting for thin film formation as shown in Figure 2.6[44]. Combination of homogenous inorganic particles and polymer solution can also be implemented in different ways: polymer is firstly dissolved in a solvent and then MOF

fillers can be added into polymer solution[45] or filler particles and polymers are dissolved in solvents separately and then particle solution is added to polymer solution[46]. After sonication and stirring, the membranes are cast on a flat surface where all the solvent is evaporated. When the membranes are dried at room temperature, films are embedded in a vacuum oven to remove the retaining solvent.

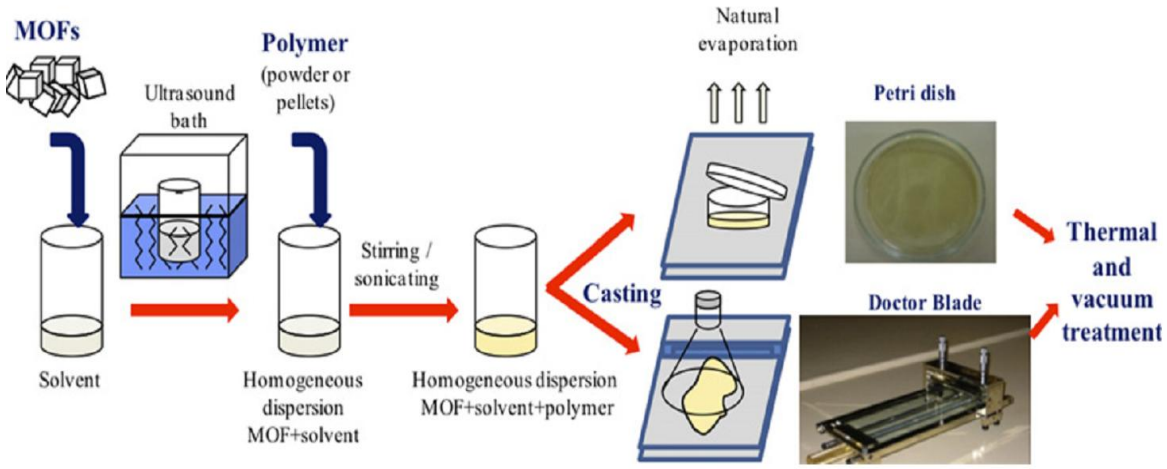

Figure 2.6: General procedure for the preparation of MOF-based MMM [44]

Determining the optimum MOF filler loading which gives high selectivity for a gas separation is very important for the effective preparation of MMMs since after a certain loading, particle agglomeration may be occurred and poor contact between the polymer matrix and fillers may be observed[47]. Figure 2.7 demonstrates the effect of loading on MMM's selectivity and permeability. MMM performance reaches an optimum value at a certain loading due to good dispersion of the fillers, but after optimum loading of fillers, agglomeration may occur since polymer chains are disrupted by the addition of excessive loading of fillers as can be seen in Figure 2.7.

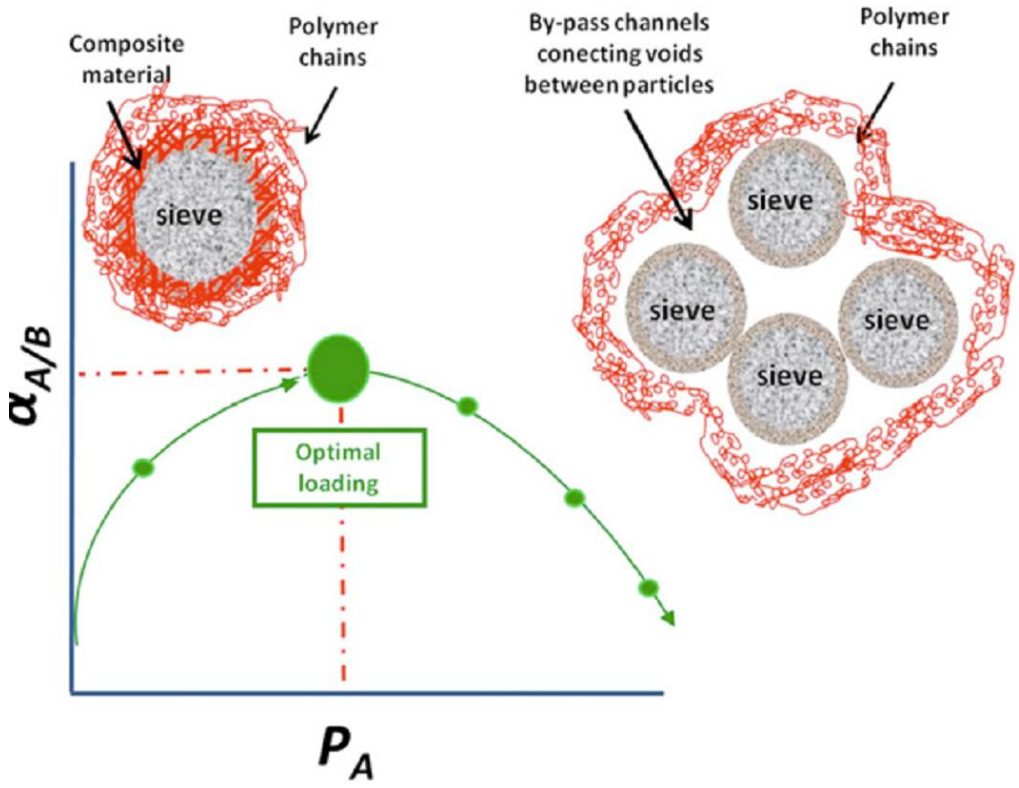

Figure 2.7: Relation between loading and separation performance [44]

Recently, MOF-based MMMs have been synthesized and their performances have been reported. Yehia and co-workers[48] synthesized the first MOF-based MMM containing copper (II) biphenyl dicarboxylate triethylenediamine in poly (3-acetoxyethylthiophene) and they observed an enhanced CH_4 selectivity relative to the pure polymer at 20 and 30 wt% of MOF loading. However, both CO_2 permeability and CO_2/CH_4 selectivity decreased. Car et al.[49] synthesized MOF-based MMMs with CuBTC and $Mn(HCOO)_2$ and the polymers poly-dimethylsiloxane (PDMS) and polysulfone (PSF) for separation of CO_2 from N_2 and CH_4. They presented that H_2 permeability and H_2/CH_4 selectivity of MMMs

was improved compared to pure polymers. However, they also reported minor improvements in ideal selectivity for CO_2 over N_2 and CH_4. The low improvement in selectivity can be associated with the leaky interface morphology as discussed by Basu et al[50]. Another study of Zhang et al.[51] showed that incorporation of Cu-BPY-HFS into Matrimid polymer enhances the separation performance of CO_2/CH_4, H_2/CO_2 and CH_4/N_2 mixtures. They claimed that Cu-BPY-HFS has the affinity towards CH_4. Hu et al.[52] incorporated CuBTC into polyimide and they showed that both H_2 permeance and selectivity increased compared to those of pure polyimide. Basu et al.[53] also studied with CuBTC/Matrimid and CuBTC/Matrimid/PSF membranes and they reported that both selectivity and permeance of CO_2 increased in CO_2/CH_4 and CO_2/N_2 gas mixtures. Perez et al.[54] reported IRMOF-1/Matrimid MMM and they observed enhancements in permeability of H_2, O_2, CO_2, N_2 and CH_4 gas pairs with very slight improvement in selectivity. In another study, Adams et al.[55] synthesized CuTPA/polyvinyl acetate MMM and reported improvements in both CO_2 permeability and ideal selectivity compared to pure polymer.

Zeolitic imidazolate frameworks (ZIFs) which are a subclass of MOFs have been also used as filler particles in MMMs. Yang et al.[56] synthesized (ZIF-7)/polybenzimidazole (PBI) MMMs and reported that H_2 permeability and selectivity of H_2/CO_2 were improved. Diaz and co-workers [57] studied ZIF-8/pristine poly(1,4-phenylene ether-ether-sulfone) membrane and they investigated CO_2 transport by using pulse field gradient NMR techniques. Liu et al.[58] and Zhang et al.[59] also used ZIF-8 fillers in fabrication of MMMs. Bae and coworkers[60] fabricated ZIF-90 based MMMs by using Ultem, Matrimid and 6FDA-DAM polyimide polymers and they measured both pure and mixture gas permeation of CO_2 and CH_4. They revealed that ZIF-90/6FDA-DAM MMMs can be good candidates for CO_2/CH_4 and CO_2/N_2 separation.

These recent studies present that MOF-based MMMs can show very high performances in gas separations. However, there are numerous MOFs that have been synthesized up to date, and even if one MOF is considered, there are hundreds of MOFs to be used as fillers. For this reason, theoretical models that can screen MOFs and identify the most promising ones for MMM applications are required. In this thesis, it is aimed to screen MOFs and model the gas permeance of MOF-based MMMs to identify the most promising MOF-polymer candidates for gas separation applications by using molecular simulations. The methodology presented in this thesis will play a critical role for design and development of MOF-based MMMs prior to experiments.

Chapter 3

COMPUTATIONAL METHODS

This chapter gives information about the computational methodology to predict gas separation performances of MOF-based MMMs. Grand Canonical Monte Carlo (GCMC) and Equilibrium Molecular Dynamics (EMD) simulation methods will be introduced to estimate equilibrium adsorption of gas molecules (adsorbates) and their diffusion coefficients, and then theoretical gas permeation models for MMMs will be described.

3.1 Predicting Gas Permeabilities through MOFs using Atomistic Simulations

Molecular simulation methods are helpful tools to screen existing and hypothetical MOFs at the atomistic scale. In this thesis, atomically detailed simulations were used to calculate gas permeation through MOFs. MOF structures were taken from Cambridge Structure Database (CSD) which includes all experimentally reported MOF structures.

To determine the separation performance of MOF-based MMMs, we have to known gas permeability values for both pure MOFs and pure polymers. The aim of this study is to estimate gas permeability through MOFs to evaluate the performance of new MOF-based MMMs. Grand-canonical Monte Carlo (GCMC) simulations were initially used to compute single component adsorption data of gas molecules. Equilibrium Molecular Dynamics (EMD) simulations were then applied to evaluate the corrected diffusivities (D_0) which are loading-dependent. The transport diffusivity (D_t) is then calculated by using the corrected diffusivity (D_o) and the thermodynamic correction factor[61], where the latter is a partial

derivative relating the adsorbate concentration, *c*, and bulk phase fugacity, *f*. Thermodynamic correction factor was defined after determining single component adsorption isotherms of each gas molecules by GCMC simulations.

$$D_t(c) = D_o(c) \cdot \frac{\partial \ln f}{\partial \ln c}. \tag{3.1}$$

After GCMC and EMD simulations, steady state fluxes (J) of each gas molecules through a MOF were calculated using shell model which estimates the diffusivities at the mean adsorbate loading based on Fick's law: [61]

$$J = -D_t(c) \cdot \nabla c \tag{3.2}$$

In this equation, ∇c is the concentration gradient of the adsorbed species based on the difference between the feed and permeate side pressures of the membrane and membrane thickness, $\nabla c = \left(c^{permeate} - c^{feed}\right)/L$ [61-62]. The gas flux in MOFs is then converted to permeability, *P* using Equation (3.3) based on the pressure drop (Δp), and membrane thickness, *L*[63].

$$P = \frac{J}{\Delta p / L}. \tag{3.3}$$

The ideal selectivity for a gas pair is defined as the ratio of permeabilities of two competing gas components (1 and 2) by using the following equation:

$$S_{1/2} = \frac{P_1}{P_2} \tag{3.4}$$

Figure 3.1 presents the computational methodology used in this study. After predicting gas permeability through MOFs, the permeability of MOF-based MMMs was estimated using permeation models. The only experimental data that were included from literature in

this study is the permeability of pure polymers for each gas species. Combining gas permeability in pure polymer and pure MOF, the performance of MOF-based MMMs was estimated using theoretical permeation models.

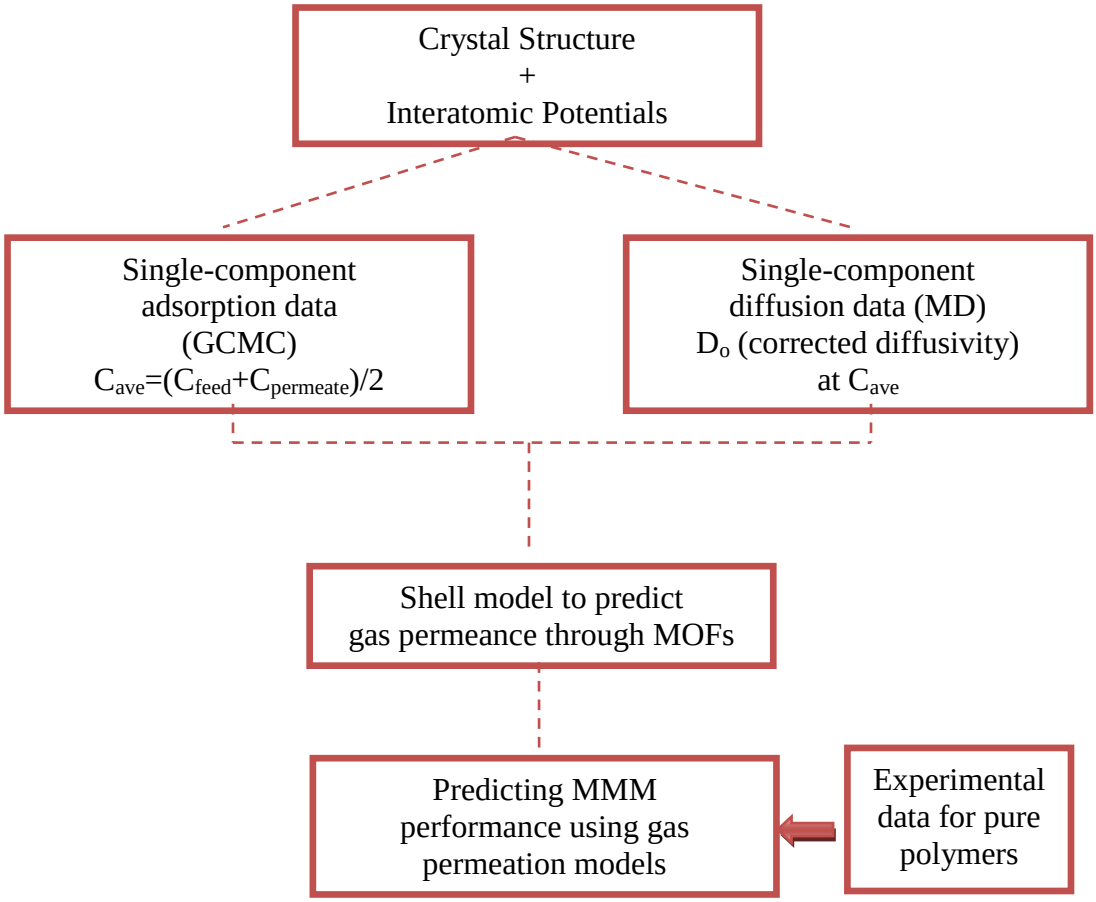

Figure 3.1: The methodology for predicting gas permeabilities through MOF-based MMMs

GCMC and EMD simulations were performed for all MOFs at room temperature (25°C) and at a feed (permeate) pressure of 2 bar (vacuum) to validate the computational results with those obtained from experimental data of MOF-based MMMs.

In simulations, models for the adsorbent (MOF structure) and the adsorbates (gas molecules such as CO_2, H_2 and CH_4) were used to compute the energetic interactions between two atoms. To describe these models, force fields are used. A force field describes the potential energy by using a set of parameters based on the interactions between atoms. The framework structures of MOFs were obtained from x-ray crystallography. The structures of MOFs were assumed to be rigid in this study. Only intermolecular interactions which consist of van der Waals and Coulomb interactions between non-bonded atoms were described. To simulate bulk phases, periodic boundary conditions were used to mimic infinite structure. By using periodic boundary conditions, simulation cells were replicated identically to avoid surface effects[64].

Lennard-Jones (LJ) 12-6 potentials were used to model repulsion and dispersion forces, and charge interactions were taken into account by using the Coulomb potential. The Lennard-Jones potential describes attractive van der Waals interactions and repulsion at short distances between nonbonded pair atoms. The Lennard-Jones potential is defined by the following formula[65]:

$$V_{LJ}(r_{ij}) = 4\varepsilon_{ij}\left[\left(\frac{\sigma_{ij}}{r_{ij}}\right)^{12} - \left(\frac{\sigma_{ij}}{r_{ij}}\right)^{6}\right] \tag{3.5}$$

Here, r is the distance between two particles (i and j). The term r^6 presents the attractive long-range forces, and the term r^{12} shows the repulsive forces, ε is a energy parameter which shows the depth of the potential well, σ is a size parameter at which the inter-particle potential is zero. To save the computational time, the long-range interactions which present the interactions between far away atoms were ignored by using a cut off radius in LJ 12-6 potentials. The potential, V_{LJ} was truncated at a distance $r = r_c$ (cut-off radius), and the simulations were performed at this distance (13 Å).

Charge interactions were considered using Coulomb potential for polar gas molecules such as CO_2. The Coulomb potential is defined by the following formula[66]:

$$V_C(r_{ij}) = \frac{q_i q_j}{4\pi\varepsilon_0 r_{ij}^2} \tag{3.6}$$

Here, q_i and q_j show the charges for i and j atoms, r_{ij} presents the separation between i and j atoms and ε_0 is the electric constant (the electrical permittivity of space).

The Coulomb potential does not only describe the polarity of gas molecules, it also takes into account the electric field generated by the framework atoms. Quantum mechanical calculations are commonly used to compute the partial charges for framework atoms. In simulations, connectivity-based atom contribution (CBAC) method was used to determine partial charges of MOFs[67]. This approximate method was developed to provide a helpful and quick source for partial charges of atoms. CBAC method assumes that the atoms with same connectivity have the same charges in different MOFs. This method has been applied in earlier studies and the charges obtained from CBAC method compared with the charges obtained from quantum mechanical calculations for adsorption isotherms of CO_2[67-68]. The atomic charges defined by CBAC method are presented in Figure 3.2. The potential, V_C was truncated at r_c and the CO_2 simulations were performed at 25 Å.

The Lorentz-Berthelot mixing rules were employed to calculate adsorbent-adsorbate and adsorbate-adsorbate LJ cross interaction parameters. Simulations at the lowest fugacity were started from an empty MOF matrix. Each simulation at higher fugacity was started from the final configuration of the previous run. Simulations consisted of a total of $3\text{x}10^7$ trial configurations which consist of $1.5\text{x}10^7$ cycles for the equilibration and $1.5\text{x}10^7$ cycles for the production step. Corrected diffusivities of single component gases in MOFs were calculated by performing 20 independent EMD simulations. Periodic boundary conditions were applied in all simulations. The size of the simulation box was set to 2x2x2 crystal unit cells.

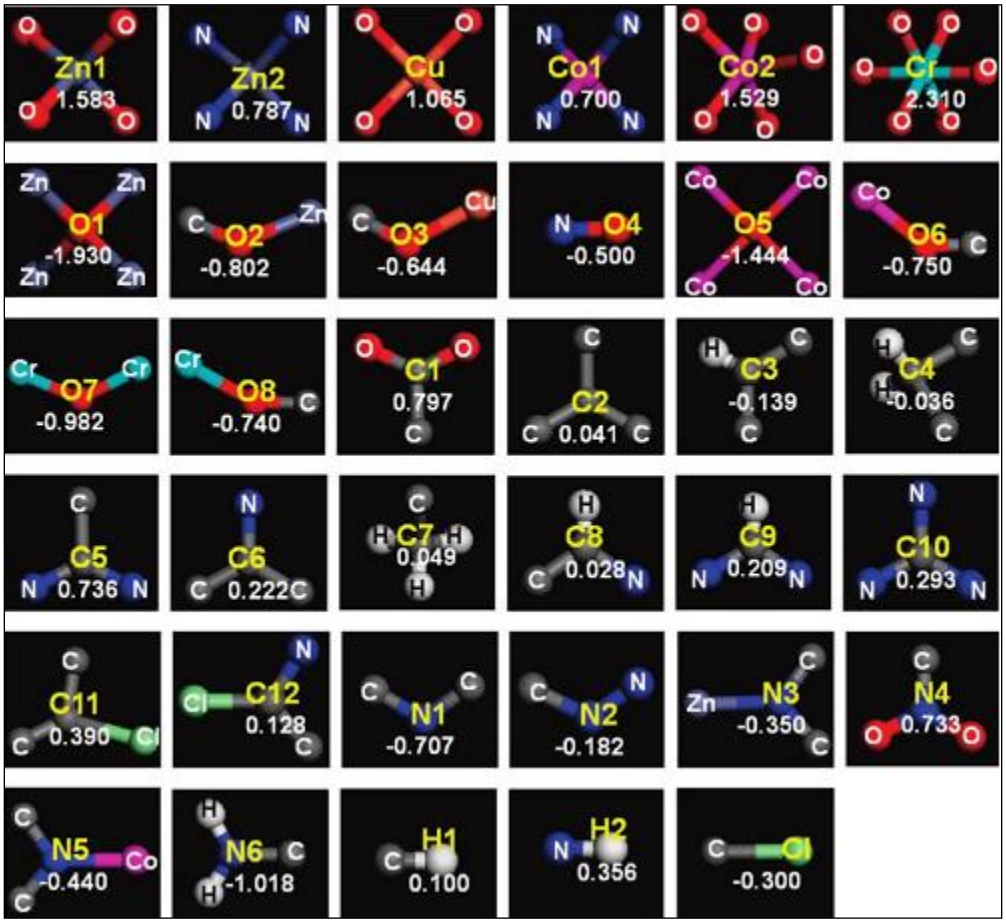

Figure 3.2: The atomic charges defined by CBAC method [67]

Spherical Lennard-Jones (LJ) 12-6 potentials were used to model adsorbate molecules, H_2 and CH_4[69-70]. H_2 and CH_4 are represented by a single sphere without charges. The Buch potential[71] was used to model H_2-H_2 interactions. To describe adsorbate-adsorbate interaction of CH_4, TraPPE force field[72] was used. The LJ potentials parameters defined by TraPPE force field was developed from the experimental vapor-liquid equilibrium data[72]. CO_2 was modeled as a three site linear molecule with three charged LJ interaction

sites located at each atom. The potential parameters were again taken from TraPPE force field developed by Potoff and Siepmann[73]. The interaction parameters are listed in Table 3.1.

Table 3.1: Interaction potential parameters for adsorbate atoms

Adsorbates	ε/*k* (K)	σ(Å)	q(e)
CH_4	148.20	3.73	-
H_2	34.20	2.96	-
$C(CO_2)$	27.00	2.80	0.70
$O(CO_2)$	79.00	3.05	-0.35

For the framework atoms in MOFs, the LJ parameters were taken from Universal force field (UFF)[74] and Dreiding[75]. UFF[74] parameters were defined based on the elements' hybridization and connectivity. Dreiding[75] force field parameters were developed for crystal structures of organic compounds. These force fields have been applied in molecular simulation studies of MOFs, and gas adsorption results obtained from (UFF)[74] and Dreiding[75] were compared with the results obtained from experimental measurements of gas adsorption, and a good agreement between simulations and experiments was found as will be shown in the next chapter[76].

3.1.1 Molecular Simulation of Adsorption

GCMC simulations have been widely used to compute adsorption isotherms. Experimental studies assume that chemical potential and the temperature inside the adsorbent is the same as that of outside of the adsorbent. Chemical potential is exactly known for ideal-gases, but for non-ideal gases, the knowledge of equation of state is required. To be consistent with experimental measurements, chemical potential, the volume and the temperature are kept constant, and the number of molecules at equilibrium is determined in GCMC simulations. During the simulation, the number of particles is

fluctuated, and adsorption isotherms are predicted by increasing pressure. Simulations consist of the random movements: particle addition, deletion and displacement which are rejected or accepted according to Boltzmann-type weighting [64].

3.1.2 Molecular Simulation of Diffusion

Diffusion is the molecular motion of the particles. Equilibrium Molecular Dynamics (EMD) simulation was used to calculate corrected diffusivity (D_0) which present the collective motion of the adsorbed molecules.

$$D_{o,i} = \lim_{t\to\infty} \frac{1}{6Nt} \left\langle \left(\sum_{l=1}^{N_i} \left[r_{il}(t) - r_{il}(0) \right] \right)^2 \right\rangle \tag{3.7}$$

Here, N is the number of the molecules, r_{il} (t) is the three dimensional position vector of molecule l of species i at time t and the angular brackets shows the ensemble average.

In EMD simulations, firstly initial velocities are randomly assigned to each particle according to Maxwell-Boltzmann distribution. The forces on the particles are then computed, and Newton's equation of motion using Verlet algorithm is integrated. Consequently, the average of measured quantities is recorded[77]. In this study, firstly GCMC simulations were used to initialize the system and then EMD simulations were performed. At NVT ensemble (constant number of particles, volume and temperature) the temperature is controlled by Nosé-Hoover thermostat[78].

3.2 Gas Permeation Models for MMMs

In this thesis, seven different permeation models were used to predict the permeation of gas species through MOFs. These models are: Maxwell, modified Maxwell, Bruggeman, Lewis-Nielson, Pal, Felske and modified Felske. Experimental data of gas selectivity and permeability of polymers were implemented into these models, and molecular simulations were performed for the prediction of gas permeabilities of MOFs.

The permeation models are categorized into two parts: models (Maxwell, Bruggeman, Lewis-Nielson, Pal) considering ideal morphology which assumes that dispersed phases are embedded into polymer matrix perfectly and there is no rigidification on matrix chain layer around the dispersed particles, and models (modified Maxwell, Felske and modified Felske) considering non-ideal morphology which considers interphase morphologies including interface voids and polymer rigidification around particles[79-80].

Maxwell model[81] is commonly used to predict gas permeability through MMMs:

$$P_r = \frac{P}{P_m} = \left[\frac{2(1-\phi) + (1+2\phi)\lambda_{dm}}{(2+\phi) + (1-\phi)\lambda_{dm}} \right] \tag{3.8}$$

In this model, λ_{dm} is the permeability ratio (P_d/P_m), P_d is the permeability of dispersed phase, P_m is the permeability of continuous phase, P_r is the relative permeability, P is the permeability in MOF/polymer MMM and ϕ is the volume fraction of MOF particles. Maxwell model is valid for low to moderate values of volume fractions ($0<\phi<0.2$) since it assumes that nearby particles do not affect the streamlines around particles. This model does not consider packing limit of particles, the effect of particle size distribution, particle shape and aggregation of particles. Bruggeman model[82] is valid for a broader range of ϕ compared to Maxwell model, however it has the same limitations with Maxwell model:

$$P_r^{(1/3)} \left[\frac{\lambda_{dm} - 1}{\lambda_{dm} - P_r} \right] = (1-\phi)^{-1} \tag{3.9}$$

Lewis-Nielson model[83] has a broad range of ϕ, ($0<\phi<\phi_m$), where ϕ_m is the maximum packing volume fraction of filler particles and assumed to be 0.64 for random close packing of uniform spheres:[79-80, 84]

$$P_r = \frac{P}{P_m} = \left[\frac{1 + 2((\lambda_{dm} - 1)/(\lambda_{dm} + 2))\phi}{1 - ((\lambda_{dm} - 1)/(\lambda_{dm} + 2))\phi\varphi} \right] \tag{3.10}$$

$$\varphi = 1 + \left[\frac{(1-\phi_m)}{(\phi_m)^2} \right] \phi \tag{3.11}$$

Lewis-Nielson model includes morphology effects on permeability since ϕ_m is related to particle size distribution, particle shape and aggregation of particles. The model reduces to Maxwell model when ϕ_m goes to 1. Pal model[85] also considers the effect of particle size distribution, particle shape and aggregation of particles. This model reduces to Bruggeman model when ϕ_m goes to 1:

$$P_r^{(1/3)} \left[\frac{\lambda_{dm} - 1}{\lambda_{dm} - P_r} \right] = \left(1 - \frac{\phi}{\phi_m} \right)^{-\phi_m} \tag{3.12}$$

Modified Maxwell model is based on the two-phase description, the polymer matrix is one phase, the dispersed particles (insert)-interface is the other phase, pseudo-insert phase[86]. This model predicts permeability of gases through pseudo-insert phase by using the following expression:

$$P_{eff} = P_I \left[\frac{2(1-\phi_s) + (1+2\phi_s)(P_d / P_I)}{(2+\phi_s) + (1-\phi_s)(P_d / P_I)} \right] \tag{3.13}$$

where P_{eff} is the effective permeability of the pseudo-insert phase, P_I is the permeability of the interphase, ϕ_s is the volume fraction of the dispersed phase within the pseudo-insert phase. The volume fraction of the dispersed phase can be estimated by using following equation:

$$\phi_s = \frac{\phi_d}{\phi_d + \phi_I} = \frac{{r_d}^3}{(r_d + l_I)^3} \tag{3.14}$$

Here, ϕ_d is the volume fraction of dispersed phase, ϕ_I is the volume fraction of the interphase, r_d is the insert radius, l_I is the interphase thickness. The permeability in MMM can be then estimated by using the following expression:

$$P_r = \frac{P}{P_m} = \left[\frac{2(1-\phi) + (1+2\phi)(P_{eff} / P_m)}{(2+\phi) + (1-\phi)(P_{eff} / P_m)} \right] \tag{3.15}$$

Modified Maxwell model is valid for low to moderate values of filler concentration like Maxwell model. At high values of filler concentration ($\phi \to \phi_m$), significant deviation from actual behavior may be occurred. Modified Maxwell does not take account for the effect of particle size distribution, particle shape and aggregation of particles. Felske model[87] considers the dispersed particles as core and the surrounding interfacial layer (rigidified interfacial layer or voids or particle pore blockage) as shell. This model gives almost the same predictions as the modified Maxwell, and it turns to the Maxwell model when δ = 1, when the interfacial layer is not included:

$$P_r = \frac{P}{P_m} = \left[\frac{2(1-\phi) + (1+2\phi)(\beta / \gamma)}{(2+\phi) + (1-\phi)(\beta / \gamma)} \right] \tag{3.16}$$

$$\begin{aligned} \beta &= (2+\delta^3)\lambda_{dm} - 2(1-\delta^3)\lambda_{\mathrm{lm}} \\ \gamma &= (1+2\delta^3) - (1-\delta^3)\lambda_{dI} \end{aligned} \tag{3.17}$$

Here, δ is the ratio of outer radius of interfacial shell to core radius, ϕ is the volume fraction of core-shell particles, λ_{lm} is the permeability ratio of P_I/P_m and λ_{dI} is the permeability ratio of P_d/P_I. This model is also applicable for low volume fraction of particles.

Modified Felske model was developed to demonstrate permeation behavior in MMMs by considering the morphology and packing factor of particles:

$$P_r = \frac{P}{P_m} = \left[\frac{1 + 2((\beta-\gamma)/(\beta+2\gamma))\phi}{1 - ((\beta-\gamma)/(\beta+2\gamma))\phi\rho} \right] \tag{3.18}$$

This model turns into original Felske model when ϕ_m is equal to 1 and it reduces to Lewis-Nielson model when δ = 1. If both of these parameters are equal to 1, this model gives

Maxwell model. In this thesis, the values of parameters, ϕ_m and δ were obtained from the study of Shimekit et al.[80] as 0.64 and 1.18, respectively for Matrimid/carbon molecular sieve (CMC) MMMs. The parameters were listed in Table 3.2.

Table 3.2: Parameters of the permeation models used for predicting permeability of CH_4 and CO_2 in IRMOF-1/Matrimid MMMs [88]

	ϕ_m	ϕ_s	δ
CH_4	0.64	0.74	1.18
CO_2	0.64	0.92	1.18

Chapter 4

VALIDATION OF MIXED MATRIX MEMBRANE MODELS

This chapter presents the comparison of calculation predictions with the available experimental measurements to identify the best predicting permeation models.

4.1 Comparing predictions of permeation models with experimental data of MOF-based MMMs for CO_2/CH_4 gas separations

The pure gas permeabilities of CO_2 and CH_4 in IRMOF-1/Matrimid and mixed gas permeabilities of CO_2/CH_4:35/65 in CuBTC/Matrimid MMMs were investigated. For IRMOF-1/Matrimid and CuBTC/Matrimid MMMs, molecular simulations were performed at 2 bar and 10 bar, respectively at 35°C. The membrane thickness was used as 35 μm, and the permeate pressure was taken as 10^{-6} bar (evacuated pressure) to mimic experimental measurements.

Perez et al.[54] measured CO_2 and CH_4 permeation through pure Matrimid and IRMOF-1/Matrimid membranes. The structure of IRMOF-1 (MOF-5) which consists of Zn_4O clusters linked by three 1, 4-benzenedicarboxylate molecules was given in Figure 4.1. Its pore size is 11 Å, and it has a cubic three-dimensional structure [54].

In Table 4.1 comparison of experiments[54] and model predictions for pure gas permeabilities (Barrer) of CO_2 and CH_4 in IRMOF-1/Matrimid MMMs was demonstrated.

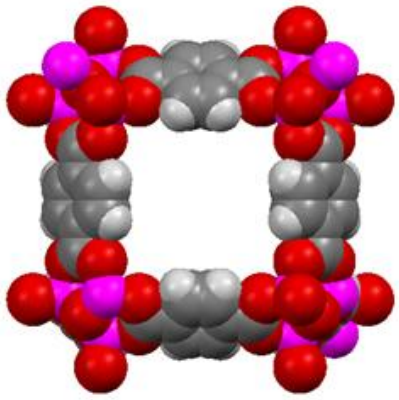

Figure 4.1: The structure of IRMOF-1 in [010] direction, atoms: Zn: violet, O: red, C: gray, H: white

Table 4.1: Comparison of experiments [54] and model predictions for pure gas permeabilities (Barrer) of CO_2 and CH_4 in IRMOF-1/Matrimid MMMs.

Weight % of IRMOF-1	Experiments	Maxwell	Bruggeman	Lewis-Nielson	Pal	Modified Maxwell	Felske	Modified Felske
CO_2								
0	9.00±0.1							
10	11.10±1.4	14.53	15.74	14.99	16.28	13.26	11.44	11.60
20	13.80±2.8	20.02	25.14	22.35	28.66	17.18	13.45	14.04
30	20.20±1.4	25.54	37.74	32.11	50.69	20.83	15.15	16.40
CH_4								
0	0.22±0.02							
10	0.22±0.04	0.36	0.38	0.37	0.40	0.30	0.28	0.28
20	0.34±0.04	0.49	0.61	0.55	0.70	0.37	0.33	0.34
30	0.45±0.06	0.62	0.92	0.79	1.24	0.44	0.37	0.40

As can be seen in Table 4.1, the permeability of both CO_2 and CH_4 in IRMOF-1/Matrimid MMM was increased with the addition of MOF particles. Maxwell, Bruggeman, Lewis-Nielson and Pal models overestimated both CO_2 and CH_4 permeability data compared to the experimental measurements. Figures 4.2 and 4.3 present the comparison of experimental data with the model predictions for permeability of CO_2 (CH_4) in IRMOF-1/Matrimid membranes. For each model, the weight per cent of IRMOF-1 increases from 10% to 30%.

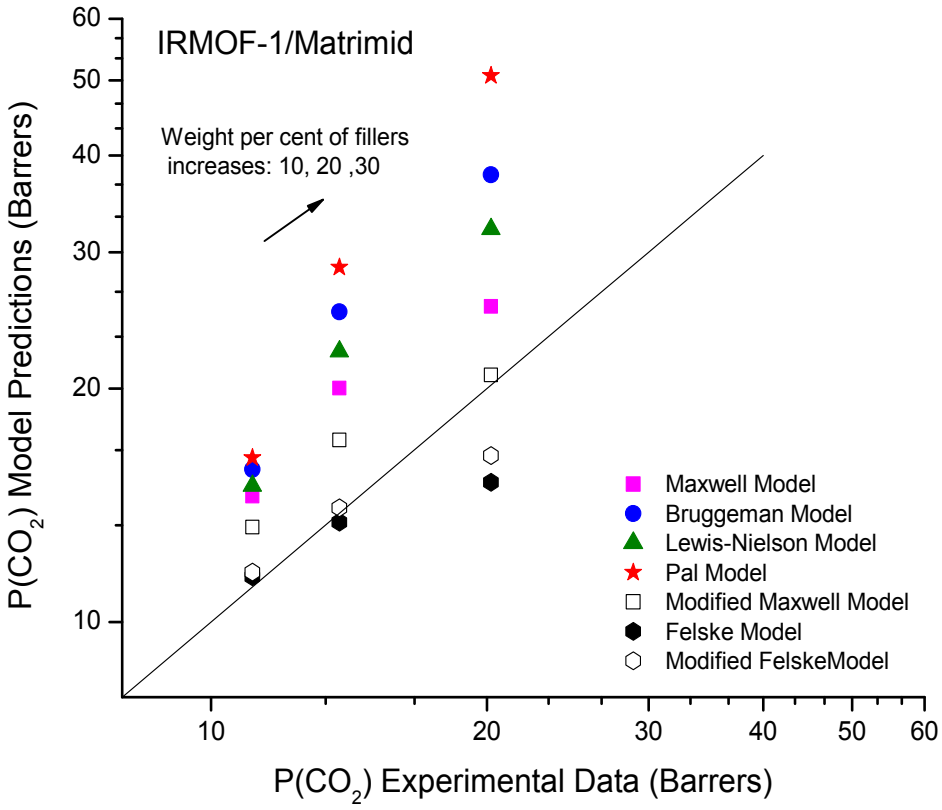

Figure 4.2: Comparison of pure gas permeabilities of CO_2 in IRMOF-1/Matrimid MMMs using different models. Experimental data is taken from Perez et al.[54]

As can be seen in Figures 4.2 and 4.3, the modified Maxwell, Felske and modified Felske models are close to the straight line which shows the good agreement between experiments and molecular simulations.

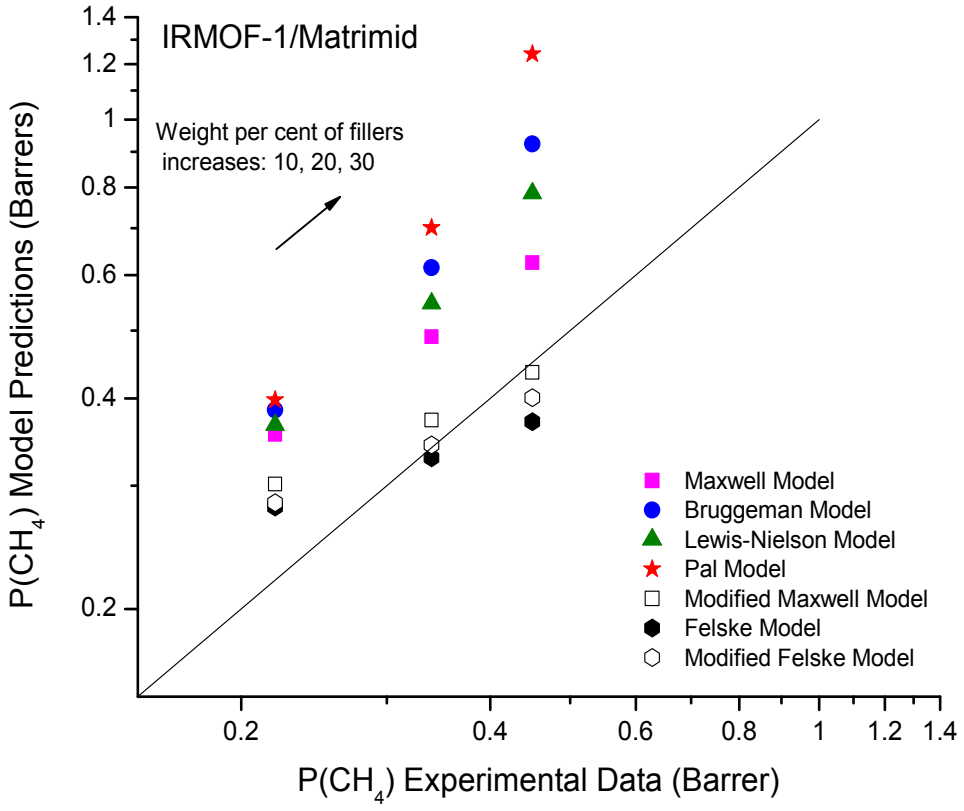

Figure 4.3: Comparison of pure gas permeabilities of CH_4 in IRMOF-1/Matrimid MMMs using different models. Experimental data is taken from Perez et al.[54]

The percentage average absolute relative error (AARE %) values for CO_2 and CH_4 permeation data were also calculated using the following equation:

$$AARE\,\% = \frac{100}{N}\sum_{i=1}^{N}\left|\frac{P_i^{\,cal} - P_i^{\exp}}{P_i^{\exp}}\right| \tag{4.1}$$

In Equation 4.1, $P_i^{\,cal}$ is the permeability which is calculated by models and $P_i^{\exp}$ is the permeability measured by experiments and N is the number of data points. The AARE% values for CO_2 and CH_4 in IRMOF-1/Matrimid membranes are presented in Table 2. The estimated AARE% values of the permeation models were ordered in two groups: For models that consider ideal morphology: Pal model > Bruggeman model > Lewis–Nielsen model > Maxwell model. For models that consider interfacial morphology: modified Maxwell model > Felske model > modified Felske model[88].

Table 4.2: Comparison of AARE% values for CO_2 and CH_4 permeation data in IRMOF-1/Matrimid MMMs

Permeation model	CO_2 AARE%	CH_4 AARE%
Modified Felske	8.37	13.60
Felske	10.20	16.04
Modified Maxwell	15.68	16.64
Maxwell	34.15	48.07
Lewis-Nielson	51.99	67.26
Bruggeman	70.25	86.94
Pal	101.76	120.89

The AARE% results showed that the Modified Felske model is the best predicting model among all models. This model considers both interphase morphology and packing intensity of particles. The Maxwell model is the best predicting model among the models that consider ideal morphology. Based on the results shown in Table 4.2, the modified Felske and the Maxwell model were used for mixed matrix membrane calculations.

Another widely studied MOF, CuBTC (HKUST-1) was also investigated as the dispersed phase in polymers, and the gas permeation in CuBTC based MMMs was compared with the available experimental data of Basu et al[89]. CuBTC has a three dimensional network, and it has 9 Å diameter as main channels and tetrahedral pockets which have 5 Å diameter. They are linked on by triangular windows that have 3.5 Å diameters. The framework structure of CuBTC is presented in Figure 4.4.

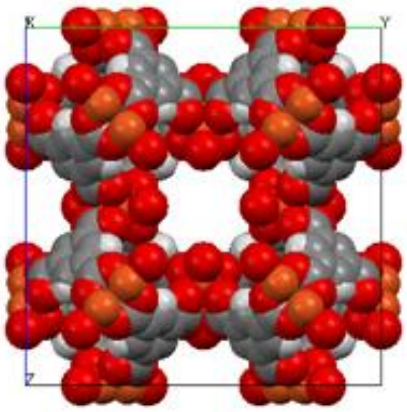

Figure 4.4: The structure of CuBTC in [100] direction, atoms: Cu: orange, O: red, C: gray, H: white

Figure 4.5 shows the mixed gas permeabilities of CO_2/CH_4:35/65 mixture through CuBTC/Matrimid MMMs at 35°C and 10 bar. Simulations for the mixture gas permeation data were compared with the results of the experimental study of Basu et. al[89]. The predictions of Maxwell and modified Felske models were again in a good agreement with the experimental measurements compared to the other models.

Results so far revealed that the Maxwell model exhibits higher permeation values when the volume fraction of dispersed particles increases compared to the modified Felske model since the Maxwell model assumes ideal-morphology and it does not take into account the

effect of interfacial layer. In addition, the term of permeability ratio $\lambda_{dm} = P_d / P_c$ affects the Maxwell equation substantially since the permeability values of dispersed phase (MOFs) are very high compared to the pure polymer phase, and for each calculation this ratio is multiplied with the loading factor ϕ (volume fraction of dispersed phase). Thus, the ratio will increase due to high permeability values of MOFs. On the other hand, this permeability ratio does not take place in the modified Felske model. Hence, it gives lower prediction values.

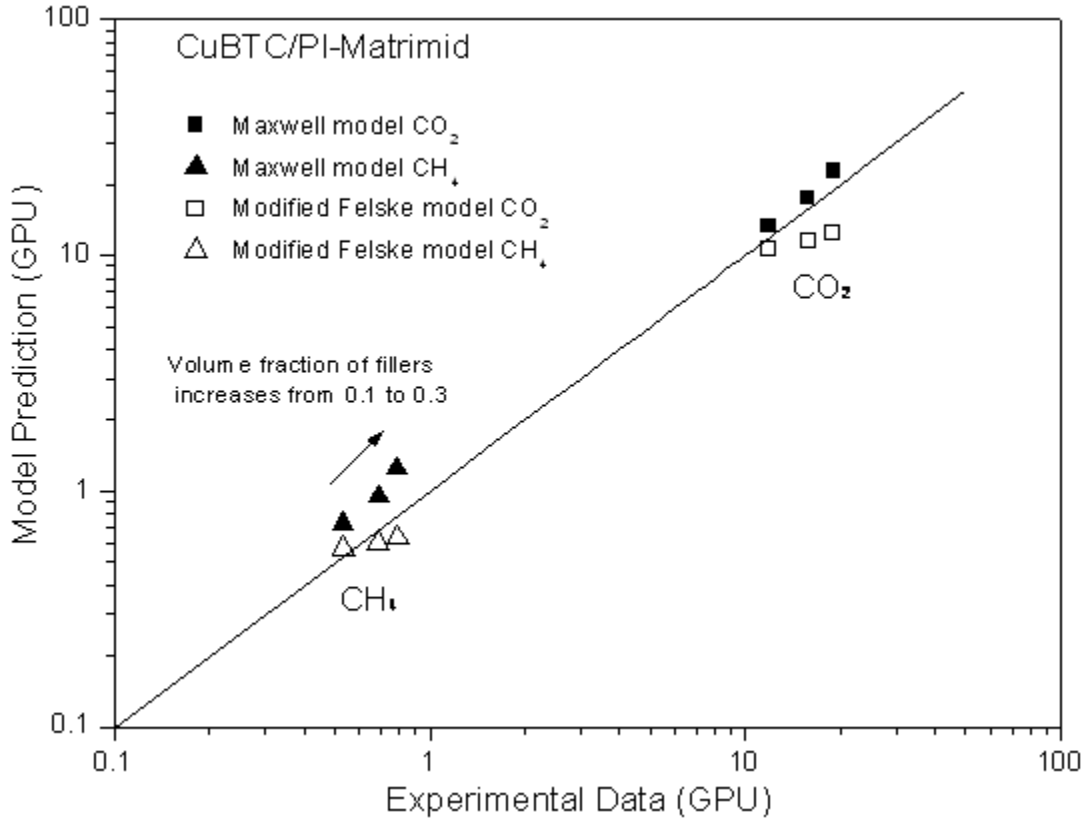

Figure 4.5: Comparison of mixed gas permeabilities of CO_2/CH_4:35/65 mixture in CuBTC/Matrimid MMMs. Experimental data is taken from Basu et al.[89] (1GPU=1 Barrer/μm)

4.2 Comparing predictions of permeation models with experimental data of MOF-based MMMs for CH_4/H_2 gas separations

The Maxwell and modified Felske models were used to make predictions for the pure gas permeabilities of H_2 and CH_4 through IRMOF-1/Matrimid[54], Cu-BPY-HFS/Matrimid[90], CuBTC/PSF[49], and CuBTC/PDMS[49] membranes. Perez et al.[54] synthesized IRMOF-1/Matrimid MMM with 0, 10, 20 and 30% loading of IRMOF-1 at 35^{o}C and they used 2000 Torr (~2.6 atm) as the inlet pressure and 1mtorr as the evacuated line pressure for the permeation measurements. Zhang et al.[90] synthesized Cu-BPY-HFS/ Matrimid MMM at 35^{o}C with 0, 10, 20, 30, 40 % loading and used 1500 Torr (~1.95 atm) as the inlet pressure for the gas permeance experiments. In simulations, 2 bar and 10^{-6} bar were used for the inlet and outlet pressures, respectively at 25^{o}C considering the same MOF loadings with the experimental works. For the calculation of modified Felske model, the maximum packing volume fraction of fillers ϕ_m was used as 0.64 for random close packing of uniform spheres and the ratio of the outer radius of the interfacial shell to the core radius, δ was taken as 1.11.

Figures 4.6 and 4.7 present the comparison of predicted $H_2(CH_4)$ permeation with the experimental measurements. Closed (open) symbols represent predictions of Maxwell (modified Felske) model. The loadings of the MOFs in the MMMs are in the range of 5% to 40%. Figure 4.6 demonstrates that modified Felske is compatible with the experimental data for pure H_2 permeability. Indeed, it gives better predictions compared to Maxwell model since modified Felske model considers the interphase morphology between polymers and MOFs. Using modified Felske is more reasonable for the performance assessment of MMMs. For pure CH_4, the same trend can be seen in Figure 4.7. The predictions of Maxwell model are worse than modified Felske model. Especially for Cu-BTC/PDMS membrane, the calculated permeability values using the Maxwell model are different than the experimental data since the model deviates when the loading of the fillers

increases from 10% to 40%. The Maxwell model is applicable for low to moderate volume fractions ($0 < \phi < 0.2$) [91]. For this reason, the predictions of modified Felske are more reasonable.

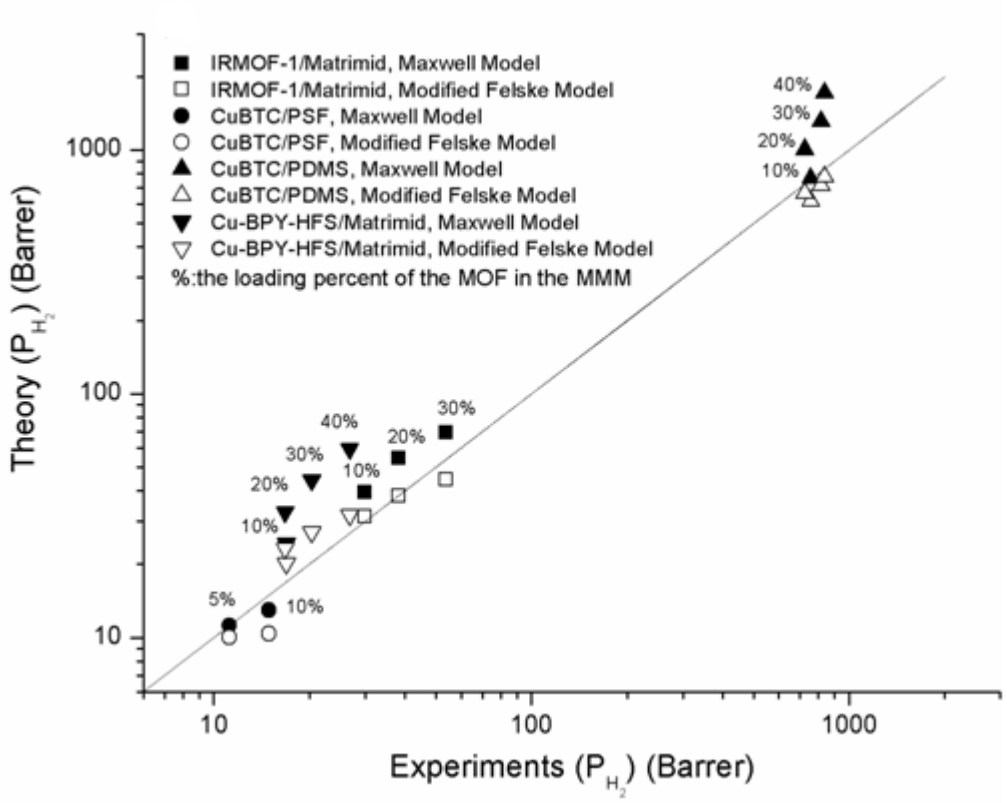

Figure 4.6: Comparisons between experimental measurements and theoretical predictions for permeabilities of H_2 in IRMOF-1/Matrimid, CuBTC/PSF, CuBTC/PDMS and Cu-BPY-HFS/Matrimid MMMs. Experimental data is taken from references [49, 51, 54].

.

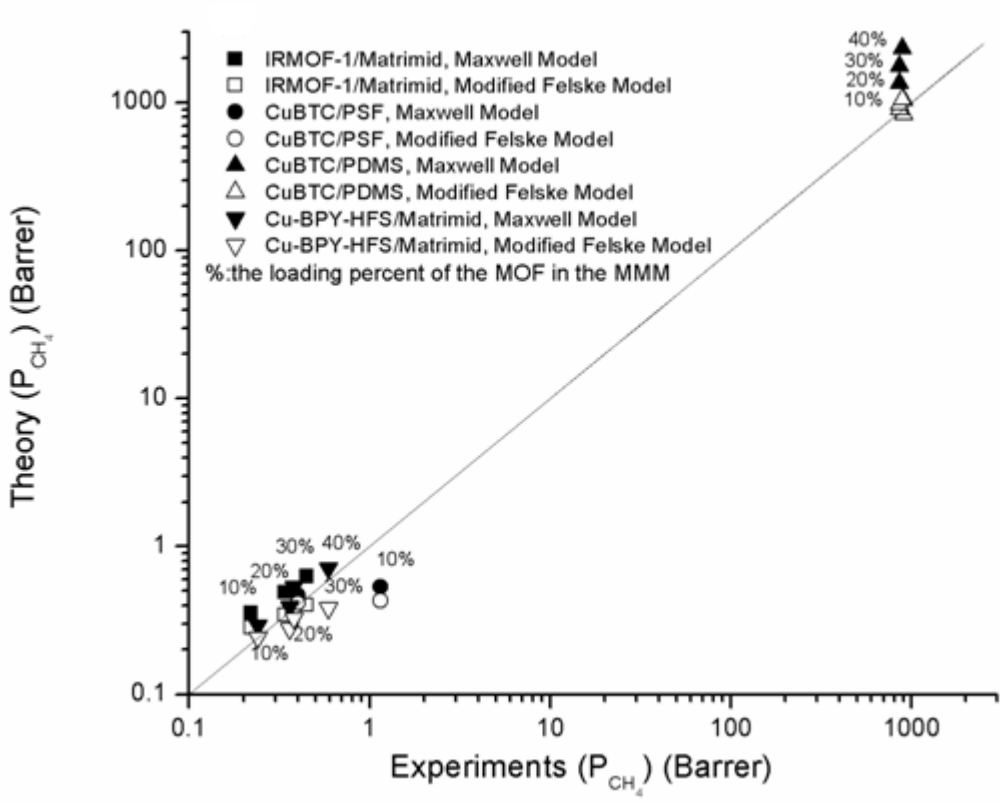

Figure 4.7: Comparisons between experimental measurements and theoretical predictions for permeabilities of CH_4 in IRMOF-1/Matrimid, CuBTC/PSF, CuBTC/PDMS and Cu-BPY-HFS/Matrimid MMMs. Experimental data is taken from references [49, 51, 54].

Erucar and Keskin[92] presented that there is a good agreement between experimental measurements and theoretical predictions for CH_4/H_2 permeance. This means new MOF-based MMMs can be studied by using the Maxwell and modified Felske models. Hypothetical or synthesized MOFs can be screened for CO_2/CH_4 and H_2/CH_4 gas separations to identify the most promising MOFs prior to experimental efforts.

Chapter 5

PREDICTIONS FOR NEW MOF-BASED MIXED MATRIX MEMBRANES (MMMs)

This chapter presents theoretical predictions for new MOF-based MMMs for CO_2/CH_4 and H_2/CH_4 separations, and the methodology for selecting appropriate MOF/polymer pairs for high performance MMMs.

5.1 Motivation

CO_2/CH_4 separation is very important for industrial applications since CO_2 reduces the energy content of the natural gas. In addition, CO_2 is acidic and it causes pipeline corrosion[93]. MMMs provide an opportunity as an efficient gas separation technology for natural gas purification due to the preferential permeation of CO_2. In this thesis, H_2/CH_4 separation was also investigated. H_2 is a clean and renewable energy source. The demand for H_2 energy has been increasing due to the limited energy sources. H_2 is commonly produced by steam reforming process. In this process, H_2 is separated from the impurities such as CH_4[94]. In this thesis, the gas separation performance of new MOF-based MMMs for CO_2/CH_4 and H_2/CH_4 gas mixtures were investigated by using atomistic and continuum modeling. The Maxwell and the modified Felske models were used to estimate the gas permeabilities through MMMs.

5.2 MOFs and Polymers

In this thesis, eighteen different MOFs were studied. The crystal structures were obtained from Cambridge Structural Database (CSD). Sixteen of MOFs were designated by their reference codes in CSD. These MOFs are BACMOH10, BAHGUN, BIMDIL, FOHQUO, GITTIN, LUNBAX, LUNBEB, LUMZUO, MABJOP, MABJUV01, MIHHOA, MIHHIU, MIHHUG, OFERUN, QAMXIL and ZUQPOQ. MMIF and $Zn(bdc)(ted)_{0.5}$, were also studied as filler particles since MMIF has very high CO_2 ($2.4x10^5$) and H_2 ($2.7x10^5$) selectivity whereas $Zn(bdc)(ted)_{0.5}$ has very low CO_2 (0.9) and H_2 (0.35) selectivity for CO_2/CH_4 and H_2/CH_4 separations, respectively[95-96].

These eighteen different MOFs have small pore diameters between 3-3.7 Å, and large pore diameters between 3.7-11.6 Å. Structural information of MOFs are given in Table 5.1. Figure 5.1 and 5.2 show the permeability and selectivity values for pure MOFs and pure polymers for CO_2 and H_2, respectively. The polymers studied in this thesis were chosen from the current Robeson's upper bound[7] for CO_2/CH_4 and H_2/CH_4 separations as can be seen in Figure 5.1 and Figure 5.2, respectively.

For CO_2/CH_4 separation, PVSH doped polyaniline, polypyrrole, polyimide TADATO/DSDA (1/1)-DDBT, poly(diphenyl acetylene) 3a, Matrimid, 6FDA-based polyimide, PIM-1 and PTMSP were studied. PVSH doped polyaniline has high CO_2 selectivity (2200) but low CO_2 permeability (0.03 Barrer) whereas PTMSP has very high CO_2 permeability ($1.9x10^4$ Barrer) but very low selectivity (4.42). Other polymers have moderate selectivity/permeability.

Table 5.1: Structural information of MOFs

MOF	Unit Cell Parameters	
	a, b, c (Å)	α, β, γ (^{0})
BACMOH10	16.05, 9.62, 7.46	90, 90, 90
BAHGUN	5.00, 24.97, 11.10	90, 98.86, 90
BIMDIL	8.47, 8.47, 14.44	90, 90, 90
FOHQUO	6.88, 14.36, 15.80	90, 101.69, 90
GITTIN	17.27, 17.27, 17.27	90, 90, 90
LUMZUO	14.68, 22.06, 18.50	90, 94.62, 90
LUNBAX	14.60, 21.97, 18.29	90, 94.94, 90
LUNBEB	14.45, 21.88, 18.03	90, 94.88, 90
MABJOP	21.01, 13.05, 8.53	90, 100.68, 90
MABJUV01	21.19, 13.19, 8.52	90, 100.31, 90
MIHHIU	13.86, 15.10, 19.43	90, 90, 90
MIHHOA	13.78, 15.06, 19.35	90, 90, 90
MIHHUG	13.87, 15.12, 19.30	90, 90, 90
MMIF	15.14, 15.14, 8.98	90, 90, 120
OFERUN	16.99, 16.99, 17.00	90, 90, 90
QAMXIL	10.45, 19.99 ,10.01	90, 90, 90
ZUQPOQ	11.07, 21.82, 7.95	90, 90, 90
$Zn(BDC)(TED)_{0.5}$	14.90, 14.90, 19.14	90, 90, 90

For H_2/CH_4 separations, sulfonated polyimide (DAPHFDS(H)), polyimide (6FDA-mMPD), polymide (6FDA-DDBT), Hyflon, Teflon (AF-2400), poly(trimethylsilypropyne-

co-phenylpropyne) and polytrimethylsilypropyne were studied as can be seen in Figure 5.2. Poly(trimethylsilypropyne-co-phenylpropyne) and polytrimethylsilypropyne polymers have very low H_2 selectivity (0.953 and 1.13, respectively) but high H_2 permeability ($2x10^4$and $1.7x10^4$ Barrer, respectively) whereas sulfonated polyimide has high H_2 selectivity (325) but very low permeability (52 Barrer). Other polymers have moderate H_2 selectivity and permeability (selectivity in the range of 5.5-121, permeability in the range of 106-3300 Barrer).

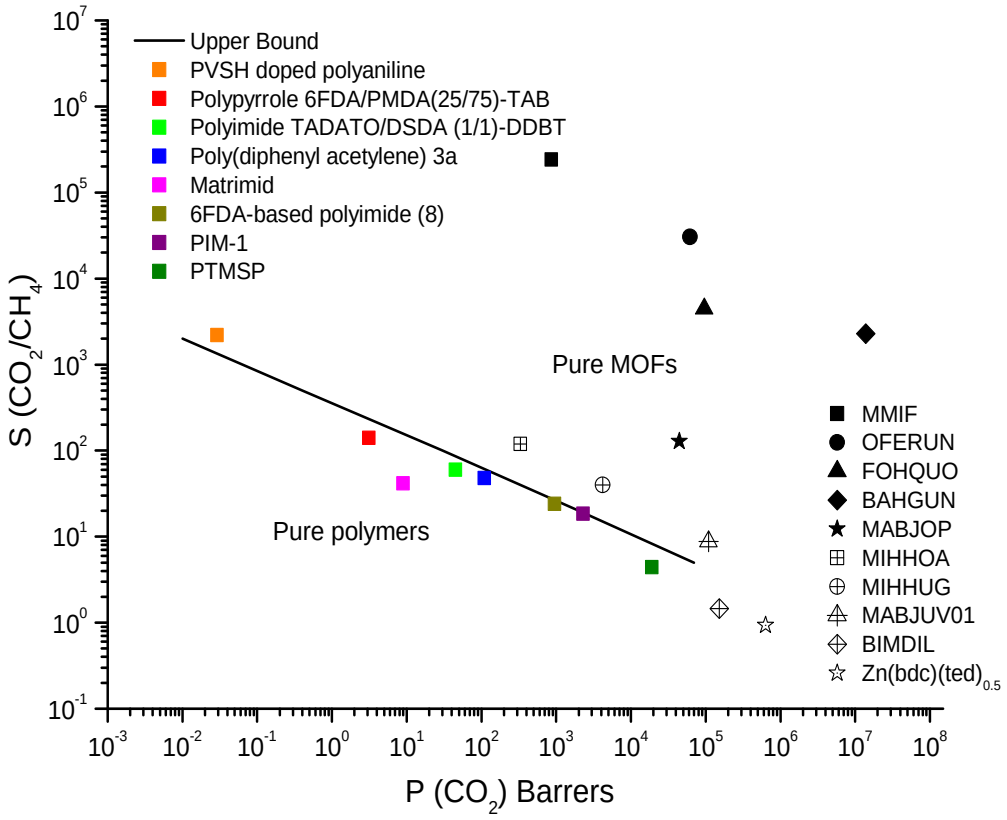

Figure 5.1: CO_2 selectivity and permeability of pure polymers and pure MOFs

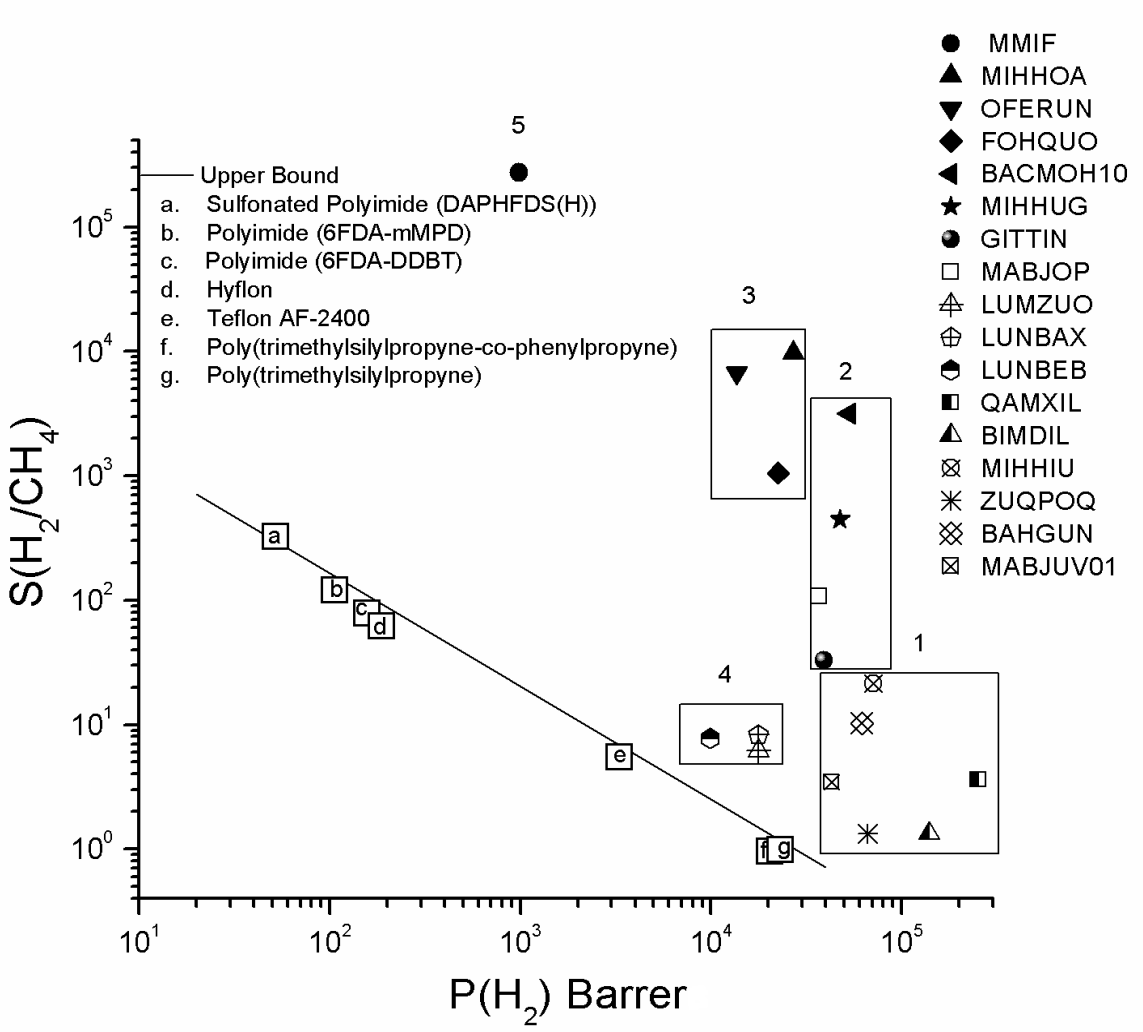

Figure 5.2: H_2 selectivity and H_2 permeability of pure polymers and pure MOFs

In Figure 5.2, seventeen MOFs were categorized into 5 different groups based on their permeability and selectivity values. The first group consists of BAHGUN, BIMDIL, MIHHIU, MABJUV01, QAMXIL and ZUQPOQ. These MOFs have high H_2 permeabilities (5×10^4-2.5×10^5 Barrer) and low H_2 selectivities (ranging from 1.3 to 21). The MOFs belong to second group are BACMOH10, GITTIN, MABJOP and MIHHUG.

These MOFs have high H_2 selectivities (33-3186) and high H_2 permeabilities (3-5×10^4 Barrer). The third group consists of MOFs which are FOHQUO, MIHHOA and OFERUN, and they present very high H_2 selectivities but low H_2 permeabilities (<3×10^4 Barrer). LUNBAX, LUNBEB and LUMZUO are the members of the fourth group presenting MOFs with low H_2 permeabilities (<1.8×10^4 Barrer) and low H_2 selectivities (<8). MMIF was separated from other groups due to its extraordinarily high H_2 selectivity and low H_2 permeability (981 Barrer). Zn(bdc)(ted)$_{0.5}$ was not included in Figure 5.2 due to its very low H_2 selectivity (0.35). The aim of this classification is to introduce an approach to determine the performances of MOF-based MMMs prior to extensive calculations.

5.3 Predicting performances of new MOF-based MMMs for CO_2/CH_4 separation

In the previous chapter, the Maxwell and the modified Felske models were validated by comparing the theoretical predictions with the experimental data of IRMOF-1/Matrimid and Cu-BTC/Matrimid membranes. The validation results showed that new MOF-based MMMs can be studied with these models prior to experimental efforts.

BAHGUN, BIMDIL, FOHQUO, MABJOP, MABJUV01, MIHHOA, MIHHUG, MMIF, OFERUN, and Zn(bdc)(ted)$_{0.5}$ were investigated as filler particles in the polymers which were defined by Robeson's data of CO_2/CH_4 separations[7] to predict the gas permeance through new-MOF based MMMs. In Table 5.2, CO_2 selectivities and permeabilities of these MOFs were demonstrated. As can be seen in Table 5.2, MMIF has the highest CO_2/CH_4 selectivity. MMIF has the narrow pores (3.3 Å) which are smaller than the kinetic diameter of CH_4 (3.7 Å) and larger than that of CO_2 (3.1 Å). Thus, CO_2 can diffuse rapidly through the pores of MMIF whereas CH_4 cannot diffuse since CH_4 experiences larger energy barrier for diffusion compared to that of CO_2. The considerable decrease in CH_4 permeability affects the overall selectivity. Among these MOFs, BAHGUN has the highest CO_2 permeability (>10^7 Barrer) since it has a highly porous

structure. Only BIMDIL and $Zn(bdc)(ted)_{0.5}$ have low CO_2 selectivities, 1.5 and 0.9, respectively. The CO_2 selectivities of the pure polymers which are poly(diphenyl acetylene) 3a (47.8) and Matrimid (41.7) are close to that of MIHHUG. Other MOFs offer high CO_2 selectivity compared to that of pure polymers which are illustrated in Figure 5.1.

Table 5.2: CO_2 selectivities and permeabilities of pure MOFs

MOF	Permeability (Barrer)		$S(CO_2/CH_4)$
	P_{CO_2}	P_{CH_4}	
BAHGUN	$1.39x10^7$	$6.05x10^3$	2290
BIMDIL	$1.52x10^5$	$1.05x10^5$	1.5
FOHQUO	9.57x104	21.4	4474.7
MABJOP	$4.42x10^4$	$3.45x10^2$	128.2
MABJUV01	$1.09x10^5$	$1.24x10^4$	8.8
MIHHOA	$3.30x10^2$	2.78	118.7
MIHHUG	$4.21x10^3$	$1.06x10^2$	39.8
MMIF	$8.66x10^2$	$3.58x10^{-3}$	$2.4x10^5$
OFERUN	$6.16x10^4$	2.02	$3.0x10^4$
$Zn(BDC)(TED)_{0.5}$	$6.30x10^5$	$6.74x10^5$	0.9

Figures 5.3-5.8 present predicted CO_2 selectivities and permeabilities of MMIF/polymer, MABJOP/polymer and BIMDIL/polymer membranes for CO_2/CH_4 separations. MMIF, MABJOP and BIMDIL-based MMMs were demonstrated to point out the effect of the change in selectivity and permeability of pure MOFs. MMIF has high CO_2 selectivity/low permeability, MABJOP shows mediocre CO_2 selectivity/high permeability, and BIMDIL has low CO_2 selectivity/high permeability. Other MOF-based MMMs

(BAHGUN, FOHQUO, MABJUV01, MIHHOA, MIHHUG and OFERUN) were presented in Appendix. The stars in Figures 5.3, 5.5, 5.7 (Figures 5.4, 5.6, 5.8) show the predictions of Maxwell model (modified Felske model) for selectivity/permeability performances of MMMs where volume fraction of the filler particles increases from 0.1 to 0.5.

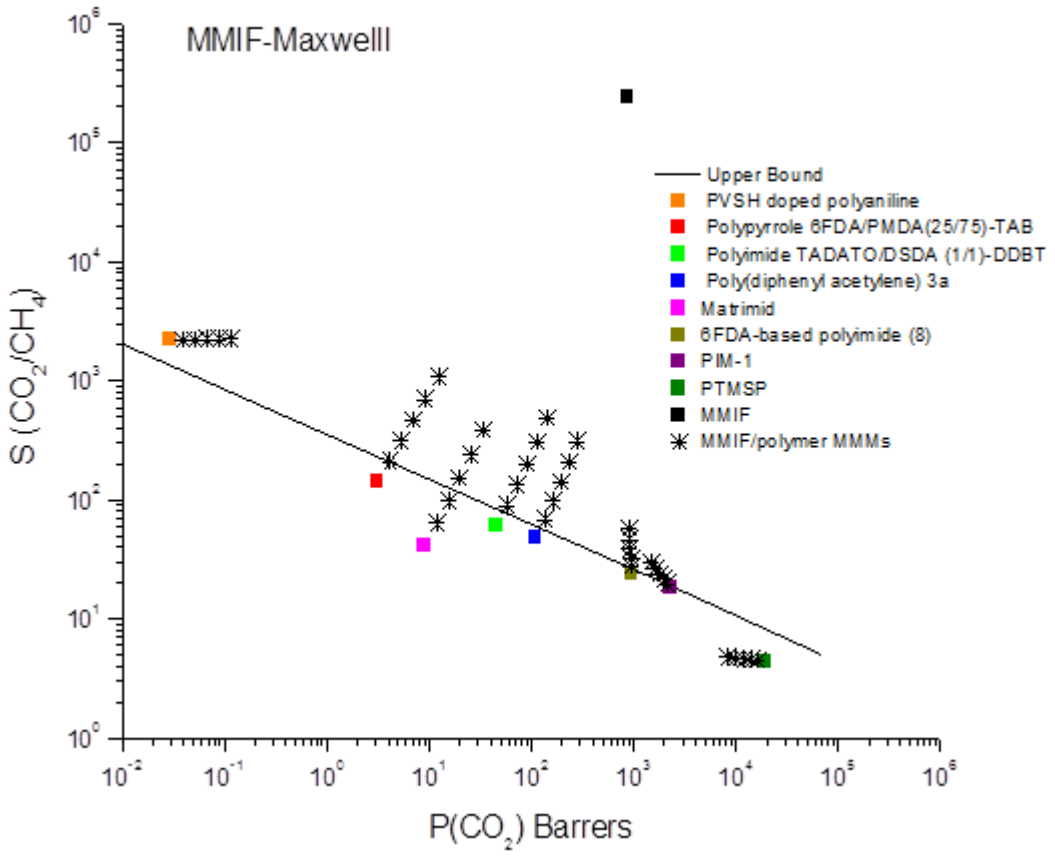

Figure 5.3: Maxwell model predictions for CO_2 selectivity and permeability of MMMs having filler particles MMIF. Squares represent the performance of pure polymers and pure MOF, stars represent the performance of MMMs with filler particles having volume fractions of 0.1, 0.2, 0.3, 0.4 and 0.5.

Figures 5.3 and 5.4 show that a MOF exhibiting high CO_2 selectivity/low CO_2 permeability can affect the performances of various polymers for CO_2/CH_4 separations. As can be seen in Figures 5.3 and 5.4, when MMIF was embedded into polymer matrices, both the selectivity and permeability of CO_2 was improved for polypyrrole, polyimide, poly(diphenyl acetylene) and Matrimid since MMIF has higher selectivity/permeability compared to these polymers. For example, pure Matrimid has a CO_2 selectivity of 41.7 (CO_2 permeability of 9 Barrer) whereas MMIF/Matrimid membrane has a CO_2 selectivity of 150.7 (CO_2 permeability of 20.1 Barrer) at a filler volume fraction of 0.3 (Figure 5.3). For PTMSP and PIM-1, the permeability of CO_2 starts to decrease when the volume fraction of MMIF particles increases, but the selectivity of CO_2 over CH_4 slightly increases since MMIF has lower permeability than those of polymers. For instance, pure PTMSP has a CO_2 selectivity of 4.42 and CO_2 permeability of $19x10^3$ Barrer. When MMIF was incorporated into PTMSP, the permeability of MMIF/PTMSP membrane decreased to 12 $x10^3$ Barrer at a filler volume fraction of 0.3.

Figure 5.4 remarks that the predictions of modified Felske model is less than those of Maxwell model both for permeability and selectivity. For example, as the volume fraction of MMIF particles increases from 0 to 0.3 in Polypyrrole 6FDA/PMDA (25/75)-TAB, selectivity of CO_2 over CH_4 increases from 140 to 462.03 according to the Maxwell model whereas the Modified Felske model estimates CO_2 selectivity as 395.56. As another example, Maxwell model predicts the selectivity of MMIF/Matrimid membranes between 64 and 387 for a volume fraction range of 0.1-0.5, but modified Felske model predicts the selectivity between 51 and 135 under the same conditions. The reason why the modified Felske model predicts lower values for CO_2 permeability and selectivity than that of the Maxwell model is that modified Felske model considers the interfacial effect between the polymer and MOF phases. Comparing Figure 5.3 and 5.4 clarifies that higher volume fractions are needed to carry MMMs above Robeson's curve for the modified Felske

model. For example, the Maxwell model predicts that MMIF/Matrimid MMMs exceed the Robeson's curve at a volume fraction of 0.3. However, if the modified Felske model was used, the volume fraction of 0.5 was needed to pass the Robeson's curve under the same conditions.

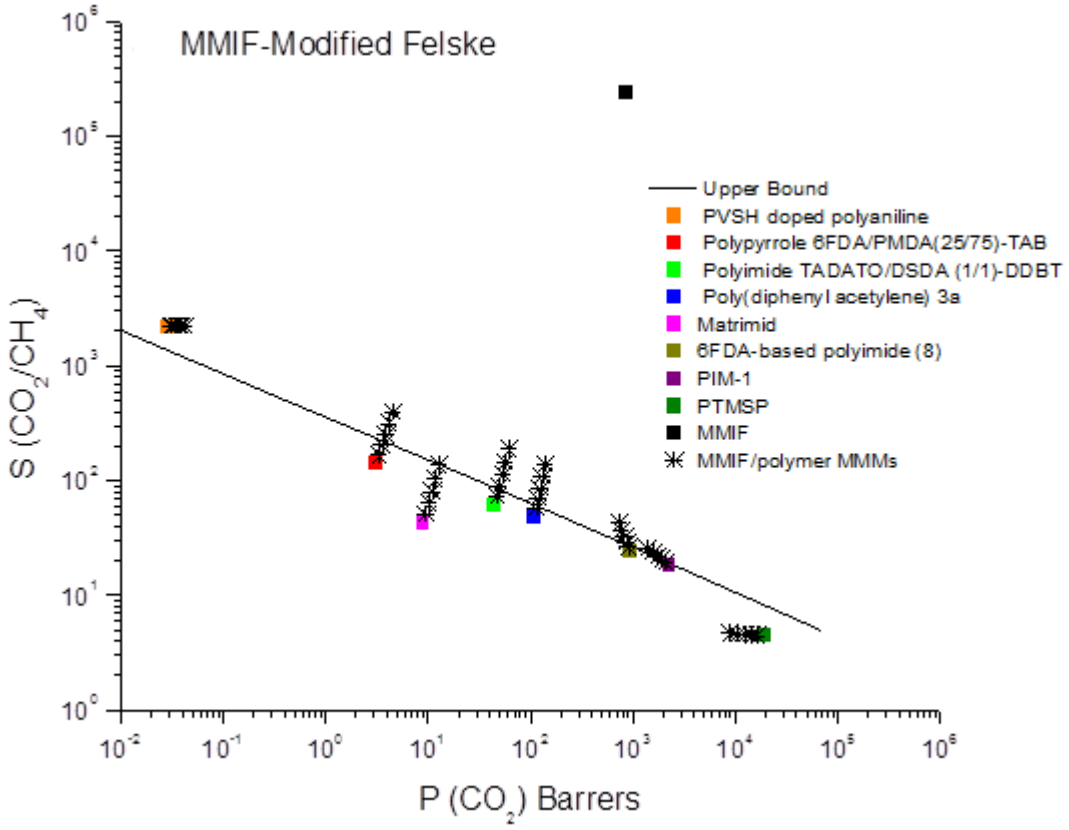

Figure 5.4: The modified Felske model predictions for CO_2 selectivity and permeability of MMMs having filler particles MMIF. Squares represent the performance of pure polymers and pure MOF, stars represent the performance of MMMs with filler particles having volume fractions of 0.1,0,2, 0.3, 0.4 and 0.5.

Figures 5.5 and 5.6 exhibit the performance of MABJOP-based MMMs for the predictions of the Maxwell and modified Felske models, respectively. Incorporation of MABJOP into PTMSP, PIM-1 and 6FDA-based polyimide improves both the selectivity and permeability. PTMSP, PIM-1 and 6FDA-based polyimide polymers have very low selectivity compared to that of MABJOP. For this reason, addition of MABJOP enhances their gas separation performance. For example, incorporation of MABJOP at a volume fraction of 0.3 can carry pure PTMSP membrane above the upper bound by increasing its selectivity from 4.42 to 8.88.

For other polymers such as Matrimid, polypyrrole and poly(diphenyl acetylene), the permeability of CO_2 was improved. However, the selectivity of CO_2 over CH_4 does not change significantly since the selectivity of MABJOP is lower than those of polymers. The predictions of the modified Felske model both in selectivity and permeability were again found to be less than the predictions of Maxwell model. Figures 5.7 and 5.8 show the performances of BIMDIL-based MMMs. Since diffusion rates of CO_2 and CH_4 are very close (~10^{-5} cm^2/s), BIMDIL has very low CO_2 selectivity (1.5), but it has very high CO_2 permeability (>10^5 Barrer).

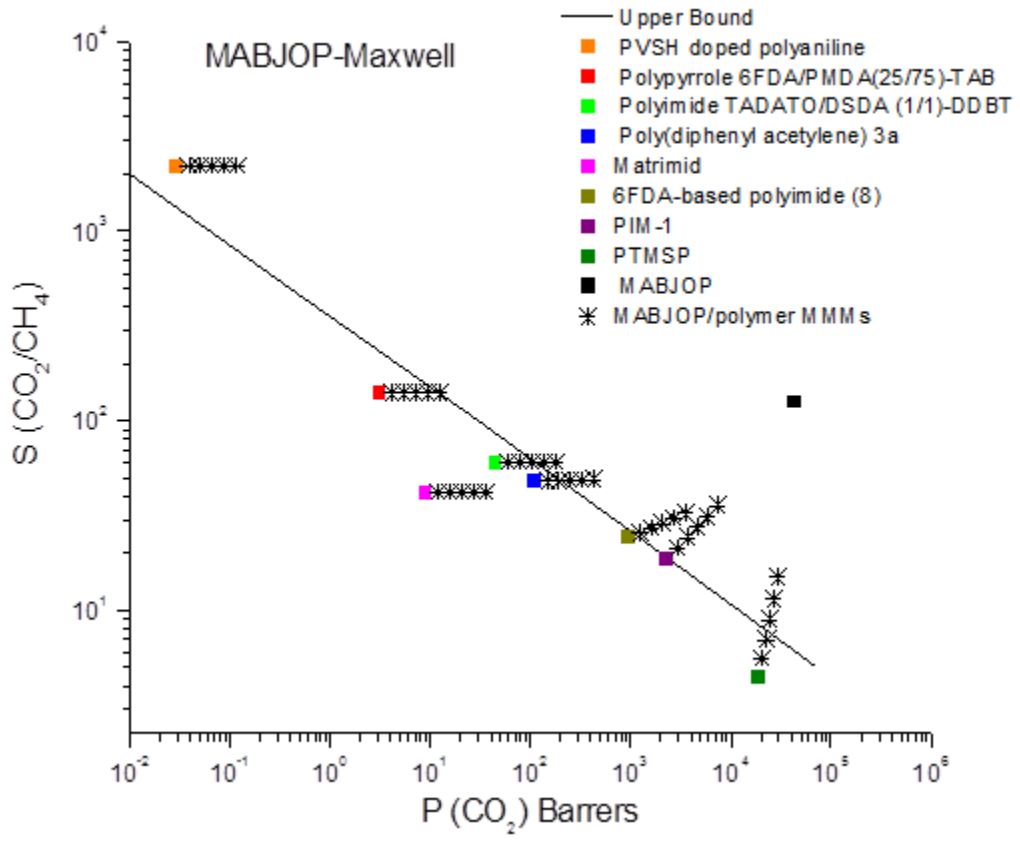

Figure 5.5: Maxwell model predictions for CO_2 selectivity and permeability of MMMs having filler particles MABJOP. Squares represent the performance of pure polymers and pure MOF, stars represent the performance of MMMs with filler particles having volume fractions of 0.1, 0.2, 0.3, 0.4 and 0.5.

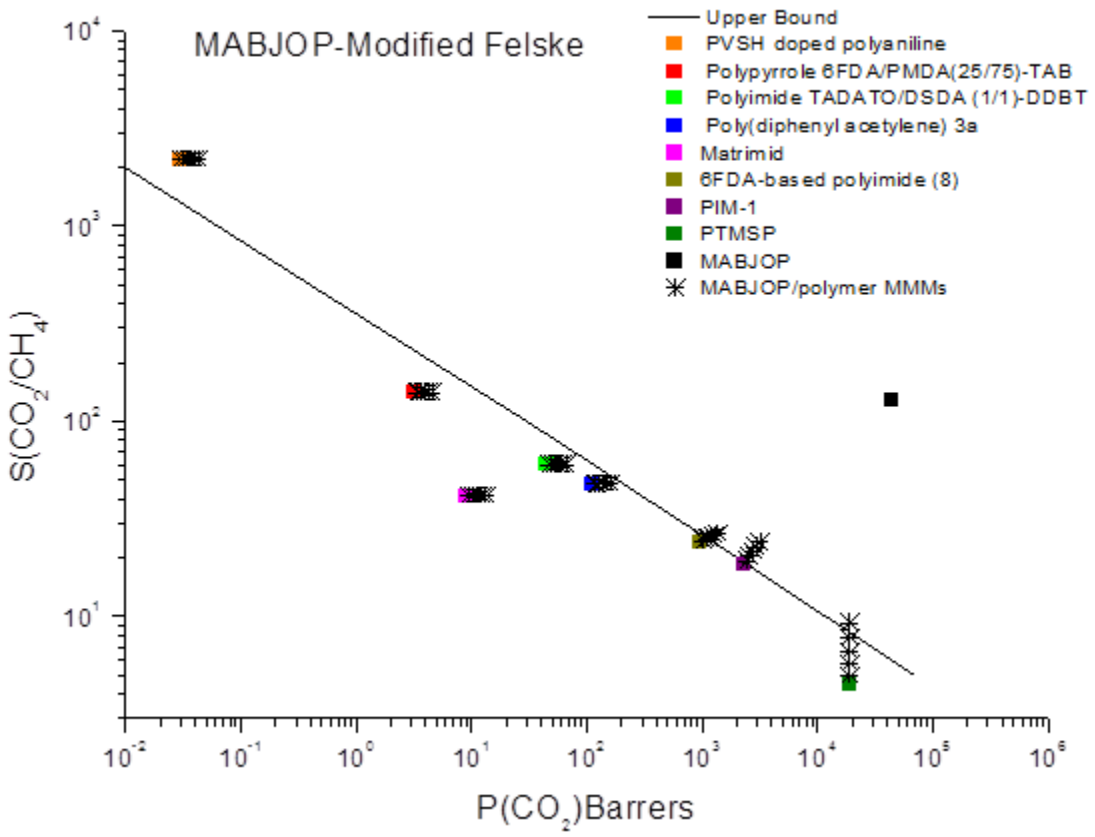

Figure 5.6: The modified Felske model predictions for CO_2 selectivity and permeability of MMMs having filler particles MABJOP. Squares represent the performance of pure polymers and pure MOF, stars represent the performance of MMMs with filler particles having volume fractions of 0.1, 0.2, 0.3, 0.4 and 0.5.

As can be observed from Figures 5.7 and 5.8, addition of BIMDIL into pure polymers does not affect the selectivity. In addition, a slight decrease in selectivity can be seen although CO_2 permeability increases. Only for BIMDIL/PTMSP membrane, CO_2 selectivity sharply decreased since this polymer has also very low selectivity like BIMDIL.

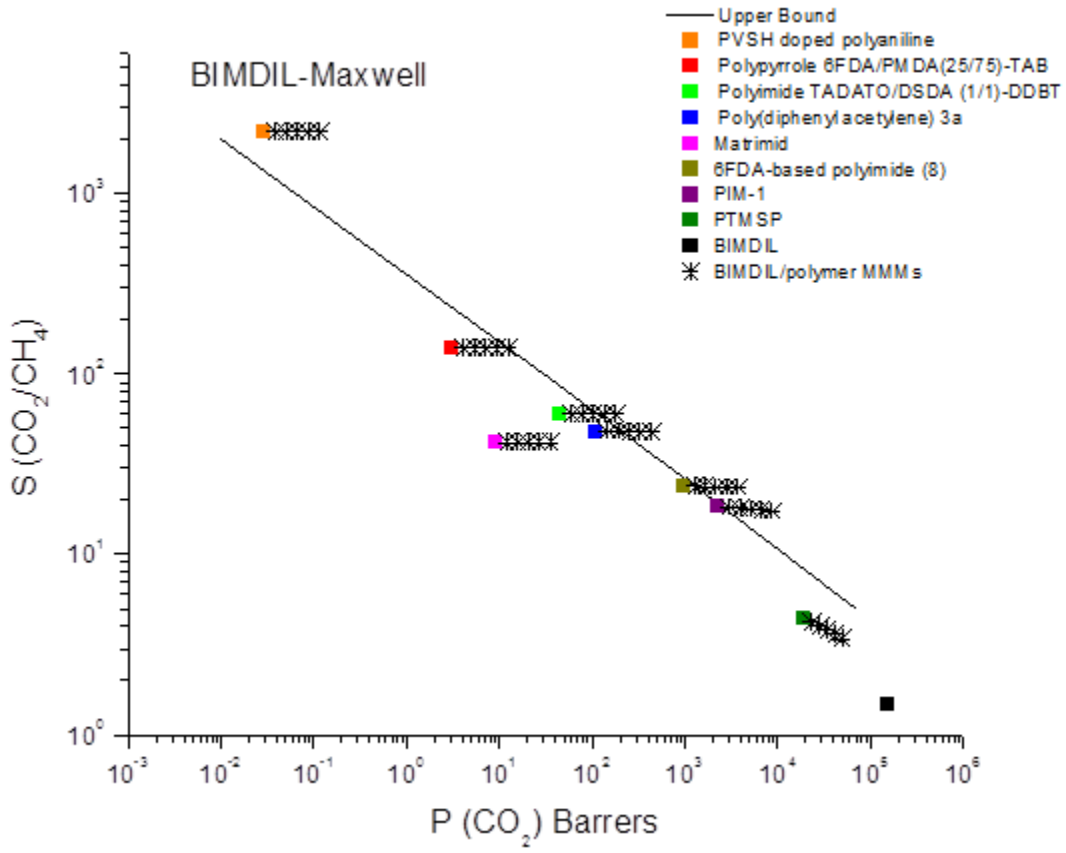

Figure 5.7: Maxwell model predictions for CO_2 selectivity and permeability of MMMs having filler particles BIMDIL. Squares represent the performance of pure polymers and pure MOF, stars represent the performance of MMMs with filler particles having volume fractions of 0.1, 0.2, 0.3, 0.4 and 0.5

Predictions of the Maxwell and the modified Felske Models suggest that as the volume fraction of BIMDIL particles increased, CO_2 permeability is enhanced, but selectivity enhancement cannot be observed. Thus, Figures 5.7 and 5.8 indicate that using a MOF which has low CO_2 selectivity/high permeability as filler particles in polymers is not a convenient way to enhance the gas selectivity of MMMs.

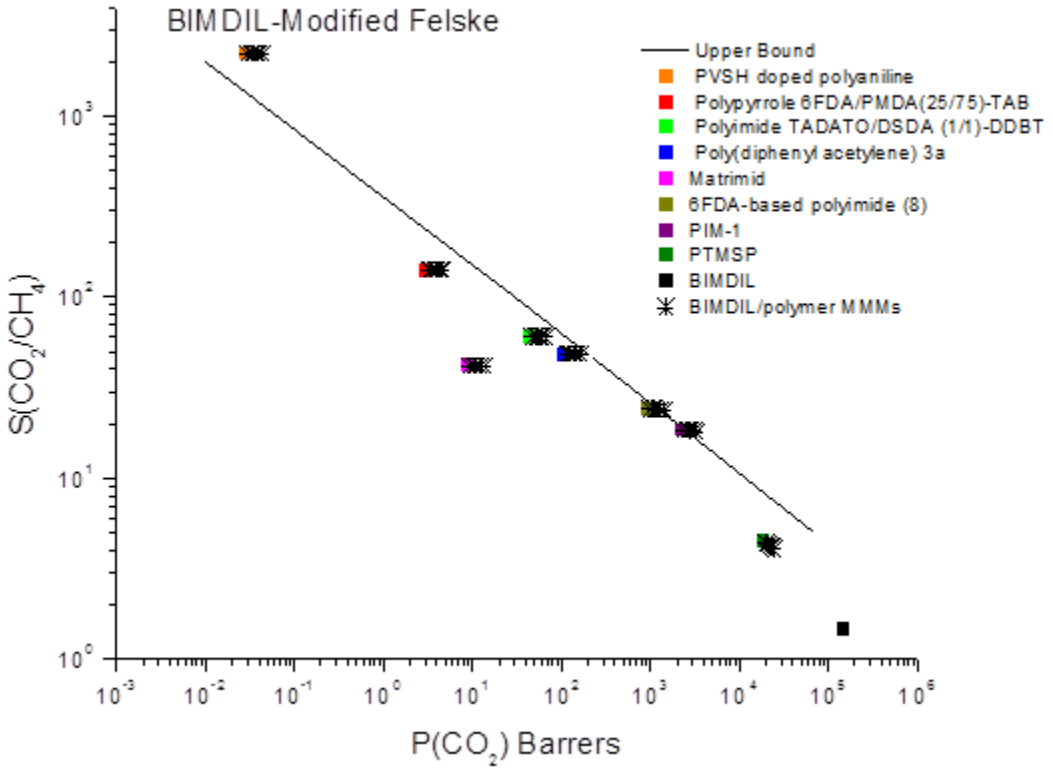

Figure 5.8: The modified Felske model predictions for CO_2 selectivity and permeability of MMMs having filler particles BIMDIL. Squares represent the performance of pure polymers and pure MOF, stars represent the performance of MMMs with filler particles having volume fractions of 0.1, 0.2, 0.3, 0.4 and 0.5.

Figures 5.3-5.8 emphasize that MOF/polymer matching is very important to enhance the separation performance of MMMs. For example, for a pure polymer membrane which has high CO_2 selectivity but low CO_2 permeability such as PVSH doped polyaniline, MOF's identity is unimportant since addition of MMIF and BIMDIL as filler particles, did not change the CO_2 selectivity. Moreover, permeability of CO_2 increased. On the other hand, for the polymers which are highly permeable but unselective such as

PTMSP, the identity of MOF is significant. If a highly selective, but unremarkably permeable MOF such as MMIF is used as filler particles in this type of polymers, CO_2 selectivity of MMMs enhances at the expense of CO_2 permeability reduction. On the contrary, if a highly permeable, but unnotably selective MOF such as BIMDIL is used as filler particles, CO_2 permeability of MMMs improves at the expense of CO_2 selectivity reduction. As can be seen in Figures 5.3-5.8, the majority of the pure polymers have mediocre CO_2 selectivity/high permeability. Hence, using a MOF which has high CO_2 selectivity such as MMIF, OFERUN, FOHQUO and BAHGUN as filler particles carries the pure polymers above the upper bound.

There are numerous different MOFs in CSD, and screening these MOFs to examine the best MOF/polymer pair is extremely important to develop high performance MMMs. In this thesis, it is aimed to find a correlation between the energy barrier to CO_2 permeability and the CO_2 selectivity in MOFs to screen MOFs without doing detailed calculations. The CO_2 and CH_4 diffusivities in each MOF were calculated with EMD simulations, and the energy barrier for diffusion was estimated by using the following equation:

$$E_{trans}^{CO_2} = -\ln\left(\frac{n \cdot D^{CO_2}}{\upsilon \cdot a^2}\right) \cdot R \cdot T \tag{5.1}$$

In Equation 5.1, $E_{trans}^{CO_2}$ is the transition energy barrier for diffusion of CO_2 (kJ/mol), n is the dimension of the pores (1 or 2 or 3), R is the gas constant (8.314 J $K^{-1}mol^{-1}$), υ is the pre-exponential factor (taken to be 10^{12} s^{-1}), D^{CO_2} is the corrected diffusivity of CO_2 calculated from EMD simulations, a is the cage-to-cage distance in MOFs and T is temperature (K).

Figure 5.9 shows the relationship between the energy barrier to CO_2 diffusion and CO_2 permeability. The higher energy barrier for diffusion causes the lower permeability of CO_2. For instance, MIHHOA has the maximum energy barrier for diffusion, 28.03 kJ/mol whereas it has the minimum CO_2 permeability (3.30×10^2 Barrer). The pore size and the

topology of MOFs significantly affect the diffusion of the gas molecules. The narrow pores provide an inconvenient path for the diffusion of gas molecules. The diffusion occurs at the expense of permeability reduction. BAHGUN, $Zn(bdc)(ted)_{0.5}$ and BIMDIL have high CO_2 permeability ($P_{CO2}>10^5$ Barrer), and low energy barrier. The diffusion of CO_2 through these MOFs is rapid due to their pore structures. However, CH_4 molecules can also rapidly diffuse through these MOFs. For this reason, CO_2/CH_4 selectivities of these MOFs are very low. For an efficient separation, both high selectivity and permeability are needed. Thus, the relationship between the energy barrier to CO_2 diffusion and CO_2 permeability agrees with the prediction results which reveal that addition of BAHGUN, $Zn(bdc)(ted)_{0.5}$ and BIMDIL as filler particles do not yield the selectivity. However, these MOFs can be good candidates for highly selective polymers such as PVSH doped polyaniline to carry the pure polymer above the upper bound by increasing the permeability without changing the selectivity.

This correlation will be very useful to predict the separation performance of MOFs prior to extensive calculation. In addition, it is possible to predict the alternative MOF/polymer combinations that can show high performance as MMMs by doing only EMD simulations.

Figure 5.10 demonstrates the relationship between the energy barrier to CO_2 diffusion and CO_2/CH_4 selectivity. The correlations suggest that there are two regions in this figure: one is for highly CO_2 selective MOFs such as MMIF, BAHGUN, OFERUN and FOHQUO, and the latter is for low-mediocre CO_2 selective MOFs such as MIHHOA and BIMDIL. The results also showed that as the energy barrier for diffusion increases, CO_2 selectivity of MOFs starts to increase since the permeabilities of gases decrease. CH_4 requires larger energy barrier than CO_2 due to the larger kinetic diameter of CH_4 (3.7 Å) compared to that of CO_2 (3.1 Å). For this reason, the decrease in CH_4 permeability is much more pronounced than the decrease in CO_2 permeability. Thus, the CO_2 selectivity

increases with the considerable decrease in CH_4 permeability. Overall, Figures 5.9 and 5.10 can give a hint for the assessment of MOF/polymer combinations without making detailed calculations. Erucar and Keskin[88] reported that this correlation will be helpful for selecting MOF/polymer combinations for MMMs for CO_2 separation applications.

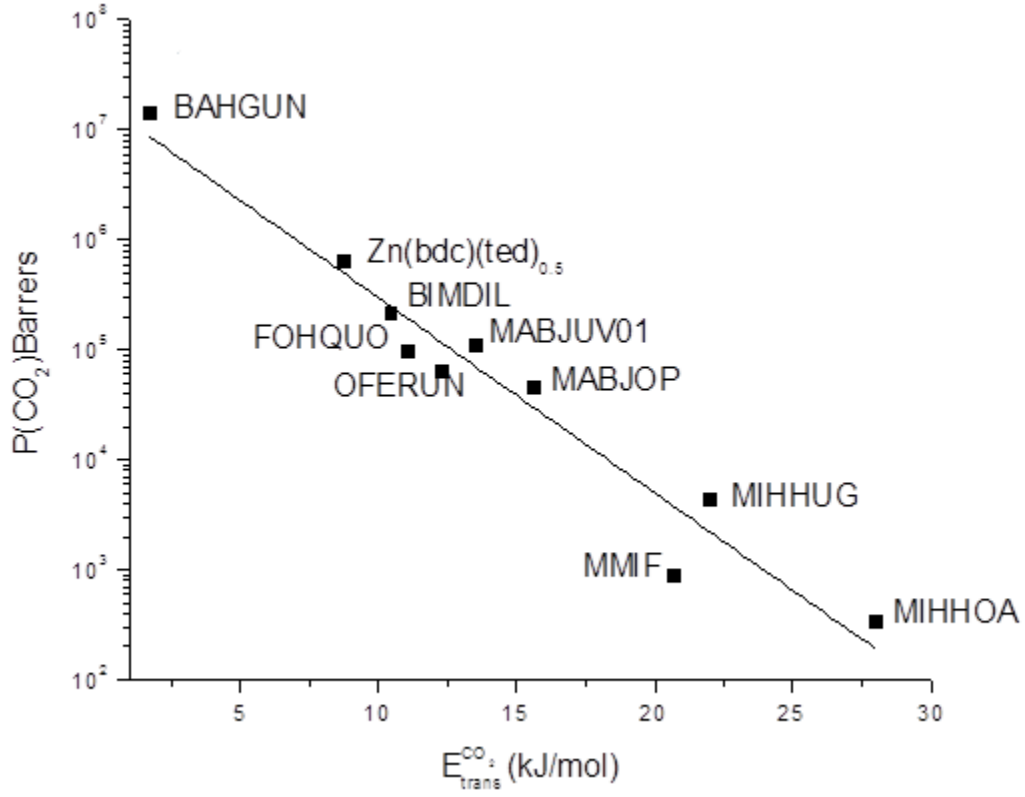

Figure 5.9: Relation between the energy barrier to CO_2 diffusion and CO_2 permeability

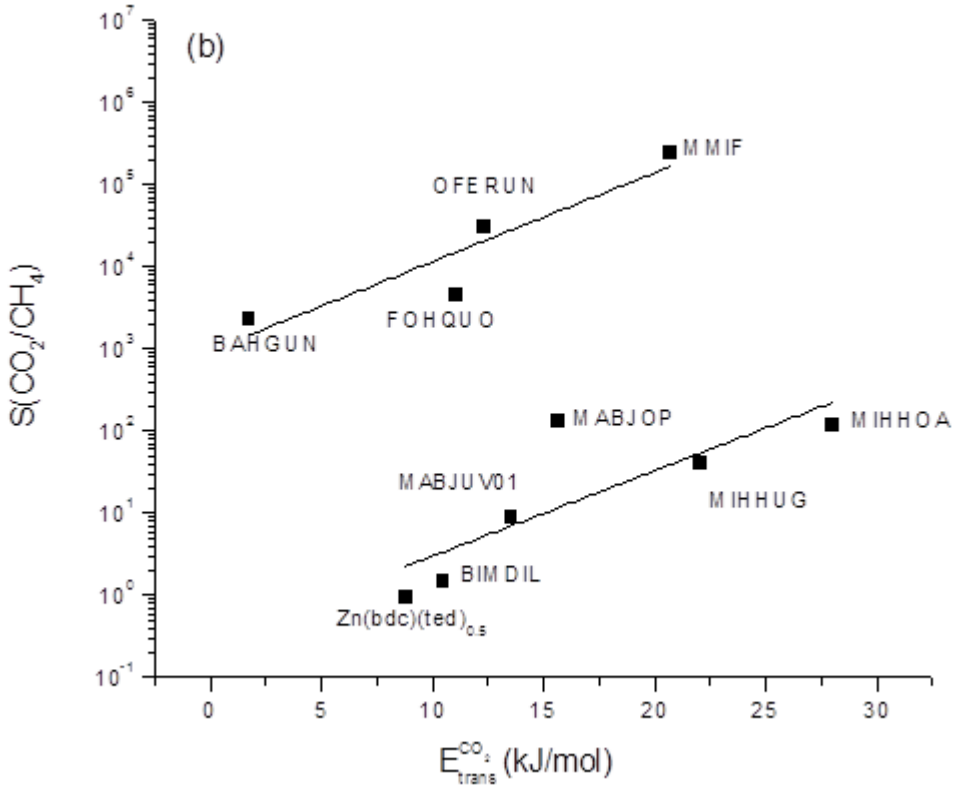

Figure 5.10: Relations between the energy barrier to CO_2 diffusion and CO_2/CH_4 selectivity

5.4 Predicting performances of new MOF-based MMMs for H_2/CH_4 separation

Since there are numerous MOFs that are presented in CSD, developing easy and fast methods to screen large number of MOFs for specific interest has been demanded. In order to develop a strategy, seventeen MOFs were categorized into 5 different groups based on the H_2 permeabilities and selectivities as discussed in the previous "MOFs and polymers" section. This categorization will constitute a convenient way for choosing new MOFs as filler particles because one can easily make predictions about the performance of new

MOF-based MMMs by determining a MOF's selectivity and permeability without extensive calculations.

The MOF groups are listed as follows: The fist group consists of MOFs with high permeability/low selectivity (BAHGUN, BIMDIL, MIHHIU, MABJUV01, QAMXIL and ZUQPOQ), the second group consists of MOFs with both high permeability/high selectivity (BACMOH10, GITTIN, MABJOP and MIHHUG), the third group consists of MOFs with low permeability/high selectivity (FOHQUO, MIHHOA and OFERUN), the fourth group consists of MOFs with low permeability/low selectivity, and the last group consists of a single MOF, MMIF which has extraordinary high selectivity/low permeability. The performances of these new MOFs-based MMMs were predicted using the Maxwell and the modified Felske models. One MOF was selected in each group as a representative candidate for H_2/CH_4 gas system: BAHGUN, MIHHUG, FOHQUO, LUNBEB and MMIF, respectively. The results of other MOFs were given in Appendix.

Figures 5.11(a) and (b) illustrate the performance of BAHGUN-based MMMs. Stars represent the performance of MMMs with MOFs volume fractions of 0.1, 0.2, 0.3, 0.4 and 0.5. Incorporation of BAHGUN (from the first group) into polymers improved both the selectivity and permeability of polytrimethylsilylpropynes (PTMSPs) significantly since BAHGUN has higher H_2 selectivity and permeability than pure PTMSPs. The first group has high permeability and low selectivity. For this reason, addition of MOFs from this group into polymers increases H_2 permeability of polyimides and Hyflon without changing their selectivity significantly. For example, H_2 permeability of Hyflon increases from 3300 to 6716 Barrer when the volume fraction of BAHGUN is equal to 0.3. BAHGUN/Hyflon MMM can exceed the upper bound due to this permeability enhancement.

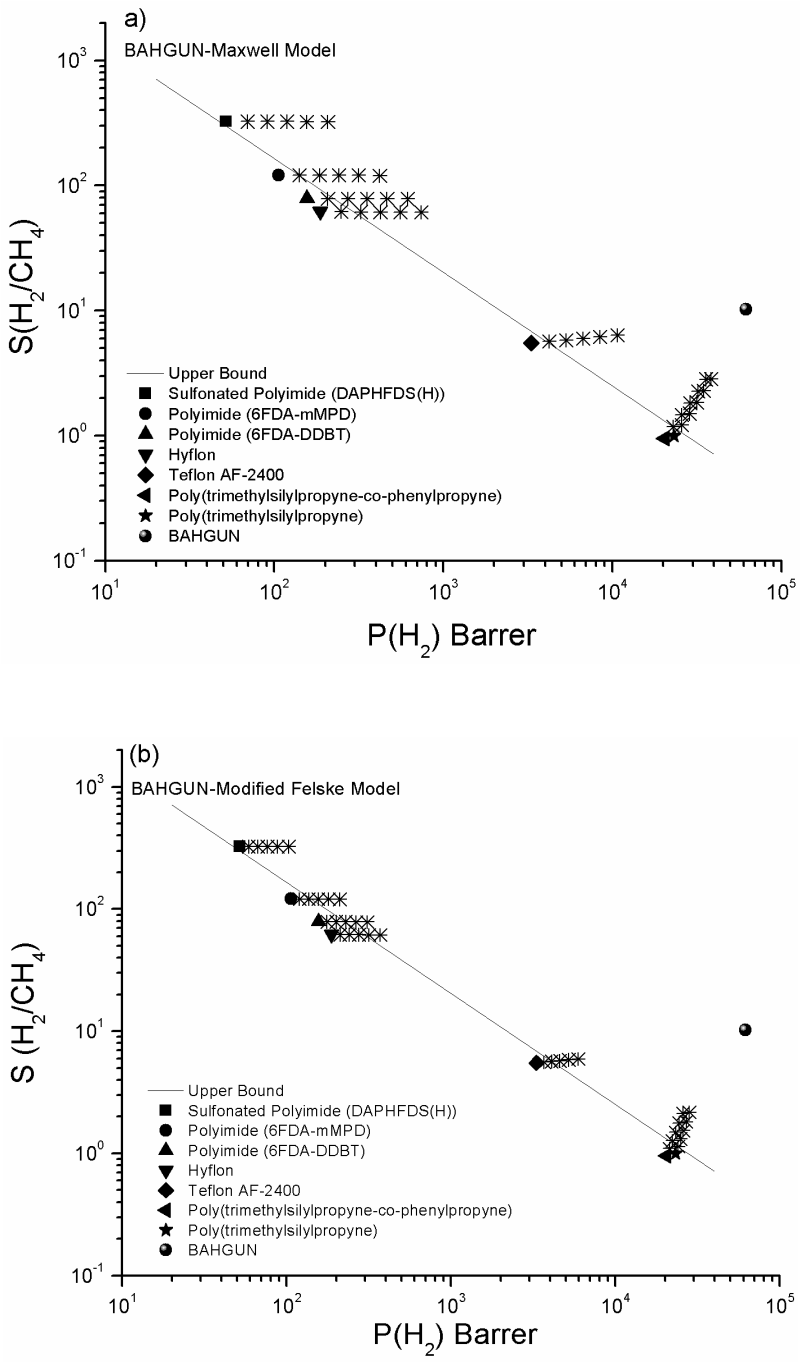

Figure 5.11: Predictions of Maxwell (a) and modified Felske (b) models for H_2 selectivity and H_2 permeability of BAHGUN-based MMMs

MIHHUG (from the second group) was chosen to demonstrate the performance of membranes made from MOFs of the second group and the results are shown in Figures 5.12 and 5.13. The second group enhanced the performance of all polymers since these MOFs have both high selectivity and high permeability. Thus, addition of a small fraction of these MOFs can carry all the polymers well above the upper bound. The improvements can be seen clearly for Teflon and PTMSPs. For example, the selectivity (the permeability) of Teflon increases from 5.5 (3300 Barrer) to 11 (5233 Barrer) at a 0.2 volume fraction of MIHHUG. Figures 5.11-5.13 demonstrate that for the polymers lying at the bottom of the upper bound, the identity of a MOF has a critical role.

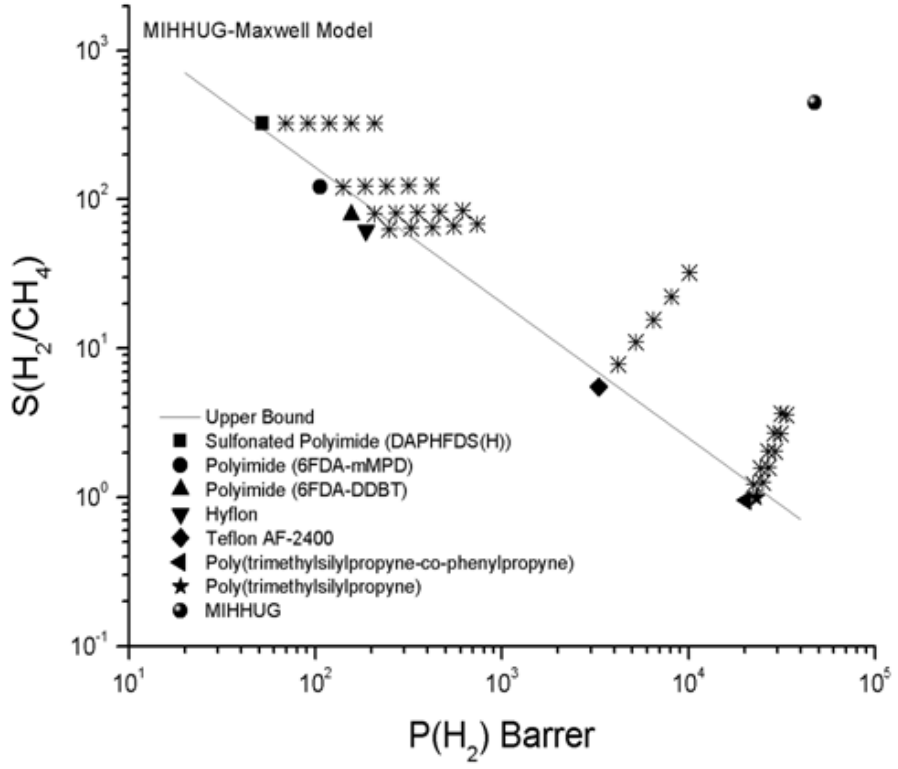

Figure 5.12: Predictions of Maxwell model for H_2 selectivity and H_2 permeability of MIHHUG-based MMMs

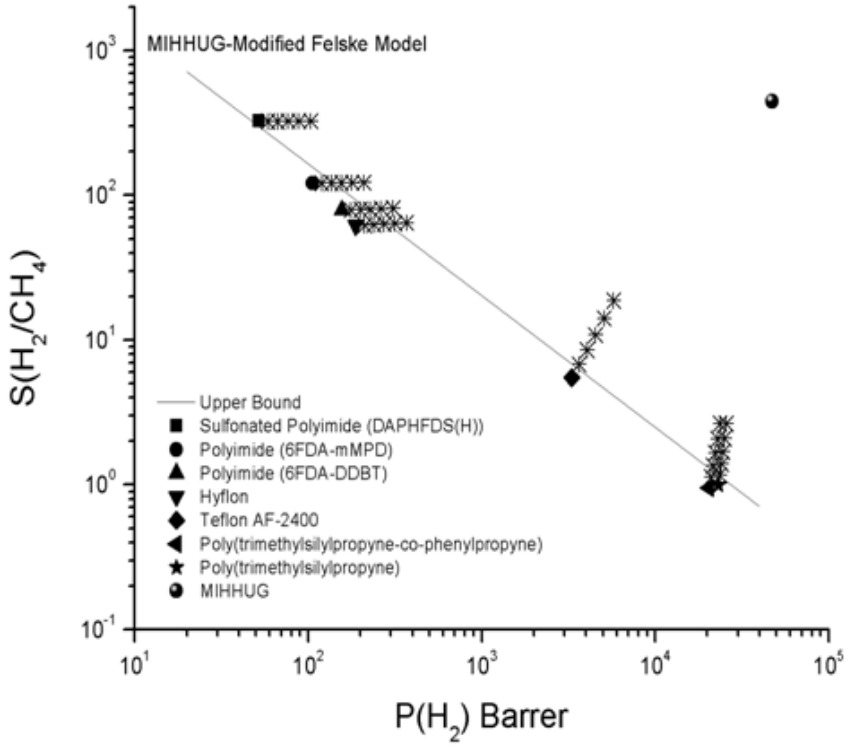

Figure 5.13: Predictions of modified Felske model for H_2 selectivity and H_2 permeability of MIHHUG-based MMMs

Incorporation of FOHQUO (from the third group) into polymers can increase the selectivity of PTMSPs without making a significant change in their permeability since the MOFs in this group have similar permeabilities to those of PTMSPs (Figures 5.14 (a) and (b)). As discussed before, the predictions of Maxwell model are more optimistic than those of the modified Felske model. For example, Maxwell model predicts that H_2 permeability is increased from 20400 to 20800 Barrer, but modified Felske model predicts that it decreases to 19400 Barrer when FOHQUO is embedded into polytrimethylylypropyne-cophenylpropyne (PTMSP-cPP) at a volume fraction of 0.2.

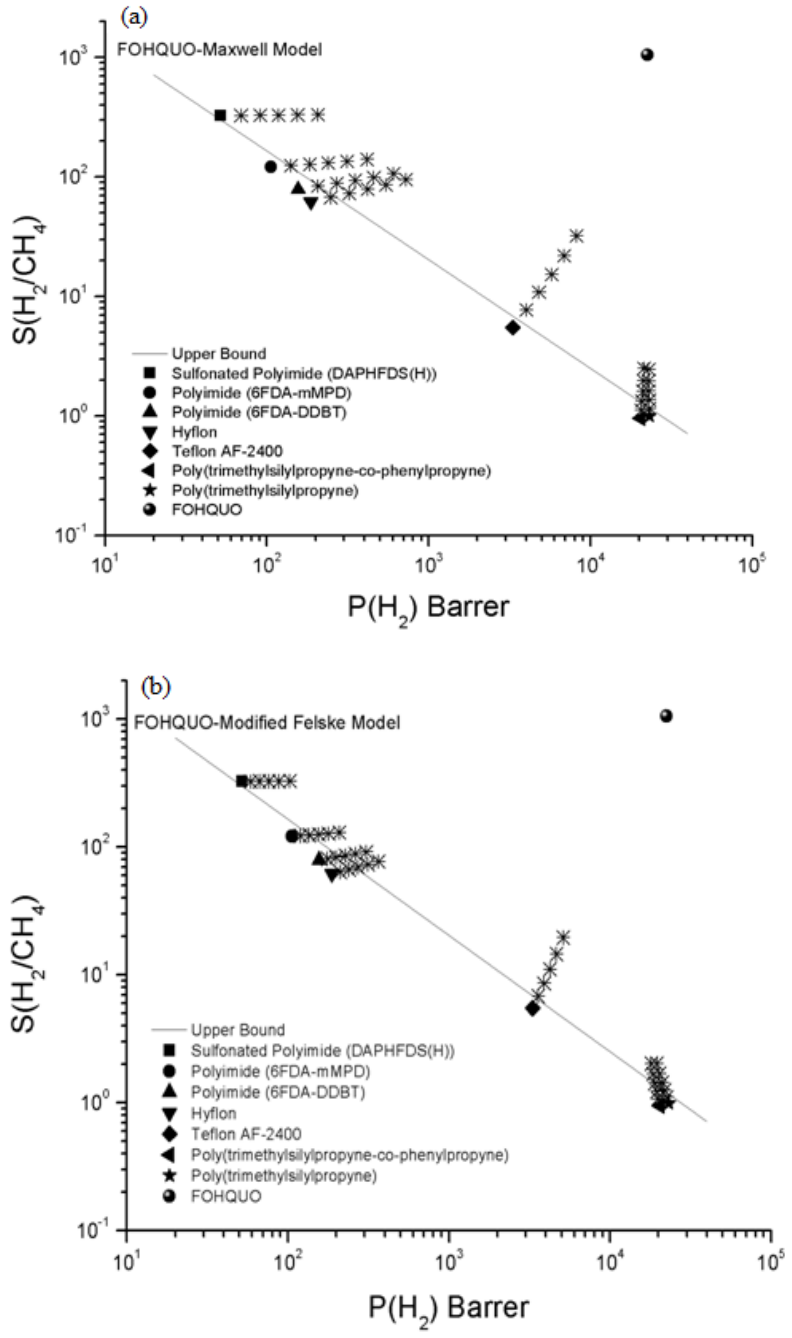

Figure 5.14: Predictions of Maxwell (a) and modified Felske (b) models for H_2 selectivity and H_2 permeability of FOHQUO-based MMMs

Figures 5.15 and 5.16 highlight the importance of MOF/polymer matching by showing the performance of LUNBEB-based MMMs. Addition of the MOFs from the fourth group into polymers increases the permeability of polyimides without changing their selectivities significantly, improves both selectivity and permeability of Teflon, and increases the selectivities of PTMSPs but decreases their permeability. This group will be helpful to enhance the performance of polymer membranes which already have high selectivity but low permeabilities such as polyimides. Incorporation of MOFs from the fourth group into this type of polymers will be sufficient to carry these polymers above the upper bound.

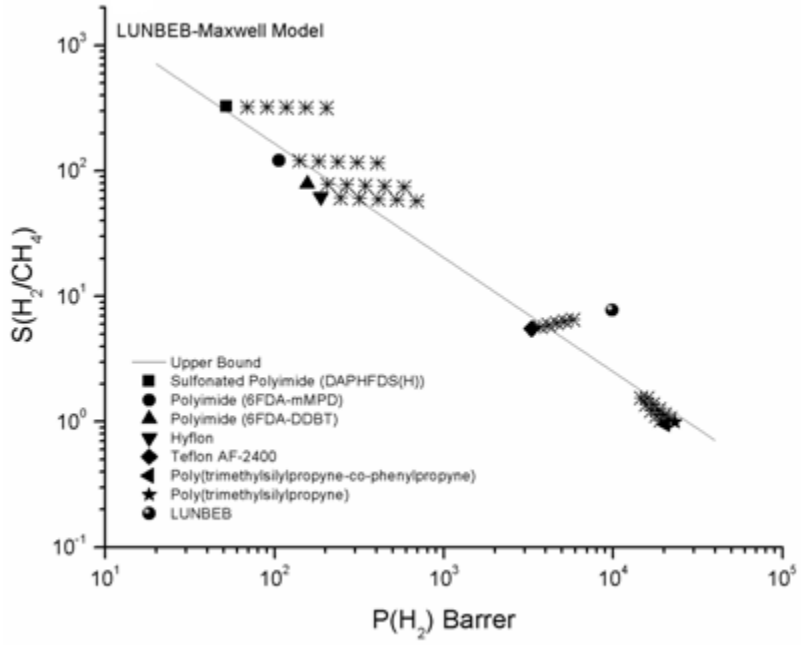

Figure 5.15: Predictions of Maxwell model for H_2 selectivity and H_2 permeability of LUNBEB-based MMMs

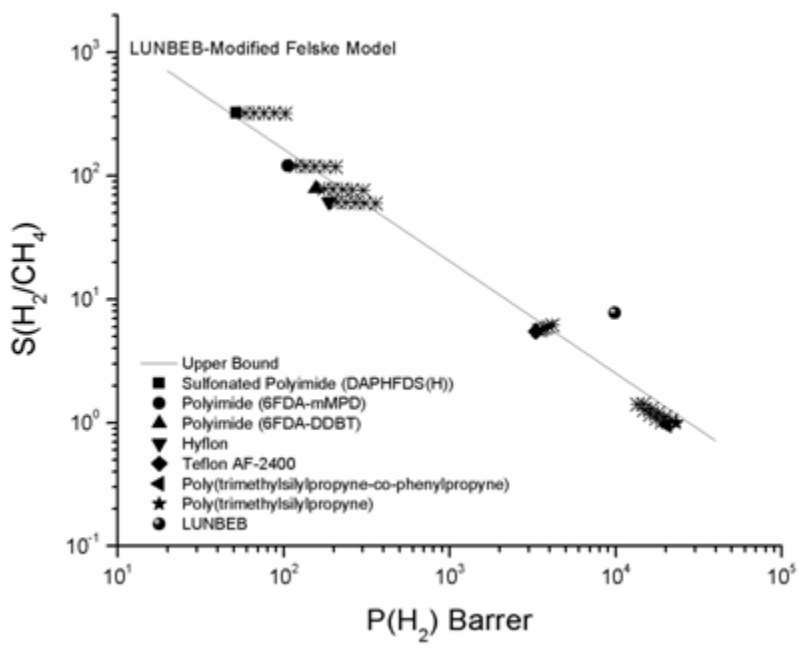

Figure 5.16: Predictions of modified Felske model for H_2 selectivity and H_2 permeability of LUNBEB-based MMMs

Finally, the impact of using a MOF which has extraordinarily high H_2 selectivity but low permeability as filler particles was investigated. As can be seen in Figures 5.17 (a) and (b), MMIF can significantly improve both selectivity and permeability of polyimides. For instance, the selectivity (permeability) of polyimide 6FDA-DDBT increases from 78.8 (156 Barrer) to 156 (225 Barrer) at a MOF volume fraction of 0.2. Thus, using a highly selective MOF with different types of polyimides will provide very promising membranes for H_2 separation. The permeabilities of Teflon and PTMSPs decreased when MMIF was used as filler particles although H_2 selectivity was increased. For example, permeability of Teflon (PTMSPs) decreased from 3300 (23200) to 2467 (14616) Barrer although selectivity was increased from 5.5 (0.99) to 6.8 (1.03). The reason for the decrease in the permeability is that MMIF has lower permeability than Teflon (PTMSPs).

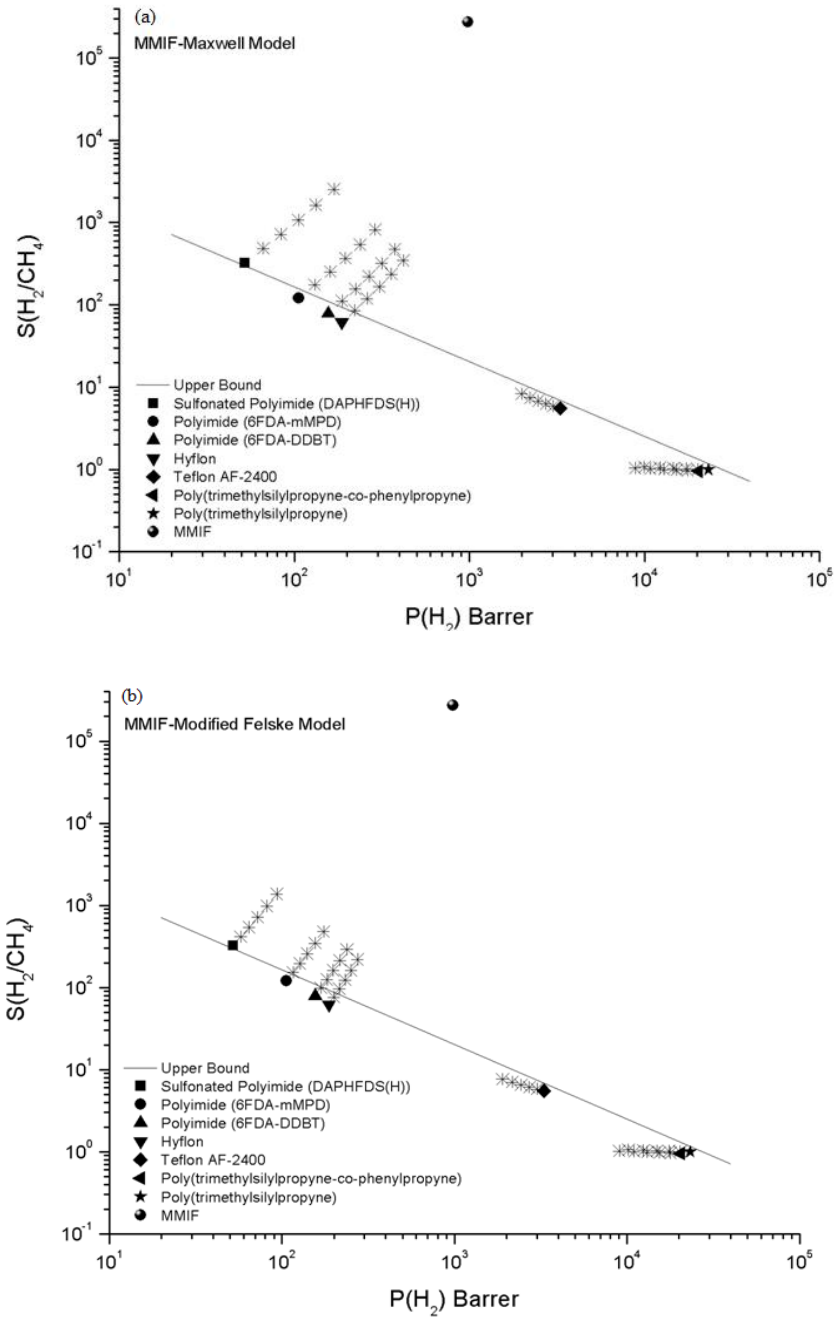

Figure 5.17: Predictions of Maxwell (a) and modified Felske (b) models for H_2 selectivity and H_2 permeability of MMIF-based MMMs

Erucar and Keskin[92] concluded that MOF/polymer matching is very important to enhance the separation performance of MMMs. The polymers that were studied for H_2/CH_4 separation were very close to upper bound. Thus, it was easy to carry them above the upper bound using a small fraction of MOFs. In this thesis, it was also aimed to find out the characteristics of MOFs to improve the performance of the polymer which are far away from the upper bound. For this motivation, the most widely used polymers, Matrimid, PSF and PDMS were studied in the following section.

5.4.1 Selecting appropriate MOF/polymer pairs for high performance MMMs

Matching appropriate MOF/polymer pairs is very important to obtain high performance MMMs. To develop a strategy for choosing the best MOF/polymer pair, real polymer/hypothetical MOF systems and hypothetical polymer/real MOF systems were investigated. Figures 5.18-5.22 show the performances of MMMs which are consisted of hypothetical MOFs and the commercial polymers, Matrimid, PSF and PDMS. These polymers were chosen since these polymers are generally used for fabrication of MOF-based MMMs. The Matrimid has high selectivity/low permeability (83.3, 17.5 Barrer), the PSF has medium selectivity/medium permeability (24.5/9.7 Barrer), and the PDMS has low selectivity/high permeability (0.74/577.6 Barrer), respectively[49, 54]. To determine the hypothetical MOFs, three different scenarios were considered:

1) increasing selectivity without changing permeability,

2) increasing both selectivity and permeability,

3) increasing permeability without changing selectivity.

The Maxwell and the modified Felske models were used to estimate the selectivity and permeability characteristics of the hypothetical MOFs. In Figure 5.18-5.22, the hypothetical MOFs were presented as: MOF-1 (scenario 1), MOF-2 (scenario 2), MOF-3 (scenario 2) and MOF-4 (scenario 3). The location of real MOF groups that was discussed

in the previous section was also demonstrated to compare the hypothetical MOFs with the real ones. The open symbols show performances of MMMs having hypothetical MOFs as filler particles and the close symbols are the performances of pure polymers and pure MOFs. The volume fraction of MOFs was increased from 0.1 to 0.5 to be consistent with the experiments.

In Figures 5.18 and 5.19, the performances of hypothetical MOFs/Matrimid-based MMMs were demonstrated. Results showed that pairing Matrimid with MOF-1 (MOF-4) increases only the selectivity (permeability) and carry Matrimid to approach the upper bound without exceeding it.

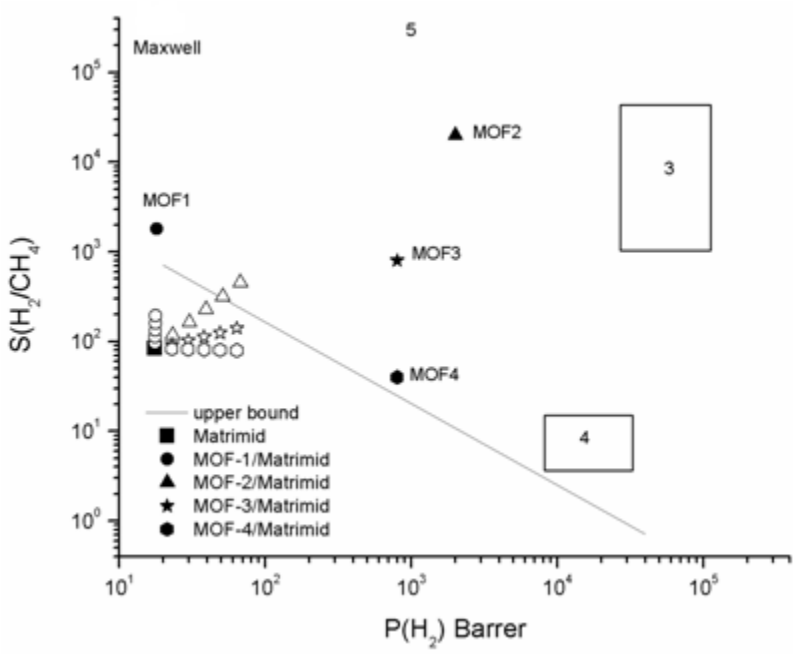

Figure 5.18: Effects of hypothetical MOFs on the performance of Matrimid-based MMMs. The open symbols are the predictions of Maxwell model for the performances of MMMs with filler volume fractions of 0.1, 0.2, 0.3, 0.4 and 0.5.

When MOF-2 was used as filler particles, Matrimid can surpass the upper bound. Matching Matrimid with a MOF which has similar permeability and selectivity characteristics to MOF-2 such as MMIF will yield the performance of MMMs. The MOFs of the third group can also carry Matrimid above the upper bound because they have higher selectivity and permeability than MOF-3.

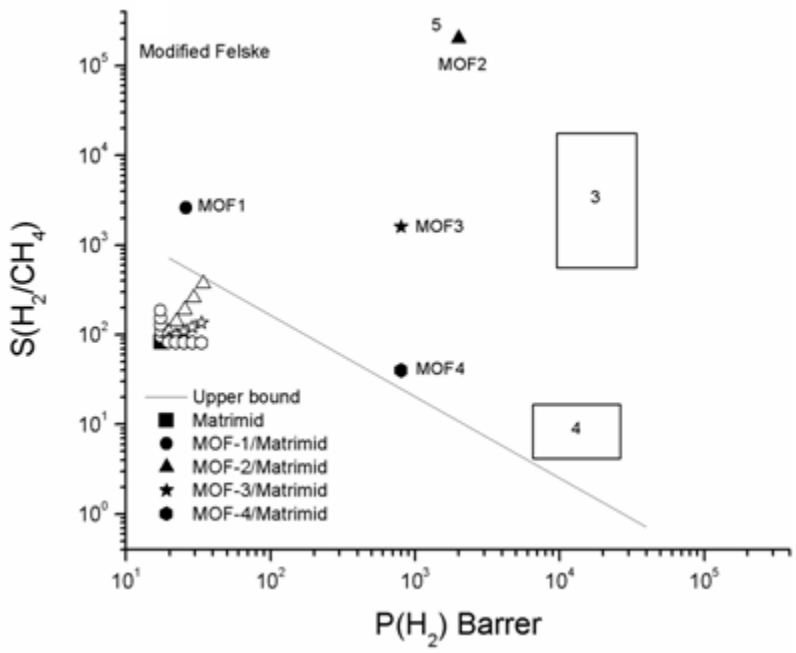

Figure 5.19: Effects of hypothetical MOFs on the performance of Matrimid-based MMMs. The open symbols are the predictions of modified Felske model for the performances of MMMs with filler volume fractions of 0.1, 0.2, 0.3, 0.4 and 0.5.

Figures 5.20-5.22 show that matching a MOF from the third group can improve both selectivity and permeability of PSF and PDMS membranes due to the location of the hypothetical MOF-3.

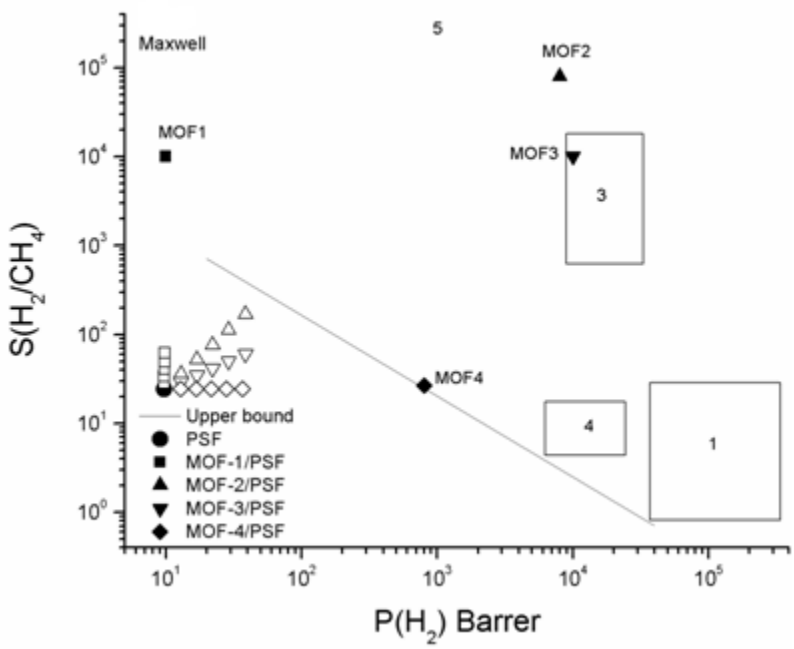

Figure 5.20: Effects of hypothetical MOFs on the performance of PSF-based MMMs. The open symbols are the predictions of Maxwell model for the performances of MMMs with filler volume fractions of 0.1, 0.2, 0.3, 0.4 and 0.5.

The first or fourth group MOFs enhances the performance of PSF and PDMS membranes by increasing the H_2 permeability of both polymers without decreasing selectivity since MOF-4 falls into the these groups. Unlike Matrimid, the hypothetical MOFs cannot carry PSF and PDMS above the upper bound as can be seen in Figures 5.20-5.22 due to the lower selectivity and permeability characteristics of PSF and PDMS compared to Matrimid. By using Figures 5.18-5.22, it is possible to estimate the performance of a MOF-based MMM by identifying the location of the MOF.

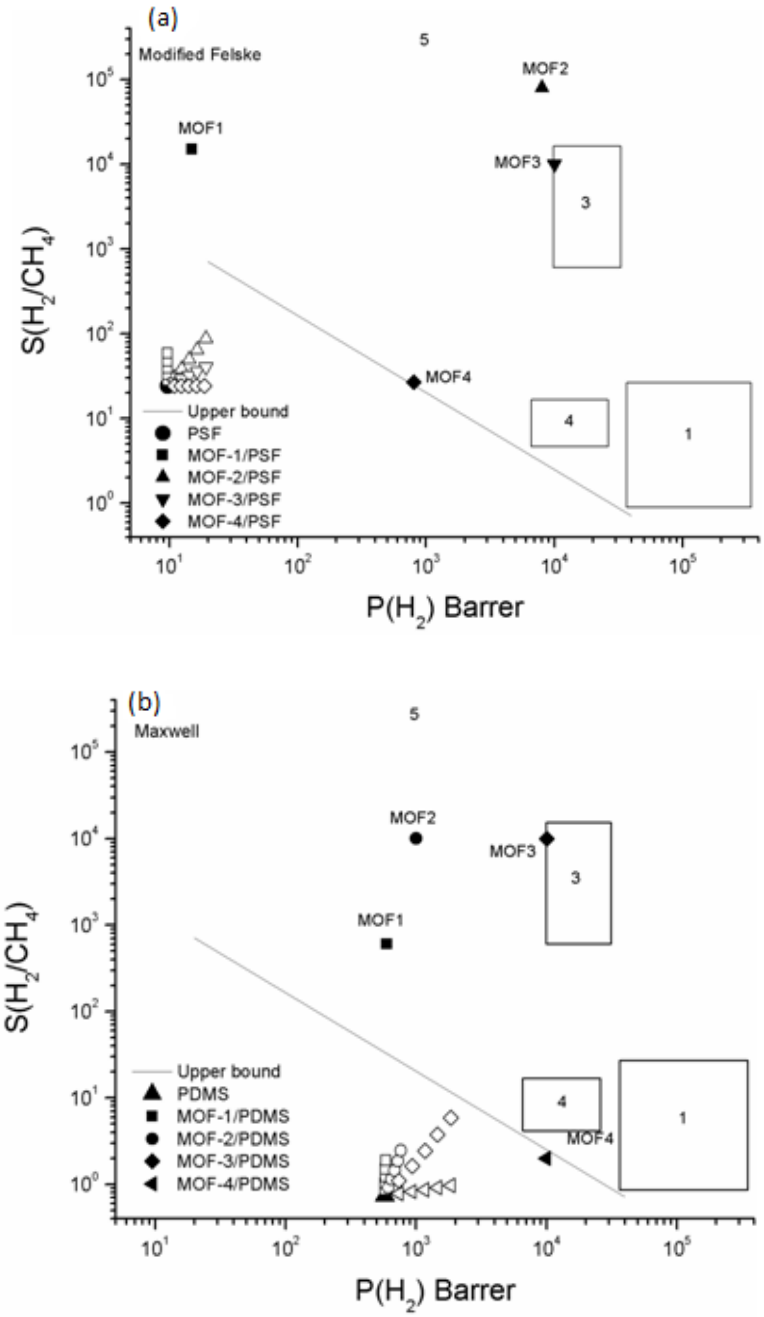

Figure 5.21: Effects of hypothetical MOFs on the performance of PSF(a) and PDMS(b)-based MMMs. The open symbols are the predictions of theoretical models for the performances of MMMs with filler volume fractions of 0.1, 0.2, 0.3, 0.4 and 0.5.

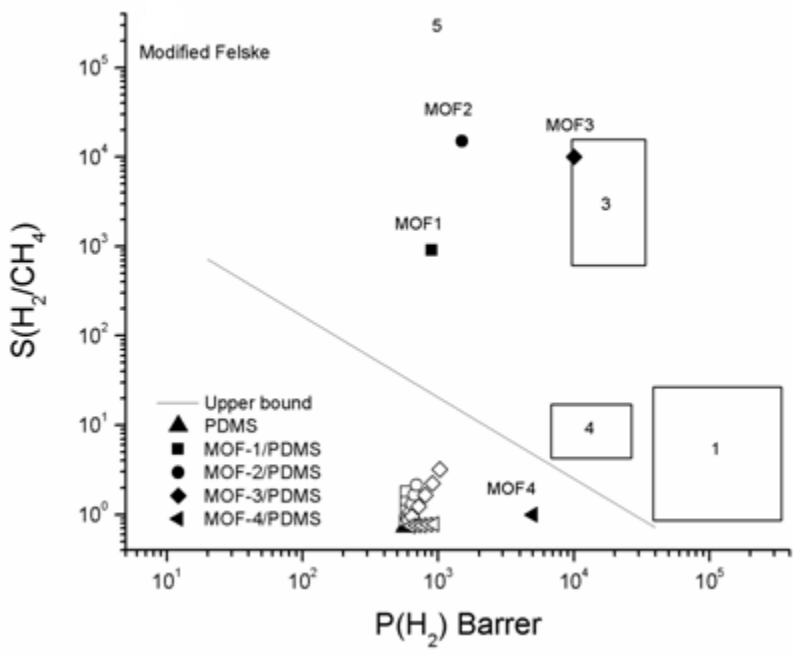

Figure 5.22: Effects of hypothetical MOFs on the performance of PDMS-based MMMs. The open symbols are the predictions of modified Felske model for the performances of MMMs with filler volume fractions of 0.1, 0.2, 0.3, 0.4 and 0.5.

Results so far show that in order to enhance the performance of MMMs, one should also consider pure polymer's characteristics in addition to pure MOF's characteristics to carry polymers above the upper bound. For this reason, hypothetical polymers were also examined to determine which polymers can yield the maximum performance when used in combination with MOFs. In Figure 5.23, six hypothetical polymers that lie along the Robeson's upper bound were presented for H_2/CH_4 separation. MIHHOA and ZUQPOQ were used as filler particles to represent a highly selective and a weakly selective MOF, respectively. The open (closed) stars represent the modified Felske model predictions for the performance of ZUQPOQ/polymer (MIHHOA/polymer) MMMs.

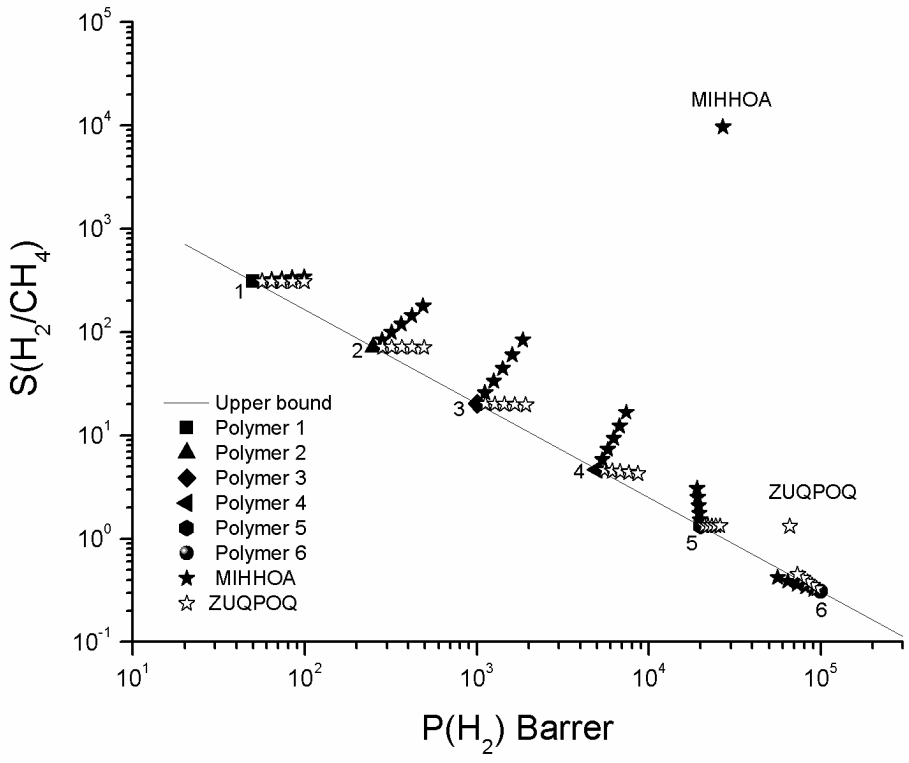

Figure 5.23: Predictions of modified Felske model for the performances of hypothetical polymer/MOF membranes. The open (closed) stars represent the predictions for the performance of ZUQPOQ/polymer (MIHHOA/polymer) MMMs.

Figure 5.23 demonstrates that if the polymer has a high H_2 selectivity, but low permeability such as polymer-1, adding a MOF can enhance the polymeric membrane's permeability with little or no change in the membrane's selectivity. Herein, the identity of the MOF appears to be unimportant. Similarly, the identity of the MOF is not critical for the polymer which has a very low H_2 selectivity but high permeability such as polymer-6. In this case, both ZUQPOQ and MIHHOA will increase the selectivity of the pure polymers at the expense of permeability. If the polymers have mediocre selectivity and permeability for H_2 such as polymer-2 and polymer-3, the identity of MOF has a critical

importance. For example, MIHHOA increases both permeability and selectivity. However, ZUQPOQ can only improve permeability without any important change in selectivity. For a polymer which is very permeable but has a very low H_2 selectivity like polymer-5, the identity of MOF also plays a critical role to affect the performance of MMMs. For instance, ZUQPOQ, which is a permeable but unselective MOF, increases permeability but decreases selectivity slightly. On the other hand, MIHHOA, which is a highly selective MOF, increases selectivity but slightly decreases the permeability.

To summarize, the presented ways for selecting appropriate MOF/polymer pairs will be very helpful to predict the performance of MMMs without detailed calculation. In addition, these ways will also play a critical role prior to fabrication of new MOF-based MMMs.

Chapter 6

CONCLUSIONS and FUTURE PROSPECTS

In this thesis, the potential of MOF-based MMMs for gas separations was investigated using molecular simulations and theoretical permeation models. Theoretical predictions gave good agreement with the experimental results of various fabricated MOF-based MMMs including IRMOF-1/Matrimid, Cu-BTC/Matrimid, Cu-BPY-HFS/Matrimid, CuBTC/PSF, and CuBTC/PDMS for CO_2/CH_4 and H_2/CH_4 separations. Combining detailed atomistic simulations with the theoretical permeation models, the performances of new-MOF based MMMs were estimated. Eighteen different MOFs (BACMOH10, BAHGUN, BIMDIL, FOHQUO, GITTIN, LUNBAX, LUNBEB, LUMZUO, MABJOP, MABJUV01, MIHHOA, MIHHIU, MIHHUG, MMIF , OFERUN, QAMXIL, ZUQPOQ and $Zn(bdc)(ted)_{0.5}$) were studied as fillers in various polymers that are chosen from the Robeson's upper bound[7] for CO_2/CH_4 and H_2/CH_4 separations.

Experimental results of fabricated MOF-based MMMs presented that MOF/polymer matching has significant importance to develop high performance MMMs. To identify the best MOF/polymer pairs via experimental studies is challenging since fabrication of MMMs is a difficult process. Since there are numerous MOFs in Cambridge Structure Database (CSD), screening MOFs in an efficient and easy way is very important for finding the best MOF/polymer combinations prior to experimental efforts. In this thesis, the methodologies for selecting appropriate MOF/polymer pairs for high performance MMMs were described. A correlation between the energy barrier to CO_2 diffusion and CO_2 selectivity of MOFs was found. Higher energy barrier to diffusion resulted in lower

permeability of CO_2. On the contrary, the CO_2/CH_4 selectivity increased as the energy barrier to CO_2 diffusion increased due to the more pronounced decrease in CH_4 permeability. This correlation gives a hint for the separation performance of MOFs prior to extensive calculation. In addition, MOFs that were studied in this thesis were categorized into 5 groups based on their H_2 permeability and selectivity to facilitate the selection of MOFs for H_2 separations. The impact of choosing MOFs from different groups was investigated by considering real polymer/hypothetical MOF systems and hypothetical polymer/real MOF systems.

Results demonstrated that performance of the polymers which have already high CO_2 or H_2 selectivity over CH_4, but requires higher permeability to surpass the upper bound can be easily enhanced by using a MOF as filler particles. The identity of MOF for this type of polymer is not important. Both a highly selective (MIHHOA) and a weakly selective MOF (ZUQPOQ) can increase the polymeric membrane's permeability with little or no change in the membrane's selectivity. However, the polymers which are close to the upper bound have generally mediocre selectivity and permeability for H_2 and CO_2, and in this case the identity of MOF has a critical role.

This thesis illustrated that MOFs having large pores connected with narrow pore windows such as MMIF are promising candidates for the CO_2/CH_4 and H_2/CH_4 separations since CH_4 permeability is very low compared to that of CO_2 due to the very slow diffusion of CH_4 in the narrow pores.

For the future prospects, it is very important to describe the limitations of this thesis. Firstly, in this thesis MOFs were assumed as rigid structures. However, some MOFs can be flexible, and their structure can change under high pressure. For example, MIL-53 has flexible framework and decomposition of its structure under pressure is known[66]. Herein, it is critical to determine a force field which considers intramolecular interactions.

Another limitation which has to be taken into consideration is the stability of MOF-based MMMs. It was assumed that MOF is ideal, a defect-free single crystal. This situation may not be possible for the fabrication of real MOF-based MMMs since the long-term stability of the MOF-based MMMs could not be predicted using molecular simulations. However, recent experimental studies showed that MOF-based MMMs are stable and a good adhesion between MOF particle and polymers was found.

Besides, some MOFs that were studied in this thesis do not have three dimensional porosities. Thus, the gas transport is non-isotropic. Kang et al. [97] demonstrated that filler orientation has to be taken into consideration if the filler has the similar permeability with that of the polymer. They presented that the filler orientation becomes important when the permeability of the filler is similar to that of the polymer. In this thesis, MOFs have generally higher permeabilities than the pure polymers. For this reason, the orientation effect was not included. However, for the future work, considering non-ideal membrane fabrication, orientation of MOFs may be investigated to determine the effects of defects or pinholes.

As a conclusion, this thesis will be helpful to determine appropriate MOF/polymer combinations for gas separation applications. The approaches that were described in this thesis will create many opportunities for the assessment of MOF-based MMMs.

BIBLIOGRAPHY

[1] R.W. Baker, Future Directions of Membrane Gas Separation Technology, Industrial & Engineering Chemistry Research, 41 (2002) 1393-1411.
[2] P. Bernardo, E. Drioli, G. Golemme, Membrane Gas Separation: A Review/State of the Art, Industrial & Engineering Chemistry Research, 48 (2009) 4638-4663.
[3] T.-S. Chung, L.Y. Jiang, Y. Li, S. Kulprathipanja, Mixed matrix membranes (MMMs) comprising organic polymers with dispersed inorganic fillers for gas separation, Progress in Polymer Science, 32 (2007) 483-507.
[4] P.S. Goh, A.F. Ismail, S.M. Sanip, B.C. Ng, M. Aziz, Recent advances of inorganic fillers in mixed matrix membrane for gas separation, Separation and Purification Technology, 81 (2011) 243-264.
[5] P. Pandey, R.S. Chauhan, Membranes for gas separation, Progress in Polymer Science, 26 (2001) 853-893.
[6] C.J. Geankoplis, in: Transport Processes and Separation Process Principles, Prentice Hall, (2008).
[7] L.M. Robeson, The upper bound revisited, Journal of Membrane Science, 320 (2008) 390-400.
[8] Y. Yampolskii, I. Pinnau , B.D. Freeman, in: Materials Science of Membranes for Gas and Vapor Separation, John Wiley & Sons, Ltd., England, (2006).
[9] P. Meares, The Diffusion of Gases Through Polyvinyl Acetate1, Journal of the American Chemical Society, 76 (1954) 3415-3422.
[10] L.M. Robeson, B.D. Freeman, D.R. Paul, B.W. Rowe, An empirical correlation of gas permeability and permselectivity in polymers and its theoretical basis, Journal of Membrane Science, 341 (2009) 178-185.
[11] B.D. Freeman, Basis of Permeability/Selectivity Tradeoff Relations in Polymeric Gas Separation Membranes, Macromolecules, 32 (1999) 375-380.
[12] A.Y. Alentiev, Y.P. Yampolskii, Free volume model and tradeoff relations of gas permeability and selectivity in glassy polymers, Journal of Membrane Science, 165 (2000) 201-216.
[13] T.T. Moore, W.J. Koros, Sorption in Zeolites Modified for Use in Organic−Inorganic Hybrid Membranes, Industrial & Engineering Chemistry Research, 47 (2007) 591-598.
[14] M. Shah, M.C. McCarthy, S. Sachdeva, A.K. Lee, H.-K. Jeong, Current Status of Metal–Organic Framework Membranes for Gas Separations: Promises and Challenges, Industrial & Engineering Chemistry Research, 51 (2011) 2179-2199.
[15] T.C. Merkel, B.D. Freeman, R.J. Spontak, Z. He, I. Pinnau, P. Meakin, A.J. Hill, Ultrapermeable, Reverse-Selective Nanocomposite Membranes, Science, 296 (2002) 519-522.

[16] D.Q. Vu, W.J. Koros, S.J. Miller, Mixed matrix membranes using carbon molecular sieves: I. Preparation and experimental results, Journal of Membrane Science, 211 (2003) 311-334.
[17] T.-S. Chung, S.S. Chan, R. Wang, Z. Lu, C. He, Characterization of permeability and sorption in Matrimid/C60 mixed matrix membranes, Journal of Membrane Science, 211 (2003) 91-99.
[18] I.F.J. Vankelecom, C. Dotremont, M. Morobé, J.B. Uytterhoeven, C. Vandecasteele, Zeolite-Filled PDMS Membranes. 1. Sorption of Halogenated Hydrocarbons, The Journal of Physical Chemistry B, 101 (1997) 2154-2159.
[19] S. Qiu, L. Wu, G. Shi, L. Zhang, H. Chen, C. Gao, Preparation and Pervaporation Property of Chitosan Membrane with Functionalized Multiwalled Carbon Nanotubes, Industrial & Engineering Chemistry Research, 49 (2010) 11667-11675.
[20] M. Eddaoudi, H. Li, O.M. Yaghi, Highly Porous and Stable Metal−Organic Frameworks: Structure Design and Sorption Properties, Journal of the American Chemical Society, 122 (2000) 1391-1397.
[21] M. Eddaoudi, H. Li, O.M. Yaghi, Highly Porous and Stable Metal-Organic Frameworks: Structure Design and Sorption Properties, Journal of the American Chemical Society, 122 (2000) 1391-1397.
[22] H.-C. Zhou, J.R. Long, O.M. Yaghi, Introduction to Metal–Organic Frameworks, Chemical Reviews, 112 (2012) 673-674.
[23] R. Banerjee, H. Furukawa, D. Britt, C. Knobler, M. O'Keeffe, O.M. Yaghi, Control of Pore Size and Functionality in Isoreticular Zeolitic Imidazolate Frameworks and their Carbon Dioxide Selective Capture Properties, Journal of the American Chemical Society, 131 (2009) 3875-3877.
[24] S.J. James, Metal organic frameworks, Chemical Society Reviews, 32 (2003) 276-288.
[25] J.L.C. Rowsell, O.M. Yaghi, Metal-organic frameworks: a new class of porous materials, Microporous and Mesoporous Materials, 73 (2004) 3-14.
[26] K. Uemura, R. Matsuda, S. Kitagawa, Flexible microporous coordination polymers, Journal of Solid State Chemistry, 178 (2005) 2420-2429.
[27] M.A. Aroon, A.F. Ismail, T. Matsuura, M.M. Montazer-Rahmati, Performance studies of mixed matrix membranes for gas separation: A review, Separation and Purification Technology, 75 (2010) 229-242.
[28] R. Mahajan, W.J. Koros, Mixed matrix membrane materials with glassy polymers. Part 1, Polymer Engineering & Science, 42 (2002) 1420-1431.
[29] R. Mahajan, W.J. Koros, Mixed matrix membrane materials with glassy polymers. Part 2, Polymer Engineering & Science, 42 (2002) 1432-1441.
[30] M. Khayet, T. Matsuura, Determination of surface and bulk pore sizes of flat-sheet and hollow-fiber membranes by atomic force microscopy, gas permeation and solute transport methods, Desalination, 158 (2003) 57-64.

[31] D.R. Paul, D.R. Kemp, The diffusion time lag in polymer membranes containing adsorptive fillers, Journal of Polymer Science: Polymer Symposia, 41 (1973) 79-93.
[32] S. Kulprathipanja, Hoffman, Estates, Neuzil, Richard W. , Downers, Grove, , Li, Norman N., Arlington, Heights., in: US Patent Allied-Signal Inc. (Morristown, NJ), US Patent, (1988).
[33] R. Mahajan, W.J. Koros, Factors Controlling Successful Formation of Mixed-Matrix Gas Separation Materials, Industrial & Engineering Chemistry Research, 39 (2000) 2692-2696.
[34] Y.C. Hudiono, T.K. Carlisle, A.L. LaFrate, D.L. Gin, R.D. Noble, Novel mixed matrix membranes based on polymerizable room-temperature ionic liquids and SAPO-34 particles to improve CO2 separation, Journal of Membrane Science, 370 (2011) 141-148.
[35] E. Karatay, H. Kalıpçılar, L. Yılmaz, Preparation and performance assessment of binary and ternary PES-SAPO 34-HMA based gas separation membranes, Journal of Membrane Science, 364 (2010) 75-81.
[36] S. Husain, W.J. Koros, Mixed matrix hollow fiber membranes made with modified HSSZ-13 zeolite in polyetherimide polymer matrix for gas separation, Journal of Membrane Science, 288 (2007) 195-207.
[37] G. Clarizia, C. Algieri, A. Regina, E. Drioli, Zeolite-based composite PEEK-WC membranes: Gas transport and surface properties, Microporous and Mesoporous Materials, 115 (2008) 67-74.
[38] A.L. Khan, A. Cano-Odena, B. Gutiérrez, C. Minguillón, I.F.J. Vankelecom, Hydrogen separation and purification using polysulfone acrylate–zeolite mixed matrix membranes, Journal of Membrane Science, 350 (2010) 340-346.
[39] M. Pan, Y.S. Lin, Template-free secondary growth synthesis of MFI type zeolite membranes, Microporous and Mesoporous Materials, 43 (2001) 319-327.
[40] E.A. Tomic, Thermal stability of coordination polymers, Journal of Applied Polymer Science, 9 (1965) 3745-3752.
[41] J.L.C. Rowsell, O.M. Yaghi, Metal–organic frameworks: a new class of porous materials, Microporous and Mesoporous Materials, 73 (2004) 3-14.
[42] M. Eddaoudi, J. Kim, N. Rosi, D. Vodak, J. Wachter, M. O'Keeffe, O.M. Yaghi, Systematic Design of Pore Size and Functionality in Isoreticular MOFs and Their Application in Methane Storage, Science, 295 (2002) 469-472.
[43] A. Vishnyakov, P.I. Ravikovitch, A.V. Neimark, M. Bülow, Q.M. Wang, Nanopore Structure and Sorption Properties of Cu−BTC Metal−Organic Framework, Nano Letters, 3 (2003) 713-718.
[44] B. Zornoza, C. Tellez, J. Coronas, J. Gascon, F. Kapteijn, Metal organic framework based mixed matrix membranes: An increasingly important field of research with a large application potential, Microporous and Mesoporous Materials,in press, DOI: 10.1016/j.bbr.2011.03.031.

[45] Y. Zhang, I.H. Musselman, J.P. Ferraris, K.J. Balkus Jr, Gas permeability properties of Matrimid® membranes containing the metal-organic framework Cu–BPY–HFS, Journal of Membrane Science, 313 (2008) 170-181.
[46] S. Kim, E. Marand, High permeability nano-composite membranes based on mesoporous MCM-41 nanoparticles in a polysulfone matrix, Microporous and Mesoporous Materials, 114 (2008) 129-136.
[47] M.J.C. Ordoñez, K.J. Balkus Jr, J.P. Ferraris, I.H. Musselman, Molecular sieving realized with ZIF-8/Matrimid® mixed-matrix membranes, Journal of Membrane Science, 361 (2010) 28-37.
[48] H. Yehia, T.J. Pisklak, J.P. Ferraris, K.J. Balkus, I.H. Musselman, Methane facilitated transport using copper(II) biphenyl dicarboxylatetriethylenediamine/poly(3-acetoxyethylthiophene) mixed matrix membranes, Polymeric Preprints, 45 (2004) 35-36.
[49] A. Car, C. Stropnik, K.V. Peinemann, Hybrid membrane materials with different metal-organic frameworks (MOFs) for gas separation, Desalination, 200 (2006) 424-426.
[50] S. Basu, A.L. Khan, A.Cano-Odena, C. Liub, I.F.J. Vankelecom, Membrane-based technologies for biogas separations, Chemical Society Reviews, 39 (2010) 750–768.
[51] Y. Zhang, I.H. Musselman, J.P. Ferraris, K.J. Balkus, Gas Permeability Properties of Matrimid® Membranes Containing the Metal-Organic Framework Cu–BPY-HFS, Journal of Membrane Science, 313 (2008) 170-181.
[52] J. Hu, H. Cai, H. Ren, Y. Wei, Z. Xu, H. Liu, Y. Hu, Mixed-Matrix Membrane Hollow Fibers of $Cu_3(BTC)_2$ MOF and Polyimide for Gas Separation and Adsorption, Industrial & Engineering Chemistry Research, 49 (2010) 12605–12612.
[53] S. Basu, A. Cano-Odena, I.F.J. Vankelecom, Asymmetric Matrimid/[$Cu_3(BTC)_2$] mixed matrix membranes for gas separations, Journal of Membrane Science, 362 (2010) 478-487.
[54] E.V. Perez, K.J. Balkus, J.P. Ferraris, I.H. Musselman, Mixed-matrix membranes containing MOF-5 for gas separations, Journal of Membrane Science, 328 (2009) 165–173.
[55] R. Adams, C. Carson, J. Ward, R. Tannenbaum, W. Koros, Metal organic framework mixed matrix membranes for gas separations, Microporous and Mesoporous Materials, 131 (2010) 13–20.
[56] T.X. Yang, Y.C. Xiao, T.S. Chung, Poly-/metal-benzimidazole nano-composite membranes for hydrogen purification, Energy & Environmental Science, 4 (2011) 4171-4180.
[57] K. Diaz, L. Garrido, M. Lopez-Gonzalez, L.F. del Castillo, E. Riande, CO2 Transport in Polysulfone Membranes Containing Zeolitic Imidazolate Frameworks As Determined by Permeation and PFG NMR Techniques, Macromolecules, 43 (2010) 316-325.
[58] X.L. Liu, Y.S. Li, G.Q. Zhu, Y.J. Ban, L.Y. Xu, W.S. Yang, An Organophilic Pervaporation Membrane Derived from Metal-Organic Framework Nanoparticles for

Efficient Recovery of Bio-Alcohols, Angewandte Chemie International Edition, 50 (2011) 10636-10639.
[59] C. Zhang, Y. Dai, J.R. Johnson, O. Karvan, W.J. Koros, High performance ZIF-8/6FDA-DAM mixed matrix membrane for propylene/propane separations, Journal of Membrane Science, 389 (2012) 34-42.
[60] T.-H. Bae, J.S. Lee, W. Qiu, W.J. Koros, C.W. Jones, S. Nair, A High-Performance Gas-Separation Membrane Containing Submicrometer-Sized Metal–Organic Framework Crystals, Angewandte Chemie International Edition, 49 (2010) 9863–9866.
[61] D.S. Sholl, Understanding macroscopic diffusion of adsorbed molecules in crystalline nanoporous materials via atomistic simulations, Accounts of Chemical Research, 39 (2006) 403-411.
[62] J.A. Wesselingh, R. Krishna, Mass Transfer in Multicomponent Mixtures, Delft University Press, Delft, (2000).
[63] R.E. Kesting, A.K. Fritzsche, Polymeric Gas Separation Membranes, John Wiley & Sons, Inc., New York, (1993).
[64] T. Duren, Y.-S. Bae, R.Q. Snurr, Using molecular simulation to characterise metal-organic frameworks for adsorption applications, Chemical Society Reviews, 38 (2009) 1237-1247.
[65] B.Smith, Phase diagrams of Lennard-Jones fluids, Journal of Chemical Physics, 96 (1992) 8639-8640.
[66] R.B. Getman, Y.-S. Bae, C.E. Wilmer, R.Q. Snurr, Review and Analysis of Molecular Simulations of Methane, Hydrogen, and Acetylene Storage in Metal–Organic Frameworks, Chemical Reviews, 112 (2011) 703-723.
[67] Q. Xu, C. Zhong, A General Approcah for Estimating Framework Charges in Metal Organic Frameworks, The Journal of Physical Chemistry C, 114 (2010) 5035-5042.
[68] S. Keskin, Atomistic Simulations for Adsorption, Diffusion, and Separation of Gas Mixtures in Zeolite Imidazolate Frameworks, The Journal of Physical Chemistry C, 115 (2011) 800-807.
[69] V. Buch, Path-Integral Simulations of Mixed Para-D-2 and Ortho-D-2 Clusters - the Orientational Effects, Journal of Chemical Physics, 100 (1994) 7610-7629.
[70] M.G. Martin, J.I. Siepmann, Transferable Potentials for Phase Equilibria. 1. United-Atom Description of *n*-Alkanes,The Journal of Physical Chemistry B, 102 (1998) 2569-2577.
[71] V. Buch, Path-Integral Simulations of Mixed Para-D-2 and Ortho-D-2 Clusters - The Orientational Effects, Journal of Chemical Physics, 100 (1994) 7610-7629.
[72] M.G. Martin, J.I. Siepmann, Transferable Potentials for Phase Equilibria. 1. United-Atom Description of n-Alkanes, The Journal of Physical Chemistry B, 102 (1998) 2569-2577.

[73] B. Chen, J.J. Potoff, J.I. Siepmann, Monte Carlo Calculations for Alcohols and Their Mixtures with Alkanes. Transferable Potentials for Phase Equilibria. 5. United-Atom Description of Primary, Secondary, and Tertiary Alcohols, The Journal of Physical Chemistry B, 105 (2001) 3093-3104.
[74] A.K. Rappe, C.J. Casewit, K.S. Colwell, W.A. Goddard, W.M. Skiff, UFF, a full periodic table force field for molecular mechanics and molecular dynamics simulations, Journal of the American Chemical Society, 114 (1992) 10024-10035.
[75] S.L. Mayo, B.D. Olafson, W.A. Goddard, Dreiding - A Generic Force-Field For Molecular Simulations, Journal of Physical Chemistry, 94 (1990) 8897-8909.
[76] T. Düren, L. Sarkisov, O.M. Yaghi, R.Q. Snurr, Design of New Materials for Methane Storage, Langmuir, 20 (2004) 2683-2689.
[77] D. Frenkel, B. Smit, in: Understanding Molecular Simulation from Algorithms to Applications, Academic Press, (2002).
[78] P.H. Hünenberger, Thermostat Algorithms for Molecular Dynamics Simulations Advanced Computer Simulation, in: C. Dr. Holm, K. Prof. Dr. Kremer (Eds.), Springer Berlin / Heidelberg, 173 (2005) 130-130.
[79] M.A. Aroon, A.F. Ismail, T. Matsuura, M.M. Montazer-Rahmati, Performance studies of mixed matrix membranes for gas separation: A review, Separation and Purification Technology, 75 (2010) 229-242.
[80] B. Shimekit, H. Mukhtara, T. Murugesan, Prediction of the relative permeability of gases in mixed matrix membranes, Journal of Membrane Science, 373 (2011) 152-159.
[81] J.C. Maxwell, A Treatise on Electricity and Magnetism, Dover Publications, New York, (1954).
[82] D.A.G. Bruggeman, Berechnung Verschiedener Physikalischer Konstanten Von Heterogenen Substanzen. I. Dielektrizitatskonstanten Und Leitfahigkeiten Der Mischkorper Aus Isotropen Substanzen, Annalen der Physik, 416 (1935) 636-679.
[83] T.B. Lewis, L.E. Nielsen, Dynamic mechanical properties of particulate-filled composites, Journal of Applied Polymer Science, 14 (1970) 1449-1471.
[84] R. Pal, Permeation models for mixed matrix membranes, Journal of Colloid and Interface Science, 317 (2008) 191-198.
[85] R. Pal, New models for thermal conductivity of particulate composites, Journal of Reinforced Plastics and Composites, 26 (2007) 643–651.
[86] T.T. Moore, R. Mahajan, D.Q. Vu, W.J. Koros, Hybrid membrane materials comprising organic polymers with rigid dispersed phases, AIChE J., 50 (2004) 311-321.
[87] J.D. Felske, Effective thermal conductivity of composite spheres in a continuous medium with contact resistance, International Journal of Heat and Mass Transfer, 47 (2004) 3453–3461.

[88] I. Erucar, S. Keskin, Screening Metal–Organic Framework-Based Mixed-Matrix Membranes for CO2/CH4 Separations, Industrial & Engineering Chemistry Research, 50 (2011) 12606-12616.
[89] S. Basu, A. Cano-Odena, I.F.J. Vankelecom, Asymmetric Matrimid/[$Cu_3(BTC)_2$] mixed matrix membranes for gas separations, Journal of Membrane Science, 362 (2010) 478-487.
[90] Y. Zhang, I.H. Musselman, J.P. Ferraris, K.J. Balkus, Gas Permeability Properties of Matrimid® Membranes Containing the Metal-Organic Framework Cu–BPY-HFS, Journal of Membrane Science, 313 (2008) 170-181.
[91] D.Q. Vu, W.J. Koros, S.J. Miller, Mixed matrix membranes using carbon molecular sieves. II. Modeling permeation behavior, Journal of Membrane Science, 211 (2003) 335–348.
[92] I. Erucar, S. Keskin, Computational screening of metal organic frameworks for mixed matrix membrane applications, Journal of Membrane Science, 407–408 (2012) 221-230.
[93] Y.-S. Bae, K.L. Mulfort, H. Frost, P. Ryan, S. Punnathanam, L.J. Broadbelt, J.T. Hupp, R.Q. Snurr, Separation of CO2 from CH4 Using Mixed-Ligand Metal−Organic Frameworks, Langmuir, 24 (2008) 8592-8598.
[94] D. Wu, C. Wang, B. Liu, D. Liu, Q. Yang, C. Zhong, Large-scale computational screening of metal-organic frameworks for CH4/H2 separation, AIChE Journal, 58 (2012) 2078-2084.
[95] S. Keskin, High CO_2 Selectivity of A Microporous Metal-Imidazolate Framework: A Molecular Simulation Study, Industrial & Engineering Chemistry Research, 50 (2011) 8230-8236.
[96] I. Erucar, S. Keskin, Separation of CO_2 Mixtures Using Zn(bdc)$(ted)_{0.5}$ Membranes and Composites: A Molecular Simulation Study, The Journal of Physical Chemistry C, 15 (2011) 13637-13644.
[97] D.-Y. Kang, C.W. Jones, S. Nair, Modeling molecular transport in composite membranes with tubular fillers, Journal of Membrane Science, 381 (2011) 50-63.

APPENDIX

A: Predicting performances of new MOF-based MMMs for CO_2/CH_4 separation

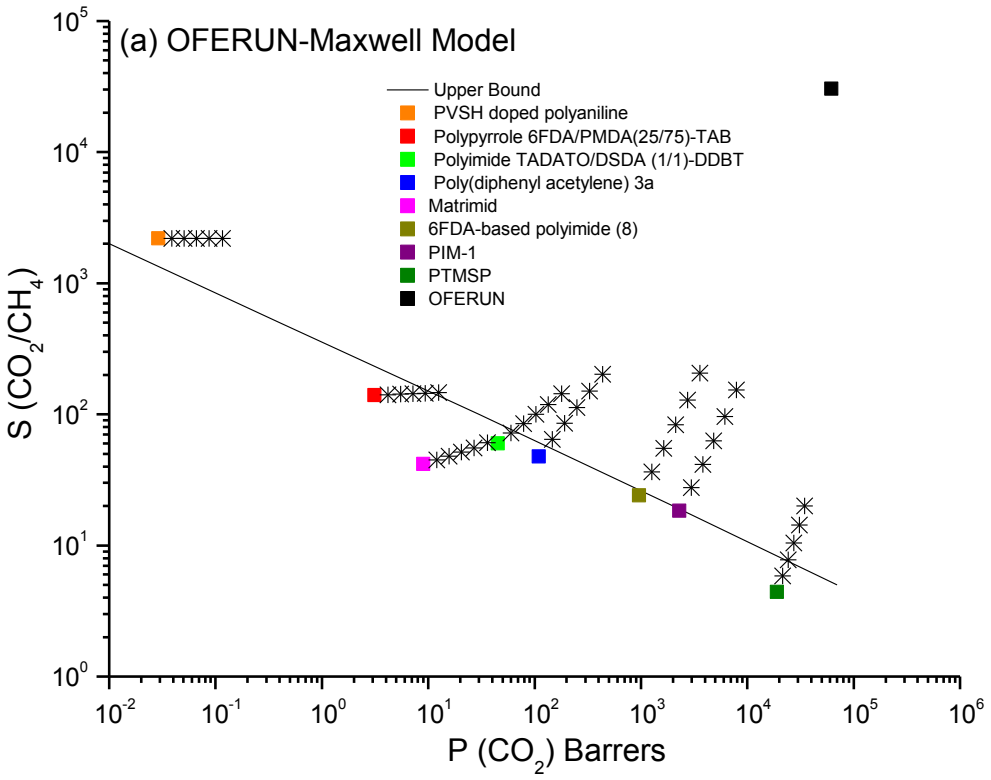

Figure A1 (a): Maxwell model predictions for CO_2 selectivity and permeability of MMMs having filler particles of OFERUN. Squares represent the performance of pure polymers and pure MOFs, stars represent the performance of MMMs with filler particles having volume fractions 0.1, 0.2, 0.3, 0.4 and 0.5.

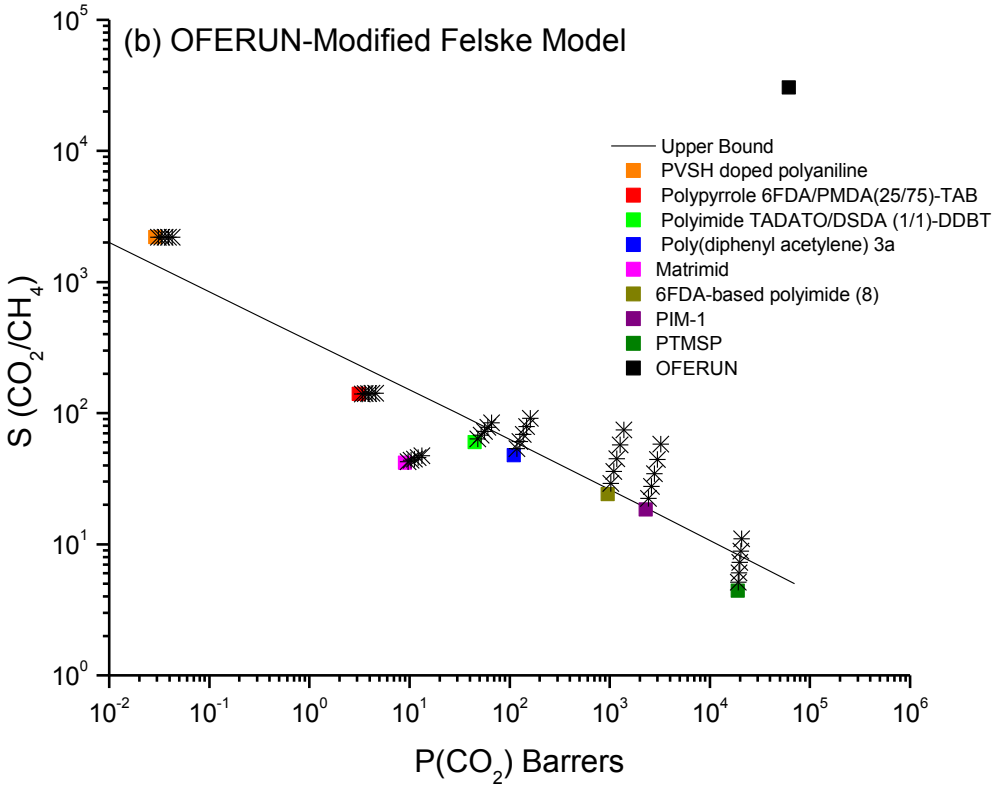

Figure A1 (b): Modified Felske model predictions for CO_2 selectivity and permeability of MMMs having filler particles of OFERUN. Squares represent the performance of pure polymers and pure MOFs, stars represent the performance of MMMs with filler particles having volume fractions 0.1, 0.2, 0.3, 0.4 and 0.5.

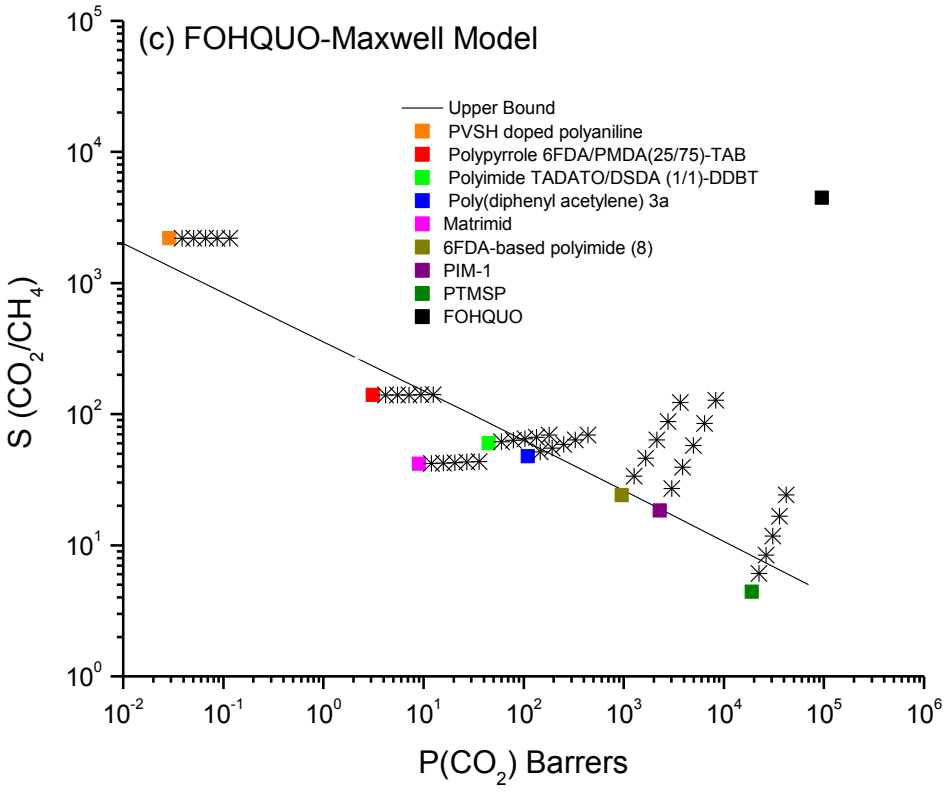

Figure A1 (c): Maxwell model predictions for CO_2 selectivity and permeability of MMMs having filler particles of FOHQUO. Squares represent the performance of pure polymers and pure MOFs, stars represent the performance of MMMs with filler particles having volume fractions 0.1, 0.2, 0.3, 0.4 and 0.5.

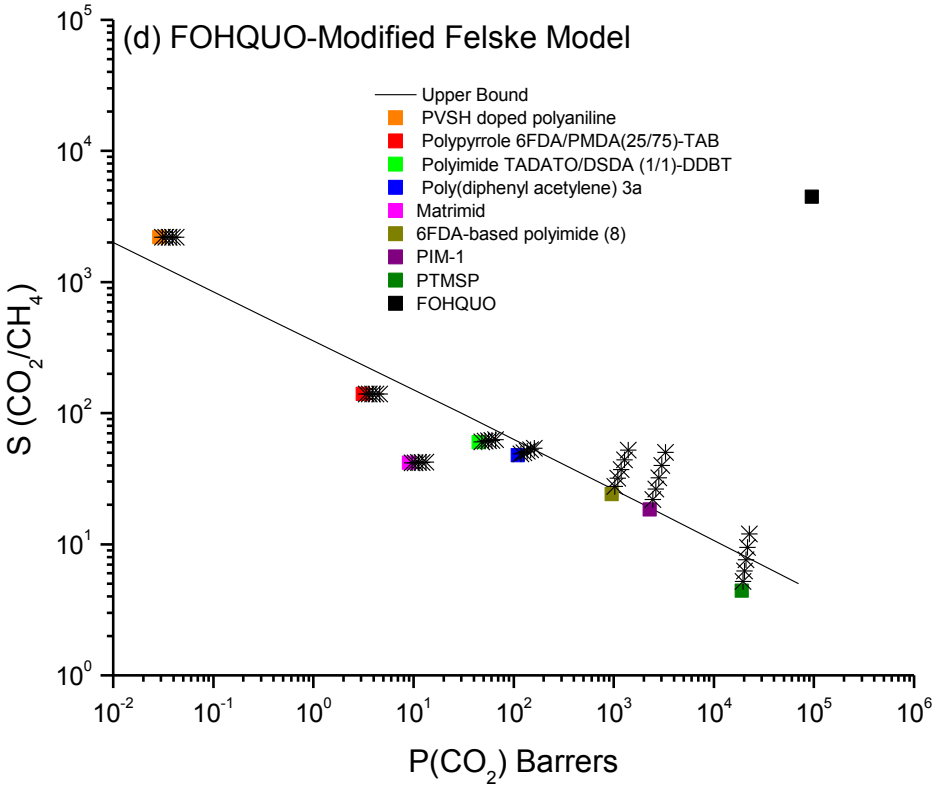

Figure A1 (d): Modified Felske model predictions for CO_2 selectivity and permeability of MMMs having filler particles of FOHQUO. Squares represent the performance of pure polymers and pure MOFs, stars represent the performance of MMMs with filler particles having volume fractions 0.1, 0.2, 0.3, 0.4 and 0.5.

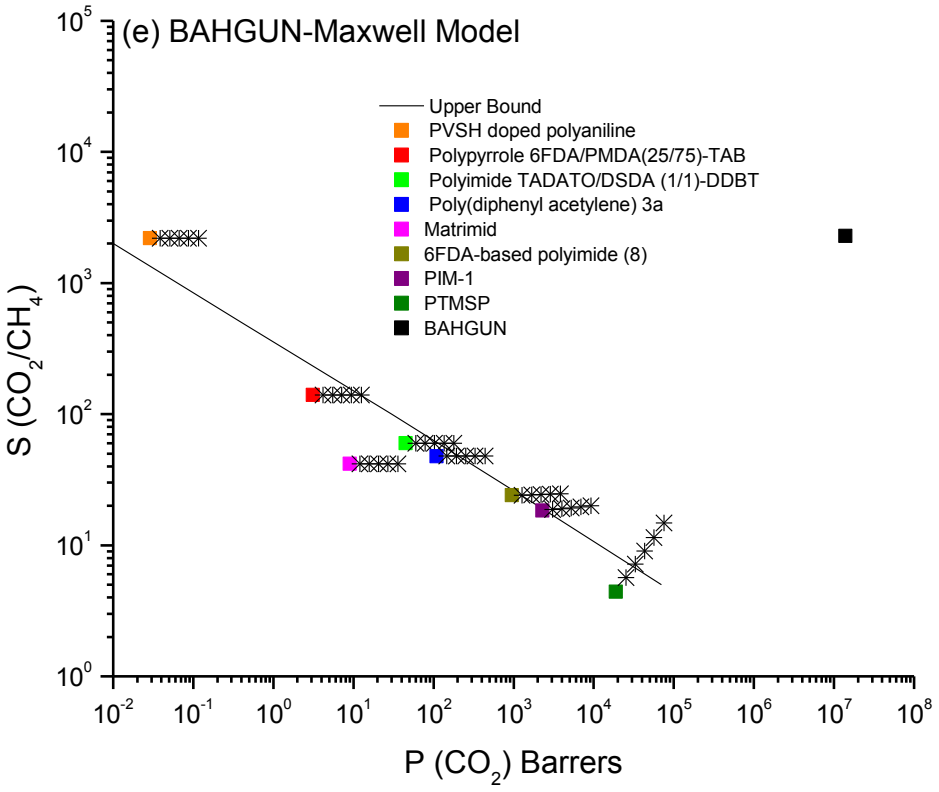

Figure A1 (e): Maxwell model predictions for CO_2 selectivity and permeability of MMMs having filler particles of BAHGUN. Squares represent the performance of pure polymers and pure MOFs, stars represent the performance of MMMs with filler particles having volume fractions 0.1, 0.2, 0.3, 0.4 and 0.5.

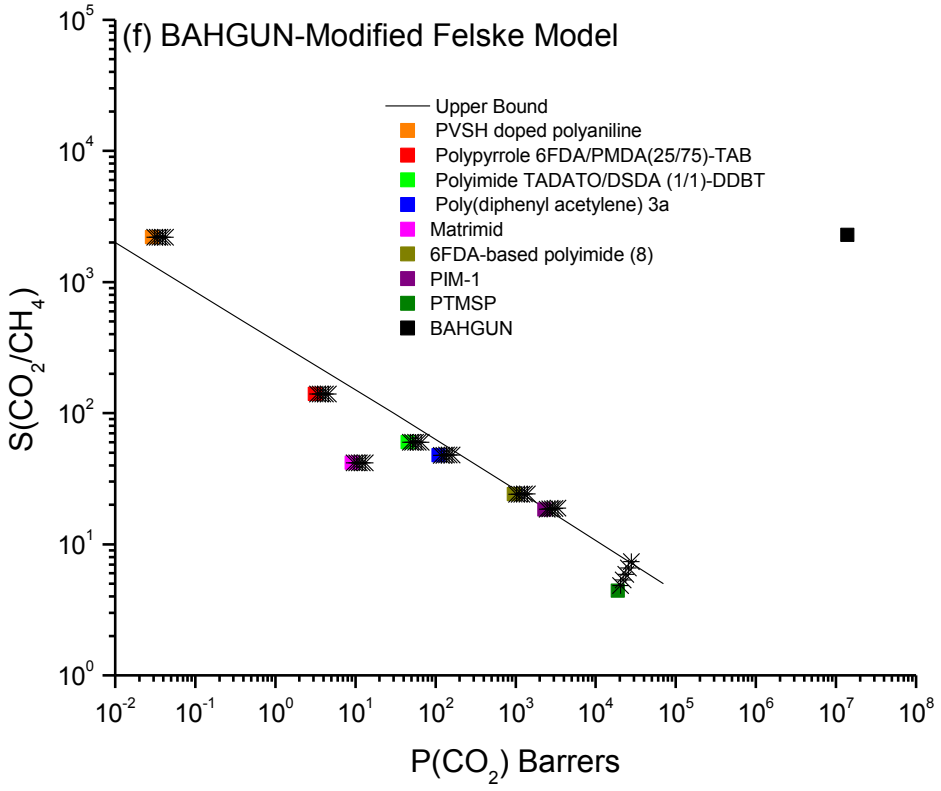

Figure A1 (f): Modified Felske model predictions for CO_2 selectivity and permeability of MMMs having filler particles of BAHGUN. Squares represent the performance of pure polymers and pure MOFs, stars represent the performance of MMMs with filler particles having volume fractions 0.1, 0.2, 0.3, 0.4 and 0.5.

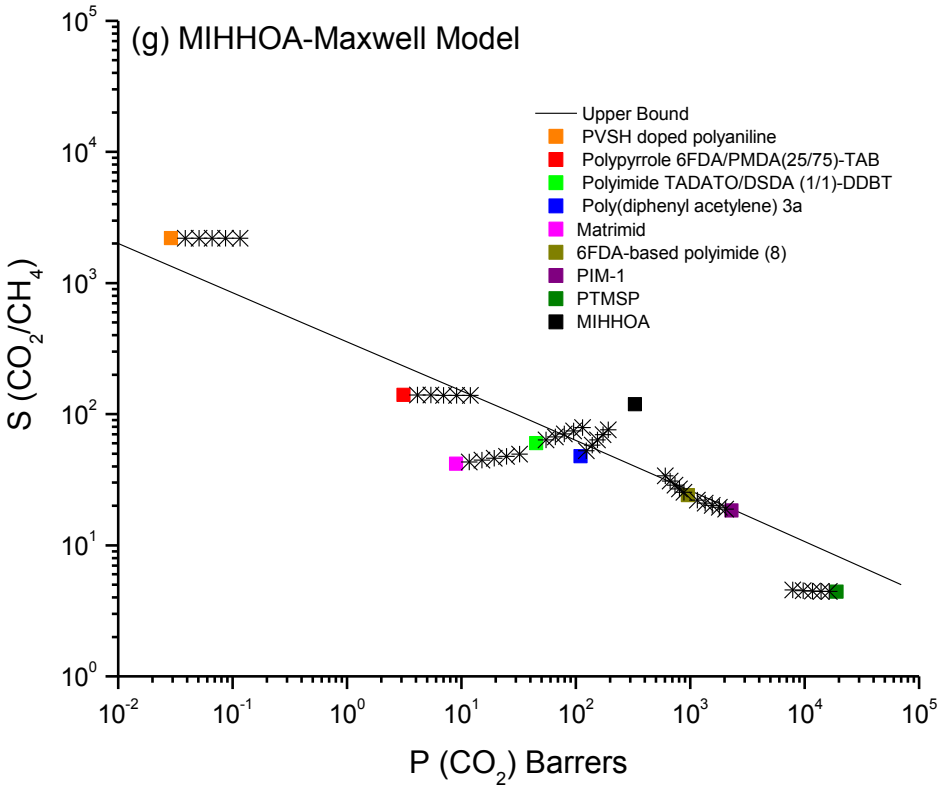

Figure A1 (g): Maxwell model predictions for CO_2 selectivity and permeability of MMMs having filler particles of MIHHOA. Squares represent the performance of pure polymers and pure MOFs, stars represent the performance of MMMs with filler particles having volume fractions 0.1, 0.2, 0.3, 0.4 and 0.5.

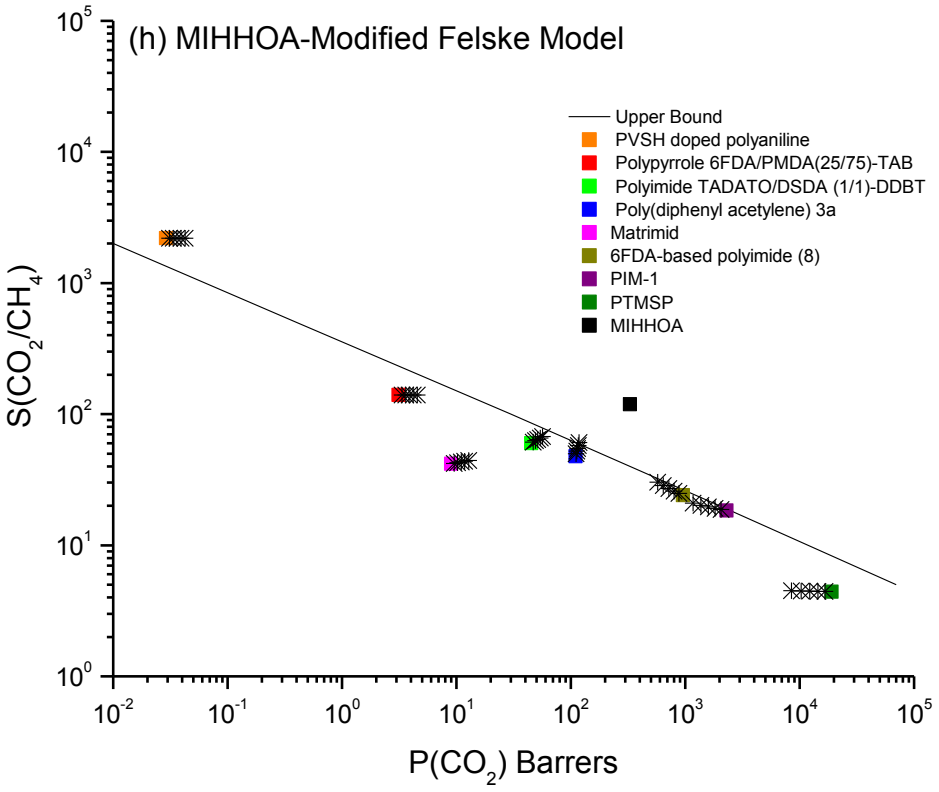

Figure A1 (h): Modified Felske model predictions for CO_2 selectivity and permeability of MMMs having filler particles of MIHHOA. Squares represent the performance of pure polymers and pure MOFs, stars represent the performance of MMMs with filler particles having volume fractions 0.1, 0.2, 0.3, 0.4 and 0.5.

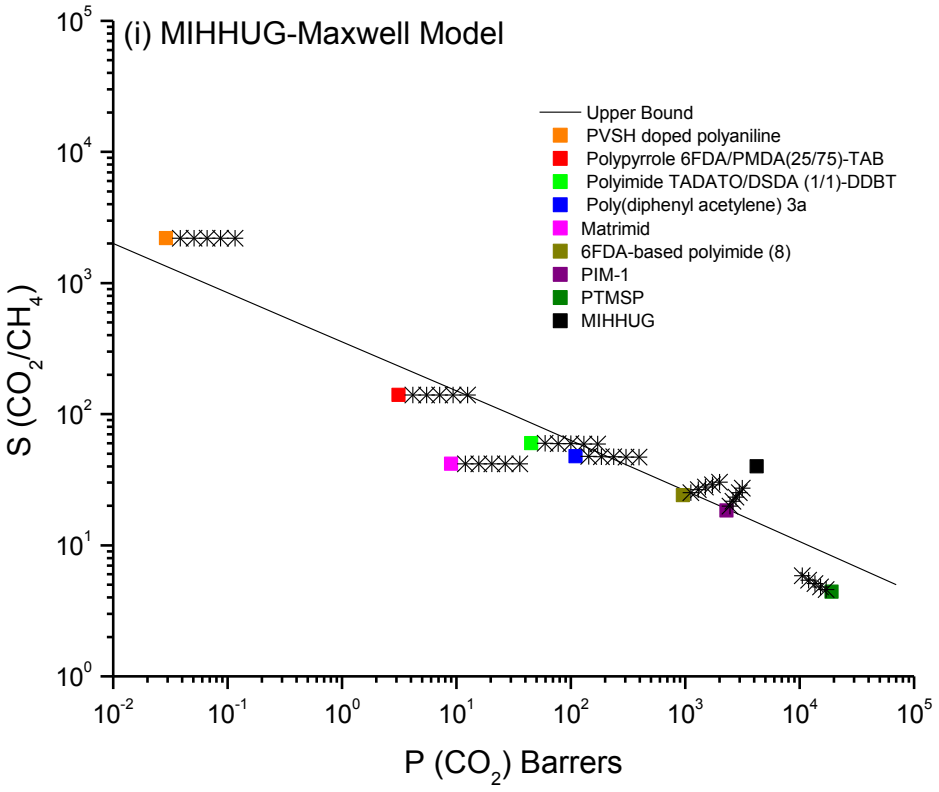

Figure A1 (i): Maxwell model predictions for CO_2 selectivity and permeability of MMMs having filler particles of MIHHUG. Squares represent the performance of pure polymers and pure MOFs, stars represent the performance of MMMs with filler particles having volume fractions 0.1, 0.2, 0.3, 0.4 and 0.5.

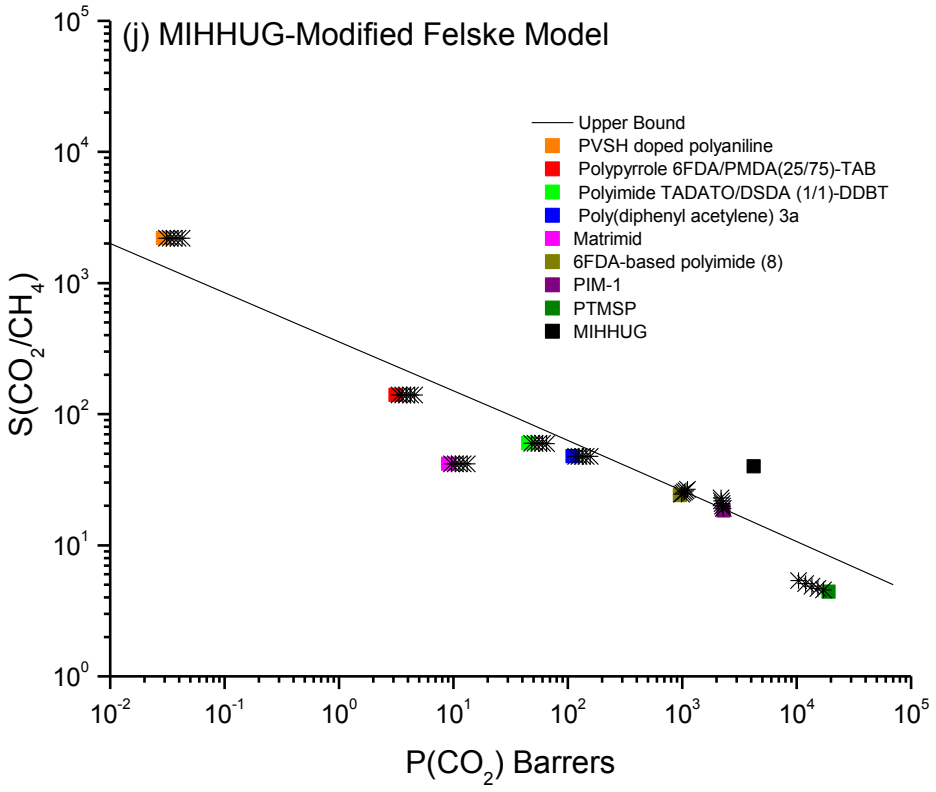

Figure A1 (j): Modified Felske model predictions for CO_2 selectivity and permeability of MMMs having filler particles of MIHHUG. Squares represent the performance of pure polymers and pure MOFs, stars represent the performance of MMMs with filler particles having volume fractions 0.1, 0.2, 0.3, 0.4 and 0.5.

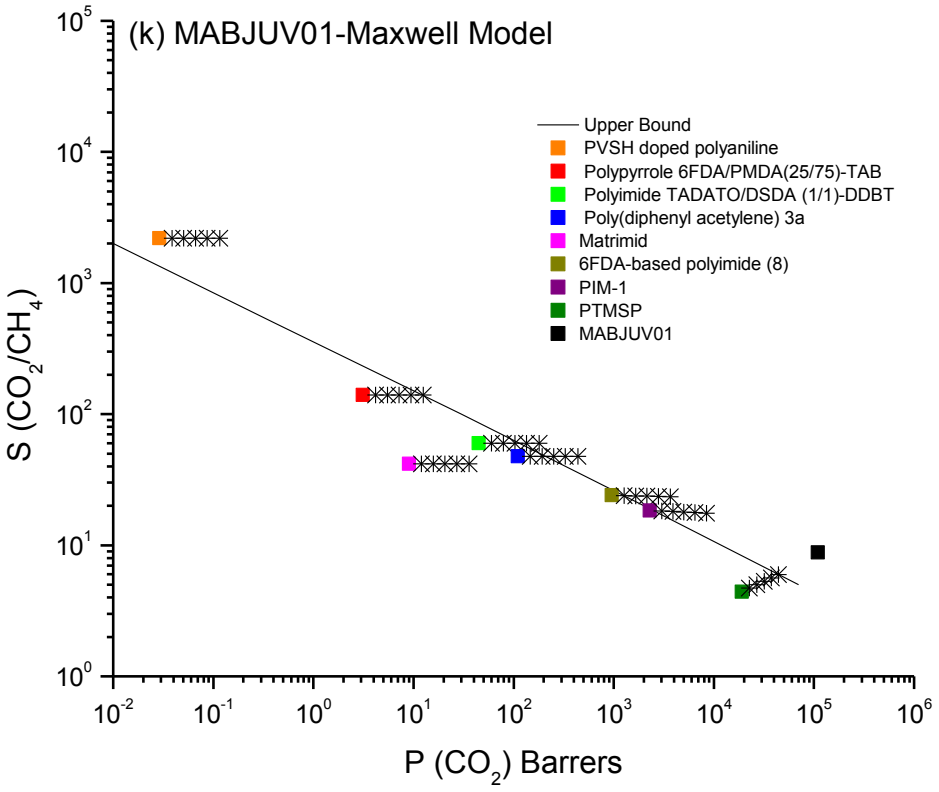

Figure A1 (k): Maxwell model predictions for CO_2 selectivity and permeability of MMMs having filler particles of MABJUV01. Squares represent the performance of pure polymers and pure MOFs, stars represent the performance of MMMs with filler particles having volume fractions 0.1, 0.2, 0.3, 0.4 and 0.5.

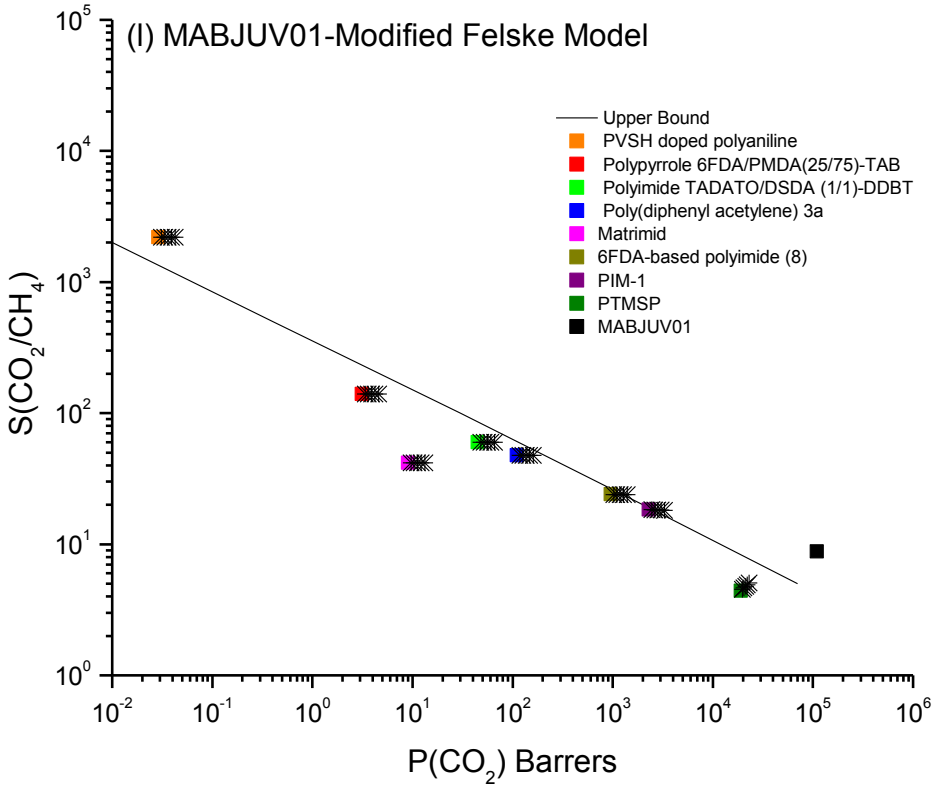

Figure A1 (l): Modified Felske model predictions for CO_2 selectivity and permeability of MMMs having filler particles of MABJUV01. Squares represent the performance of pure polymers and pure MOFs, stars represent the performance of MMMs with filler particles having volume fractions 0.1, 0.2, 0.3, 0.4 and 0.5.

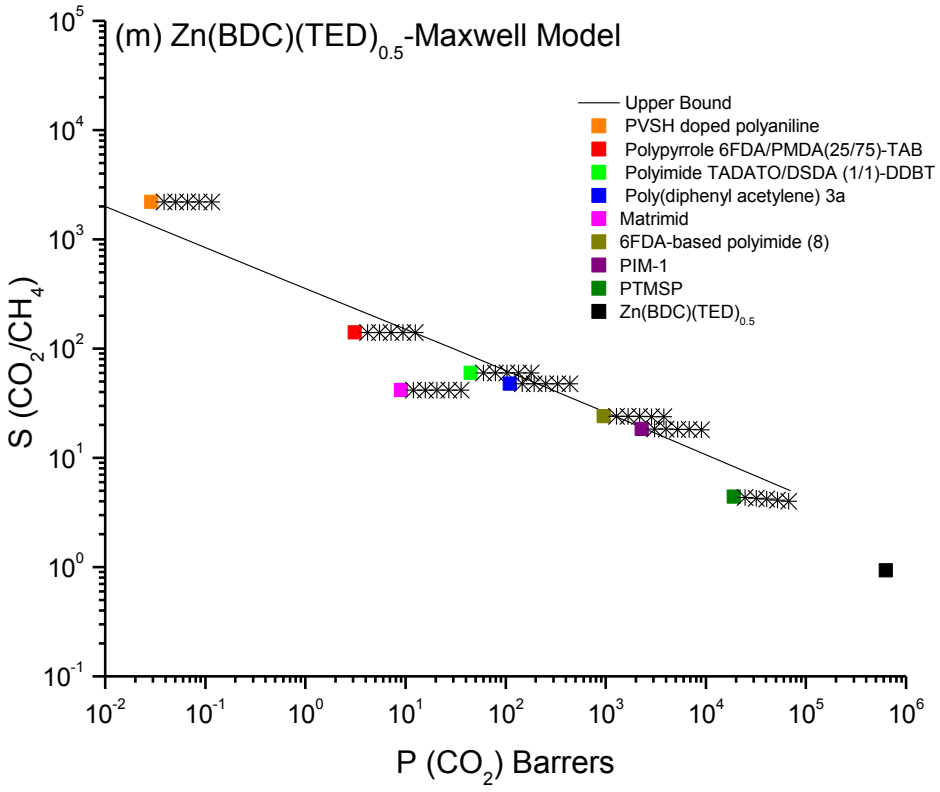

Figure A1 (m): Maxwell model predictions for CO_2 selectivity and permeability of MMMs having filler particles of $Zn(BDC)(TED)_{0.5}$. Squares represent the performance of pure polymers and pure MOFs, stars represent the performance of MMMs with filler particles having volume fractions 0.1, 0.2, 0.3, 0.4 and 0.5.

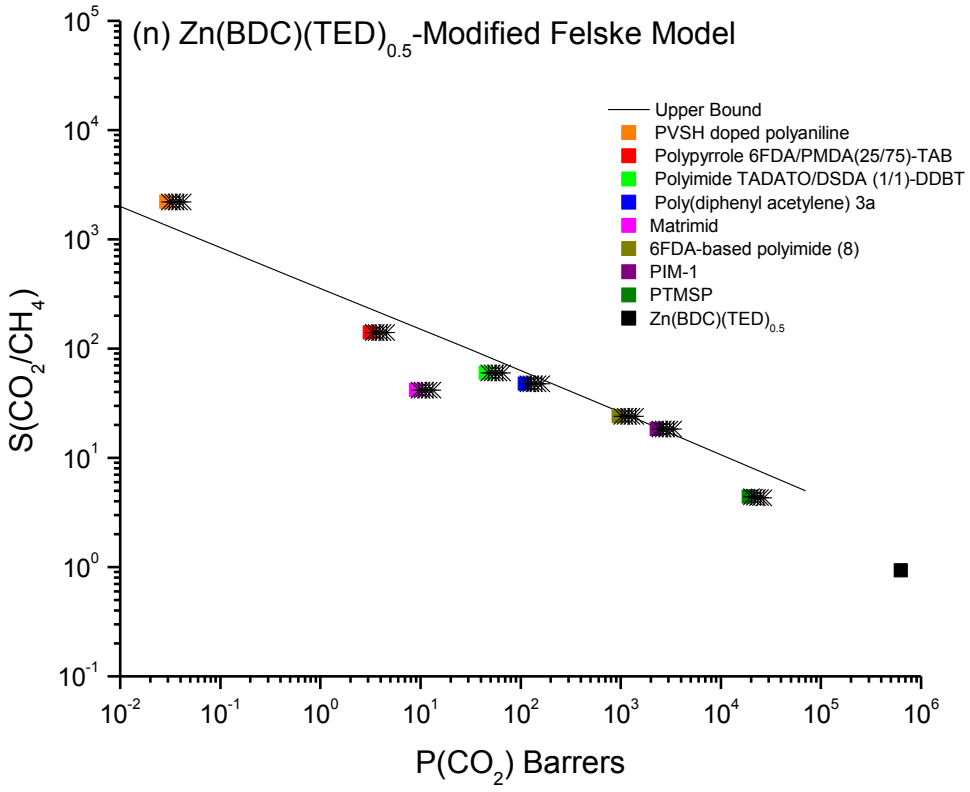

Figure A1 (n): Modified Felske model predictions for CO_2 selectivity and permeability of MMMs having filler particles of $Zn(BDC)(TED)_{0.5}$. Squares represent the performance of pure polymers and pure MOFs, stars represent the performance of MMMs with filler particles having volume fractions 0.1, 0.2, 0.3, 0.4 and 0.5

B: Predicting performances of new MOF-based MMMs for H_2/CH_4 separation

Table B1: Comparison of experiments and theory predictions for H_2 and CH_4 permeabilities (Barrer) through MOF-based MMMs.

	Loading % of MOF		0	5	10	20	30	40
IRMOF-1/ Matrimid	Experiments[1]	P_{H2}	24.4		29.90	38.30	53.80	
		P_{CH4}	0.22		0.22	0.34	0.45	
	Modified Felske	P_{H2}			31.45	38.08	44.46	
		P_{CH4}			0.28	0.34	0.40	
	Maxwell	P_{H2}			39.39	54.29	69.25	
		P_{CH4}			0.36	0.49	0.62	
Cu-BPY-HFS/ Matrimid	Experiments[2]	P_{H2}	17.50		16.91	16.75	20.34	26.74
		P_{CH4}	0.21		0.24	0.36	0.38	0.59
	Modified Felske	P_{H2}			20.17	23.21	27.14	31.79
		P_{CH4}			0.24	0.28	0.33	0.38
	Maxwell	P_{H2}			24.32	32.65	44.30	59.42
		P_{CH4}			0.29	0.39	0.53	0.71
CuBTC/PDMS	Experiments[3]	P_{H2}	577.55		756.03	724.51	815.54	836.52
		P_{CH4}	783.58		905.47	853.23	853.23	888.06
	Modified Felske	P_{H2}			619.00	665.38	717.78	777.56
		P_{CH4}			839.68	902.46	973.35	1054.24
	Maxwell	P_{H2}			768.59	1006.97	1312.79	1719.37
		P_{CH4}			1042.20	1364.76	1778.31	2327.68
CuBTC/PSF	Experiments[3]	P_{H2}	9.70	11.20	14.90			
		P_{CH4}	0.40	0.40	1.15			
	Modified Felske	P_{H2}		10.04	10.40			
		P_{CH4}		0.41	0.43			
	Maxwell	P_{H2}		11.23	12.93			
		P_{CH4}		0.46	0.53			

Table B2: Structural information and gas permeation properties of MOFs.

MOF	Unit Cell Parameters		P_{H2} (Barrer)	P_{CH4} (Barrer)	$S_{H2/CH4}$
	a, b, c	α, β, γ			
BACMOH10	16.05, 9.62, 7.46	90, 90, 90	$5.29x10^{4}$	16.60	$3.19x10^{3}$
BAHGUN	5.00, 24.97, 11.10	90, 98.86, 90	$6.18x10^{4}$	$6.05x10^{3}$	10.22
BIMDIL	8.47, 8.47, 14.44	90, 90, 90	$1.39x10^{5}$	$1.05x10^{5}$	1.33
FOHQUO	6.88, 14.36, 15.80	90, 101.69, 90	$2.25x10^{4}$	21.40	$1.05x10^{3}$
GITTIN	17.27, 17.27, 17.27	90, 90, 90	$3.92x10^{4}$	$1.19x10^{3}$	32.87
LUMZUO	14.68, 22.06, 18.50	90, 94.62, 90	$1.77x10^{4}$	$2.87x10^{3}$	6.19
LUNBAX	14.60, 21.97, 18.29	90, 94.94, 90	$1.77x10^{4}$	$2.14x10^{3}$	8.28
LUNBEB	14.45, 21.88, 18.03	90, 94.88, 90	$9.89x10^{3}$	$1.27x10^{3}$	7.76
MABJOP	21.01, 13.05, 8.53	90, 100.68, 90	$3.70x10^{4}$	345.00	107.11
MABJUV01	21.19, 13.19, 8.52	90, 100.31, 90	$4.29x10^{4}$	$1.24x10^{4}$	3.45
MIHHIU	13.86, 15.10, 19.43	90, 90, 90	$7.09x10^{4}$	$3.32x10^{3}$	21.35
MIHHOA	13.78, 15.06, 19.35	90, 90, 90	$2.70x10^{4}$	2.78	$9.70x10^{3}$
MIHHUG	13.87, 15.12, 19.30	90, 90, 90	$4.74x10^{4}$	106.00	447.41
MMIF	15.14, 15.14, 8.98	90, 90, 120	981.00	$3.58x10^{-3}$	$2.74x10^{5}$
OFERUN	16.99, 16.99, 17.00	90, 90, 90	$1.36x10^{4}$	2.02	$6.73x10^{3}$
QAMXIL	10.45, 19.99 ,10.01	90, 90, 90	$2.53x10^{5}$	$7.00x10^{4}$	3.61
ZUQPOQ	11.07, 21.82, 7.95	90, 90, 90	$6.61x10^{4}$	$5.00x10^{4}$	1.32

Table B3: Maxwell and modified Felske model predictions for gas permeation in MMMs for H_2/CH_4 separation using *Sulfonated Polyimide (DAPHFDS(H))*, [ϕ =0.3], (*P_{CH4}, P_{H2}: Barrer)

	Maxwell Model			**Modified Felske Model**		
Name	**P_{CH4}**	**P_{H2}**	**$S_{(H2/CH4)}$**	**P_{CH4}**	**P_{H2}**	**$S_{(H2/CH4)}$**
PURE POLYMER	0.16	52.00	325.00	0.16	52.00	325.00
BACMOH10	0.36	118.58	331.70	0.23	76.37	328.08
BAHGUN	0.37	118.62	324.36	0.24	76.38	324.71
BIMDIL	0.37	118.75	324.71	0.24	76.42	324.87
FOHQUO	0.36	118.20	328.99	0.23	76.26	326.84
GITTIN	0.37	118.48	324.07	0.24	76.34	324.57
LUMZUO	0.37	118.03	322.77	0.24	76.21	323.97
LUNBAX	0.37	118.03	322.78	0.24	76.21	323.98
LUNBEB	0.37	117.38	321.05	0.24	76.02	323.17
MABJOP	0.37	118.46	324.26	0.24	76.34	324.66
MABJUV01	0.37	118.51	324.06	0.24	76.35	324.57
MIHHIU	0.37	118.65	324.46	0.24	76.39	324.75
MIHHOA	0.32	118.31	366.19	0.22	76.29	344.02
MIHHUG	0.36	118.54	325.32	0.23	76.36	325.15
MMIF	0.10	105.92	1067.71	0.10	72.39	716.17
OFERUN	0.31	117.78	379.49	0.22	76.14	350.25
QAMXIL	0.37	118.80	324.84	0.24	76.44	324.93
ZUQPOQ	0.37	118.63	324.39	0.24	76.39	324.72

Table B4: Maxwell and modified Felske model predictions for gas permeation in MMMs for H_2/CH_4 separation using *Polyimide (6FDA-mMPD)*, [ϕ =0.3], (*P_{CH4}, P_{H2}: Barrer)

	Maxwell Model			**Modified Felske Model**		
Name	**P_{CH4}**	**P_{H2}**	**$S_{(H2/CH4)}$**	**P_{CH4}**	**P_{H2}**	**$S_{(H2/CH4)}$**
PURE POLYMER	0.88	106.00	121.00	0.88	106.00	121.00
BACMOH10	1.79	241.12	135.05	1.22	155.51	127.49
BAHGUN	2.00	241.29	120.55	1.29	155.60	120.84
BIMDIL	2.00	241.84	120.79	1.29	155.78	120.95
FOHQUO	1.83	239.58	131.05	1.23	155.05	125.66
GITTIN	2.00	240.72	120.44	1.29	155.39	120.74
LUMZUO	2.00	238.86	119.38	1.29	154.83	120.25
LUNBAX	2.00	238.86	119.41	1.29	154.83	120.27
LUNBEB	2.00	236.24	118.18	1.29	154.04	119.69
MABJOP	1.99	240.63	120.91	1.29	155.56	120.80
MABJUV01	2.00	240.85	120.31	1.29	155.43	120.68
MIHHIU	2.00	241.42	120.65	1.29	155.72	120.90
MIHHOA	1.26	240.02	191.20	1.01	155.18	153.91
MIHHUG	1.96	240.99	122.74	1.28	155.47	121.80
MMIF	0.54	195.72	365.80	0.55	140.42	257.00
OFERUN	1.14	237.85	208.74	0.95	154.53	162.52
QAMXIL	2.00	242.04	120.89	1.28	155.36	120.96
ZUQPOQ	2.00	241.35	120.54	1.29	155.58	120.79

Table B5: Maxwell and modified Felske model predictions for gas permeation in MMMs for H_2/CH_4 separation using *Polyimide (6FDA-DDBT)*, [ϕ =0.3], (*P_{CH4}, P_{H2}: Barrer)

	Maxwell Model			**Modified Felske Model**		
Name	**P_{CH4}**	**P_{H2}**	**$S_{(H2/CH4)}$**	**P_{CH4}**	**P_{H2}**	**$S_{(H2/CH4)}$**
PURE POLYMER	1.98	156.00	78.80	1.98	156.00	78.80
BACMOH10	3.59	354.06	98.60	2.60	228.62	87.98
BAHGUN	4.52	354.42	78.39	2.91	228.81	78.66
BIMDIL	4.52	355.61	78.59	2.91	229.21	78.75
FOHQUO	3.75	350.75	93.51	2.66	227.63	85.65
GITTIN	4.51	353.20	78.37	2.91	228.37	78.60
LUMZUO	4.52	349.23	77.31	2.91	227.17	78.11
LUNBAX	4.51	349.22	77.35	2.91	227.17	78.13
LUNBEB	4.51	343.68	76.23	2.91	225.48	77.60
MABJOP	4.46	352.99	79.08	2.91	228.73	78.61
MABJUV01	4.52	353.48	78.15	2.91	228.45	78.50
MIHHIU	4.52	354.69	78.50	2.91	229.08	78.70
MIHHOA	2.20	351.69	159.88	1.94	227.92	117.38
MIHHUG	4.33	353.77	81.65	2.85	228.54	80.11
MMIF	1.21	266.80	221.07	1.23	198.45	160.97
OFERUN	1.99	347.08	174.20	1.82	226.52	124.80
QAMXIL	4.52	356.04	78.69	2.89	228.30	78.93
ZUQPOQ	4.52	354.56	78.36	2.91	228.77	78.60

Table B6: Maxwell and modified Felske model predictions for gas permeation in MMMs for H_2/CH_4 separation using *Hyflon*, [ϕ =0.3], (*P_{CH4}, P_{H2}: Barrer)

	Maxwell Model			**Modified Felske Model**		
Name	**P_{CH4}**	**P_{H2}**	**$S_{(H2/CH4)}$**	**P_{CH4}**	**P_{H2}**	**$S_{(H2/CH4)}$**
PURE POLYMER	3.03	187.00	61.70	3.03	187.00	61.70
BACMOH10	5.02	423.83	84.37	3.79	273.88	72.26
BAHGUN	6.92	424.34	61.32	4.45	274.03	61.52
BIMDIL	6.93	426.05	61.50	4.46	274.54	61.61
FOHQUO	5.31	419.10	78.88	3.91	272.46	69.73
GITTIN	6.89	422.59	61.37	4.44	273.51	61.55
LUMZUO	6.91	416.94	60.33	4.45	271.81	61.06
LUNBAX	6.90	416.93	60.39	4.45	271.80	61.09
LUNBEB	6.89	409.08	59.39	4.44	269.40	60.61
MABJOP	6.79	422.30	62.24	4.41	273.42	61.95
MABJUV01	6.92	423.00	61.09	4.46	273.63	61.42
MIHHIU	6.91	424.73	61.44	4.45	274.15	61.58
MIHHOA	2.96	420.45	142.28	2.72	272.87	100.40
MIHHUG	6.49	423.42	65.23	4.32	273.76	63.33
MMIF	1.85	306.67	166.06	1.89	232.49	123.23
OFERUN	2.70	413.89	153.12	2.55	270.88	106.27
QAMXIL	6.93	426.67	61.59	4.46	274.72	61.65
ZUQPOQ	6.93	424.54	61.29	4.46	274.09	61.51

Table B7: Maxwell and modified Felske model predictions for gas permeation in MMMs for H_2/CH_4 separation using *Teflon AF-2400*, [ϕ =0.3], (*P_{CH4}, P_{H2}: Barrer)

	Maxwell Model			Modified Felske Model		
Name	**P_{CH4}**	**P_{H2}**	**$S_{(H2/CH4)}$**	**P_{CH4}**	**P_{H2}**	**$S_{(H2/CH4)}$**
PURE POLYMER	600.00	3300.00	5.50	600.00	3300.00	5.50
BACMOH10	373.63	6602.08	17.67	380.41	4553.16	11.97
BAHGUN	1124.10	6716.79	5.98	800.85	4592.01	5.73
BIMDIL	1352.80	7143.18	5.28	876.64	4730.37	5.40
FOHQUO	376.02	5743.93	15.28	382.45	4237.88	11.08
GITTIN	744.50	6343.91	8.52	632.28	4463.02	7.06
LUMZUO	961.65	5444.19	5.66	736.52	4116.35	5.59
LUNBAX	889.20	5443.22	6.12	704.35	4115.95	5.84
LUNBEB	760.29	4648.19	6.11	640.71	3759.61	5.87
MABJOP	515.07	6287.36	12.21	490.60	4442.75	9.06
MABJUV01	1233.56	6425.47	5.21	839.03	4491.91	5.35
MIHHIU	996.63	6808.81	6.83	751.24	4622.67	6.15
MIHHOA	366.64	5956.29	16.25	374.39	4320.20	11.54
MIHHUG	416.54	6512.65	15.64	416.09	4522.37	10.87
MMIF	365.22	2467.93	6.76	373.16	2428.29	6.51
OFERUN	366.25	5089.56	13.90	374.05	3963.89	10.60
QAMXIL	1343.88	7315.39	5.44	873.96	4783.69	5.47
ZUQPOQ	1333.27	6762.68	5.07	870.74	4607.36	5.29

Table B8: Maxwell and modified Felske model predictions for gas permeation in MMMs for H_2/CH_4 separation using *Poly(trimethylsilylpropyne-co-phenylpropyne)*, [ϕ =0.3], (*P_{CH4}, P_{H2}: Barrer)

	Maxwell Model			**Modified Felske Model**		
Name	**P_{CH4}**	**P_{H2}**	**$S_{(H2/CH4)}$**	**P_{CH4}**	**P_{H2}**	**$S_{(H2/CH4)}$**
PURE POLYMER	$2.14x10^4$	$2.04x10^4$	0.95	$2.14x10^4$	$2.04x10^4$	0.95
BACMOH10	$1.30x10^4$	$2.75x10^4$	2.11	$1.33x10^4$	$2.26x10^4$	1.70
BAHGUN	$1.59x10^4$	$2.88x10^4$	1.82	$1.56x10^4$	$2.33x10^4$	1.49
BIMDIL	$3.45x10^4$	$3.55x10^4$	1.03	$2.64x10^4$	$2.62x10^4$	0.99
FOHQUO	$1.30x10^4$	$2.10x10^4$	1.61	$1.33x10^4$	$1.90x10^4$	1.43
GITTIN	$1.36x10^4$	$2.50x10^4$	1.84	$1.38x10^4$	$2.14x10^4$	1.54
LUMZUO	$1.44x10^4$	$1.96x10^4$	1.36	$1.45x10^4$	$1.81x10^4$	1.25
LUNBAX	$1.41x10^4$	$1.96x10^4$	1.39	$1.42x10^4$	$1.81x10^4$	1.27
LUNBEB	$1.37x10^4$	$1.68x10^4$	1.23	$1.39x10^4$	$1.62x10^4$	1.17
MABJOP	$1.32x10^4$	$2.46x10^4$	1.86	$1.35x10^4$	$2.11x10^4$	1.57
MABJUV01	$1.84x10^4$	$2.58x10^4$	1.40	$1.75x10^4$	$2.17x10^4$	1.24
MIHHIU	$1.46x10^4$	$3.00x10^4$	2.05	$1.47x10^4$	$2.38x10^4$	1.62
MIHHOA	$1.30x10^4$	$2.22x10^4$	1.71	$1.33x10^4$	$1.98x10^4$	1.48
MIHHUG	$1.31x10^4$	$2.66x10^4$	2.03	$1.34x10^4$	$2.22x10^4$	1.66
MMIF	$1.30x10^4$	$1.29x10^4$	0.99	$1.33x10^4$	$1.31x10^4$	0.98
OFERUN	$1.30x10^4$	$1.82x10^4$	1.40	$1.33x10^4$	$1.72x10^4$	1.29
QAMXIL	$3.09x10^4$	$3.95x10^4$	1.28	$2.48x10^4$	$2.77x10^4$	1.12
ZUQPOQ	$2.79x10^4$	$2.94x10^4$	1.05	$2.33x10^4$	$2.36x10^4$	1.01

Table B9: Maxwell and modified Felske model predictions for gas permeation in MMMs for H_2/CH_4 separation using *Poly(trimethylsilylpropyne)*, [ϕ =0.3], (*P_{CH4}, P_{H2}: Barrer)

	Maxwell Model			Modified Felske Model		
Name	**P_{CH4}**	**P_{H2}**	**$S_{(H2/CH4)}$**	**P_{CH4}**	**P_{H2}**	**$S_{(H2/CH4)}$**
PURE POLYMER	$2.33x10^4$	$2.32x10^4$	0.99	$2.33x10^4$	$2.32x10^4$	0.99
BACMOH10	$1.42x10^4$	$3.01x10^4$	2.12	$1.45x10^4$	$2.51x10^4$	1.73
BAHGUN	$1.71x10^4$	$3.15x10^4$	1.85	$1.69x10^4$	$2.59x10^4$	1.53
BIMDIL	$3.68x10^4$	$3.93x10^4$	1.07	$2.84x10^4$	$2.93x10^4$	1.03
FOHQUO	$1.42x10^4$	$2.30x10^4$	1.62	$1.45x10^4$	$2.10x10^4$	1.45
GITTIN	$1.48x10^4$	$2.73x10^4$	1.85	$1.50x10^4$	$2.37x10^4$	1.58
LUMZUO	$1.56x10^4$	$2.15x10^4$	1.38	$1.57x10^4$	$2.00x10^4$	1.28
LUNBAX	$1.53x10^4$	$2.15x10^4$	1.41	$1.54x10^4$	$2.00x10^4$	1.30
LUNBEB	$1.48x10^4$	$1.86x10^4$	1.25	$1.50x10^4$	$1.80x10^4$	1.20
MABJOP	$1.44x10^4$	$2.68x10^4$	1.87	$1.47x10^4$	$2.34x10^4$	1.59
MABJUV01	$1.96x10^4$	$2.81x10^4$	1.43	$1.88x10^4$	$2.41x10^4$	1.28
MIHHIU	$1.58x10^4$	$3.29x10^4$	2.08	$1.59x10^4$	$2.65x10^4$	1.67
MIHHOA	$1.42x10^4$	$2.43x10^4$	1.71	$1.45x10^4$	$2.19x10^4$	1.51
MIHHUG	$1.42x10^4$	$2.90x10^4$	2.04	$1.45x10^4$	$2.46x10^4$	1.69
MMIF	$1.42x10^4$	$1.46x10^4$	1.03	$1.45x10^4$	$1.49x10^4$	1.02
OFERUN	$1.42x10^4$	$2.00x10^4$	1.41	$1.45x10^4$	$1.90x10^4$	1.31
QAMXIL	$3.29x10^4$	$4.40x10^4$	1.34	$2.66x10^4$	$3.12x10^4$	1.17
ZUQPOQ	$2.96x10^4$	$3.22x10^4$	1.09	$2.49x10^4$	$2.62x10^4$	1.05